

國立交通大學

生醫工程研究所

碩士論文

基於多重生理訊號參數之
即時無線瞌睡偵測系統



Real-time Wireless System based on Multiple Bio-signal
Parameters for Drowsiness Detection

研究生：劉育航

指導教授：林進燈 教授

中華民國 九十九年七月

基於多重生理訊號參數之即時無線瞌睡偵測系統

Real-time Wireless System based on Multiple Bio-signal Parameters for
Drowsiness Detection

研究生：劉育航

Student：Yu-Hang Liu

指導教授：林進燈

Advisor：Chin-Teng Lin

國立交通大學

生醫工程研究所



Submitted to Institute of Biomedical Engineering
College of Computer Science
National Chiao Tung University
in partial Fulfillment of the Requirements
for the Degree of
Master
in
Computer Science

July 2010

Hsinchu, Taiwan, Republic of China

中華民國九十九年七月

Real-time Wireless System based on Multiple Bio-signal Parameters for Drowsiness Detection

Student: Yu-Hang Liu

Advisor: Dr. Chin-Teng Lin

Institute of Biomedical Engineering
College of Computer Science
National Chiao Tung University

Abstract

In recent years, traffic accident is one of the critical reasons to cause deaths of drivers. Drivers' drowsiness has been implicated as a causal factor in many accidents because of the marked decline in drivers' perception of risk and recognition of danger, and diminished vehicle handling abilities. Consequently, if the mental state of drivers could be real-time monitored, drowsiness detection and warning could effectively avoid disasters such as vehicle crashes in working environments. Some previous researches used non-physiological method, as eye closure with CCD image tracking, such as the pupil recognition, blink detection or identification of the drivers head shaking frequency. However, for CCD image tracking, users couldn't move for free, and the images detecting performance were easily be interfered by external flash light. Other studies used physiological parameters to increase the accuracy of drowsy detection, like pulse wave analysis with neural network, electrooculography (EOG), electromyography (EMG), and electroencephalogram (EEG) measurement. In this study, we proposed a real-time wireless system for drowsiness detection. A wearable, wireless and real-time bio-signal acquisition system was designed for long-term

monitoring. In the other hand, not only EEG but also EOG signals were acquired by our system to increase the accuracy of drowsiness detection. Furthermore, an algorithm of drowsiness detection was also proposed to reduce the computation complexity, and was implemented in a portable DSP module with bio-feedback as bio-stimulator or buzzer. In order to estimate the level of drowsiness, a lane-keeping driving experiment was designed and the drowsiness level of drivers was indirectly assessed by the reaction time under Virtual Reality Driving Simulation Environment. The advantage of this unsupervised algorithm can remove the differences between individual and environment in different people or measurements. For the purpose of verifying the accuracy and feasibility of our proposed unsupervised algorithm, drowsiness status estimated by driving performance was compared with the results obtained by our proposed unsupervised algorithm. The results of comparison showed that our algorithm can detect driver's drowsiness status precisely. In addition, our system can be successfully applied in practice to prevent traffic accidents caused by drowsy driving.

KEYWORD: drowsiness detection, electroencephalogram, electrooculography, portable bio-signal acquisition system, DSP module, Virtual Reality Driving Simulation Environment, driving performance, unsupervised algorithm

基於多重生理訊號參數之即時無線瞌睡偵測系統

學生：劉育航

指導教授：林進燈 博士

國立交通大學生醫工程研究所

摘要

近年來，交通意外是一個造成駕駛死亡的至關重要原因，其中駕駛者的精神狀況不佳所造成車禍意外佔了絕大多數比例，所以開車駕駛瞌睡監控問題是我們嘗試克服之處，試著以人為方式來減少車禍發生。近年來相關的開車監控研究引進了生理參數來做為開車即時瞌睡狀況的比較依據，如心電圖、眼電波圖、肌電圖或腦波圖等，較影像辨識來得直接與精確，使用者可以不必受影像定位之問題影響，本論文即針對生理參數中之腦波以及眼電波參數做進一步的探討。我們設計了一套無線可攜式的多重生理訊號擷取系統以及包含生理回饋機制如電刺激器等數位訊號處理平台，再搭配非監督式分析演算法來做即時的瞌睡判斷。使用非監督式演算法的優勢在於可移除掉不同人、不同次測量中個別跟環境差異性。本論文藉由虛擬實境模擬環境所記錄下開車偏移量來當作瞌睡程度的參考，並與所發展的非監督式分析法的相互比對關係來證明此演算法對瞌睡程度偵測的能效與可行性，最後實現在數位訊號處理平台上。經由實際測試，可以成功在駕駛者有睡意時，利用電刺激器或是警示音提醒駕駛保持清醒，確保開車時的安全。

關鍵字: 瞌睡監控、腦波圖、眼電波圖、無線可攜式生理訊號擷取系統、數位訊號處理平台、虛擬實境模擬環境、開車偏移量、非監督式分析法



誌謝

本論文的完成，首先要感謝指導教授林進燈博士這兩年來的悉心指導，讓我學習到許多寶貴的知識，在學業及研究方法上也受益良多。另外也要感謝口試委員們的建議與指教，使得本論文更為完整。

其次，感謝實驗室的學長林伯昱在研究上的指導。同學智賢、璽文、佩瑄、聖翔、敬婷、佳鈴，在過去兩年研究生活中同甘共苦、相互扶持，及學姐依伶、學長家達、孟修、煒忠、寓鈞、哲睿、有德、家欣、怡然與倫德、學弟妹們俊甫、麒宇與琬茹，在研究過程中所給我的鼓勵與協助。尤其是哲睿學長、依伶學姐及伯昱學長，在研究理論及程式技巧上給予我相當多的幫助與建議，亦師亦友，讓我獲益良多。也同樣感謝實驗室助理在許多事務上的幫助。

感謝我的父母親對我的教育與栽培，並給予我精神及物質上的一切支援，使我能安心地致力於學業，也要感謝你們對我不斷的關心與鼓勵。還要謝謝我的妹妹以及 Angel 和圓圓的陪伴，使我回家時的生活充滿歡笑。此外，我也很感謝我的朋友柏任、宗穎、念平、哲羽以及可涵，同樣謝謝你們的鼓勵以及支持，讓我在沮喪或低潮時重新有動力，使我能全心投入論文之中，真心的感謝你們。

謹以本論文獻給我的家人及所有關心我的師長與朋友們。

Chapter 1 Introduction.....	1
1.1 Drowsiness Detection	1
1.2 Previous Research.....	2
1.3 Motivation.....	7
1.4 Organization of Thesis	9
Chapter 2 Material and Method.....	10
2.1 EEG Signal Acquisition	11
2.2 EOG Signal Acquisition.....	13
2.3 Virtual Reality Driving Simulation Environment	14
2.4 EEG Preprocessing	17
2.5 EOG Preprocessing	18
2.6 Unsupervised Analysis of EEG and EOG.....	19
Chapter 3 Hardware Frameworks	23
3.1 System Overview	23
3.2 Portable Bio-signal Acquisition System	24
3.2.1 Front-End Filter Circuit	26
3.2.2 Analog to Digital Converter and Digital Controller	29
3.2.3 Power Management	36
3.2.4 Wireless Transmission	38
3.3 DSP Module.....	39
3.3.1 DSP Framework.....	39
3.3.2 The Circuit of Stimulator	41
3.4 Hardware System Specification	43
Chapter 4 Unsupervised Approach	46
4.1 Driving Performance.....	46
4.2 Construction of the Alertness Model	48
4.3 Computation of the Deviation from the Subject.....	51
4.4 Computation of the Blink Duration from the Subject.....	52
Chapter 5 Results and Discussion	55
5.1 Performance of Portable Bio-signal Acquisition System and Bio-stimulator of DSP Module.....	55
5.2 Driving Performance and Unsupervised Analysis	60
5.2.1 Results of Unsupervised Analysis.....	60
5.2.2 Relationship between Driving Performance and Unsupervised Analysis	64
5.2.3 Threshold Definition and Drowsiness Classification	67

5.2.4 Test and Verify the Optimized Threshold	74
5.2.5 Comparison between MDT/MDA Only and with Blink Duration.....	75
5.2.6 DSP Module Programming	77
Chapter 6 Conclusions and Future Works	81
6.1 Conclusions.....	81
6.2 Future Works.....	83



List of Figures

Fig. 1-1: The role of driver status monitor [13]	3
Fig. 1-2: Flowchart of EEG processing in drowsy estimation system [19]	6
Fig. 1-3: Scan NuAmps Express system (Compumedics Ltd., VIC, Australia)	6
Fig. 2-1: A typical BCI system architecture	10
Fig. 2-2: International 10-20 system	13
Fig. 2-3: The recommended derivation of EOG	14
Fig. 2-4: The overview of surrounded VR scene	15
Fig. 2-5: The digitized highway scene.[56].	16
Fig. 2-6: Illustration of synchronization between the driving trajectory and bio-signal data	17
Fig. 2-7: Steps of EEG preprocessing	18
Fig. 2-8: Illustration of 5-second moving window with 4.88-second overlap	18
Fig. 2-9: Steps of EOG preprocessing	19
Fig. 2-10: The flowchart of the EEG and EOG analysis method.	22
Fig. 3-1: Illustration of hardware framework of our system	24
Fig. 3-2: Diagram of portable bio-signal acquisition unit	25
Fig. 3-3: The R_G decides the gain of preamplifier, and the high pass filter of preamplifier decided by R_G and C	27
Fig. 3-4: Simulation of preamplifier's gain response (EEG)	27
Fig. 3-5: High-pass filter and Low-pass filter circuits	28
Fig. 3-6: Simulation results in EEG channel of amplifier and band-pass filter	28
Fig. 3-7: Simulation results in EOG channel of amplifier and band-pass filter	29
Fig. 3-8: MSP430 Architecture [51]	30
Fig. 3-9: Operating flow chart in MSP430F1611	30
Fig. 3-10: Timer_A up mode for interrupt function of MSP430F1611	31
Fig. 3-11: ADC12 Block Diagram [51]	32
Fig. 3-12: Diagram of the sampling and conversion with timer A trigger	33
Fig. 3-13: Data format	33
Fig. 3-14: Result of noise cancellation by using moving average	35
Fig. 3-15: Power supply circuit in portable bio-signal acquisition system	37
Fig. 3-16: Charging circuit in our portable bio-signal acquisition system	38
Fig. 3-17: PCB Blue Tooth antenna [64]	39
Fig. 3-18: The block diagram of DSP system [64]	41
Fig. 3-19: The schematic circuit of Slave board	42
Fig. 3-20: The front-end analog and digital control circuit	43
Fig. 3-21: (a) Master board of DSP module (b) Slave board of DSP module	45

Fig. 4-1: The example of deviation event and car trajectories.....	47
Fig. 4-2: Blink features	52
Fig. 5-1: The result between two conditions.....	56
Fig. 5-2: The result of arbitrary wave test.....	57
Fig. 5-3: The position of Fengchi	58
Fig. 5-4: Result of EEG raw data and corresponding frequency spectrum	58
Fig. 5-5: Results of EEG raw data: (a) before bio-stimulation, (b) during bio-stimulation and (c) after bio-stimulation.	59
Fig. 5-6: Example 1 of driving performance and unsupervised analysis.....	61
Fig. 5-7: Example 2 of driving performance and unsupervised analysis.....	62
Fig. 5-8: Example 3 of driving performance and unsupervised analysis.....	62
Fig. 5-9: Example 4 of driving performance and unsupervised analysis.....	63
Fig. 5-10: Process of sorting analysis	65
Fig. 5-11: The relationship between MDA/ MDT/ Duration and reaction time	66
Fig. 5-12: The relationship between sensitivity and specificity	67
Fig. 5-13: Positive predictive value vs. threshold of “Combination” where the numeric in parentheses was sequentially expressed as (MDT, MDA, Duration)	70
Fig. 5-14: Sensitivity vs. threshold of “Combination” where the numeric in parentheses was sequentially expressed as (MDT, MDA, Duration)	71
Fig. 5-15: F-measure vs. threshold of “Combination” where the numeric in parentheses was sequentially expressed as (MDT, MDA, Duration)	73
Fig. 5-16: The result of comparison between MDT/MDA only and with blink duration	77
Fig. 5-17: The flowchart of DSP module program	78
Fig. 5-18: The user interface’s flowchart	80
Fig. 5-19: The block diagram of dataflow	80
Fig. 6-1: (a) top view, (b) exploded view of the proposed dry foam EEG electrode. .	83
Fig. 6-2: Frequency characteristic of the proposed dry foam electrodes on.....	85
Fig. 6-3: Impedance variation of dry foam electrode and conventional wet electrode under long-term EEG measurement.....	86
Fig. 6-4: Placements and results of measurements by using different types of electrodes	88

List of Tables

Table 2-1: Common band of EEG	12
Table 2-2: Feature of blink behaviors	14
Table 3-1: Specification for various kinds of bio-sensors	25
Table 3-2: The spec of portable bio-signal acquisition system	44
Table 3-3: The spec of DSP Module	44
Table 5-1: The description of binary classification test	67
Table 5-2: The results of binary classification test	74
Table 5-3: 10 subjects' results of validation with MDT=0.3, MDA=0.3, Duration=0.4 and threshold set as 31.5	75
Table 5-4: The results of binary classification test with only MDT and MDA	76



Chapter 1 Introduction

1.1 Drowsiness Detection

In recent years, traffic accident is one of the critical reasons to cause deaths of drivers. World Health Organization report released that the global traffic accidents killed 1.2 million lives each year and caused millions of people were injured [1]. The report stated that a daily average of 1000 persons aged 25 years of age because of the people killed in traffic accidents, of which 90 percent of the victims took place mainly in Africa and Asia, low-income countries. The report said that the 19-year-old and 15-year-old groups to the cause of death, traffic accidents ranked first, far exceeding the number of AIDS deaths. It showed that the traffic safety is the very urgent issues that need to straighten and improve.

The cause of accidents is often imputed to driver's mental state. A human in drowsiness often exhibits relative inattention to environments, eye closure, less mobility, failure to motor control and decision making [2]. Therefore, those accidents which caused by falling drowsiness usually not only endanger themselves but also involve the public. Many studies have pointed out that a driver's drowsiness can cause serious traffic accidents [3]-[6]. In 2002, the National Highway Traffic Safety Administration (NHTSA) reported that about 0.7% of drivers have been involved in a crash that they attribute to drowsy driving, amounting to an estimated 800,000 to 1.88 million drivers in the past five years [7]. The National Sleep Foundation (NSF) also reported that 51% of adult drivers had driven a vehicle while feeling drowsy and 17% had actually fallen asleep [8].

Thus, in the field of safety driving, development of methodologies for detection

drowsiness / departure from alertness in drivers has become an important area of researches. If the mental state of drivers can be real-time monitored directly, drowsiness detection and warning can effectively avoid disasters such as vehicle crashes in working environments. Recently, with the development of brain computer interface, real-time monitoring the mental states of drivers and detecting drowsiness have become feasible.

1.2 Previous Research

Drowsiness leads to decline in drivers' abilities of perception, recognition, and vehicle control and hence monitoring of drowsiness in drivers is very important to avoid road accidents [9]. Some researches used non-physiological method, as eye closure with CCD image tracking [10]-[16]. And others used physiological parameters to increase the accuracy of drowsy detection, like pulse wave analysis with neural network [20], the electrooculography (EOG) and the electromyography (EMG) measurement [17], [18], and the electroencephalogram (EEG) [19]-[21].

In 2003, Hamada et al. proposed a driver status monitor system by using CCD camera, as shown in Fig. 1-1 [13]. The CCD camera was installed in the car and focused on the user's eyes. The driver status monitor detected drowsiness from the change in the duration of eye closure during blinking and inattention from the change in the gaze direction. Using CCD camera to contribute the urgency system was a very difficult work here. There were some critical points inside, and needed to overcome. For instance, user couldn't move for free, the images detecting performance were easily be interfered by light, and the largest problem was that the system is too big, complex, and expensive to implement. The algorithm of eye tracking also needed to

use edge detecting to train data, and hence to build up a neural network to classify the drowsy status.

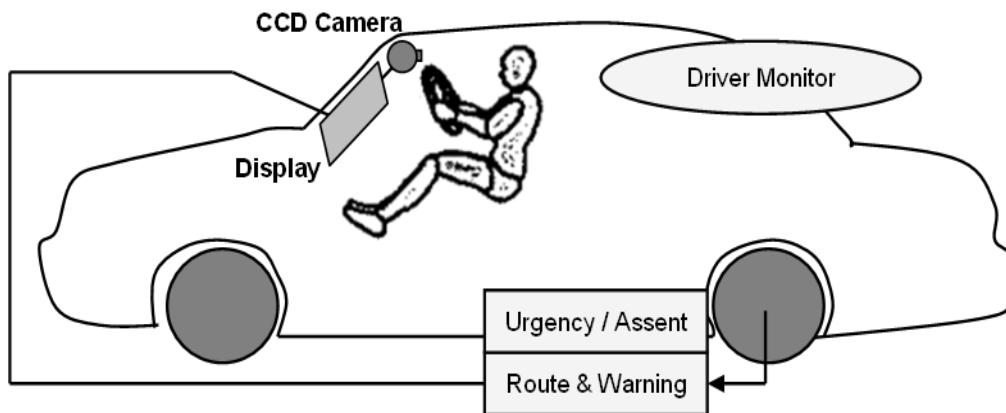


Fig. 1-1: The role of driver status monitor [13]

An alternate is to detect the moment from alertness to drowsiness by using physiological parameters. In 2005, Thum et al. used EOG as an alternative to video-based systems in detecting eye activities caused by drowsiness [18]. Rapid eye movements (REM), which occurred when one is awake, and slow eye movements (SEM), which occurred when one is drowsy, can be detected through EOG. The results showed that the detection rate for eye activities caused by drowsiness was more than 80 %. However, REM and SEM are difficult to measure when users are driving because users can not close his/her eyes when they are driving a vehicle on the road, and then SEM is hard to measure. In addition, REM and SEM are tending to the level of sleep stage not the indicator of drowsiness detection, so they can not be used as the parameters of on-line process.

In 2003, Caffier et al. proposed that the spontaneous eye blink is considered to be a suitable ocular indicator for fatigue diagnostics [24]. To evaluate eye blink parameters as a drowsiness indicator, they developed a contact free method for the measurement of eye blinks by using an infrared sensor clipped to an eyeglass frame recorded eyelid movements continuously. The parameters blink duration and

reopening time in particular change reliably with increasing drowsiness. The results demonstrate that the measurement of eye blink parameters provided reliable information about drowsiness. In 2008, Jammes et al. in order to automatically score the drowsiness level, they developed a software for identifying blinks in EOGs as their first step [23]. They recorded vertical EOG signals by surface electrodes placed above and below the eyes. The analysis of EOG velocity based on expert rules was the originality of their blink detection algorithm and more than 97.7% of blinks were detected by their algorithm. The drowsiness scale they selected was Karolinska Drowsiness Score (KDS) which would score when signs of drowsiness, i.e. long duration or small amplitude blinks were detected. Comparing the results of KDS and the results of their automatic scoring, and then they found out the correlation of these results was high. It demonstrated that blink duration and amplitude are important parameters for drowsiness detection.

Brain Computer Interface (BCI) is an interface between human and computers or machines. It is based on the translation of the specific brain activity generated by a specific thought of a human to control machines, to communicate with the outside world directly, to convey the message, and independent operations, as well as self-care purposes. BCI can be divided into three distinct modes: invasive, partially-invasive, and non-invasive BCI. Non-invasive BCI is the main stream of BCI research which has advantages of both easy application and absence of procedural risks, such as infection or cortical micro-lesions. There are several approaches to non-invasively acquire brain activities, such as magnetoencephalography (MEG), positron emission tomography (PET), functional magnetic resonance imaging (fMRI), electroencephalography (EEG) and et al. EEG is the mainstream of non-invasive BCI, because of its much fine temporal resolution,

ease of use, portability and low set-up cost. In particular, higher temporal resolution becomes the great temptation to use EEG techniques as a direct communication channel from the brain to the real world [27]-[42].

In EEG system, it was different from other physiological parameters, and moreover it owned intuitive and specific characteristics, such as alpha, theta or beta band power followed subject's own mental state. In addition, the EEG system usually needed to collect enough EEG data to analyze. The supervised methods which previously study often had been used to train a learning data, and usually implement in off-line EEG analysis. Previous studies which used supervised methods developed several kinds of brain computer interface for drowsiness detection [19], [20]. When the subject changed the state from alertness to drowsiness, the alpha rhythm will increase and beta rhythm will decrease [21]. In 2005, a drowsy estimation system was developed by combining independent component analysis (ICA), power-spectrum analysis, correlation evaluations, and linear regression model to estimate a driver's cognitive state when he/she drove a car in a virtual reality (VR)-based dynamic simulator [19]. Its flowchart of EEG processing was shown in Fig. 1-2. In the above studies, an EEG machine, Scan NuAmps Express system (Compumedics Ltd., VIC, Australia), was used to measure EEG, as shown in Fig. 1-3. It is not small, light, and wearable. Moreover, the above algorithms for drowsiness detection requires mass computation complexity, thus, they are not easy to be implemented in a portable DSP device.

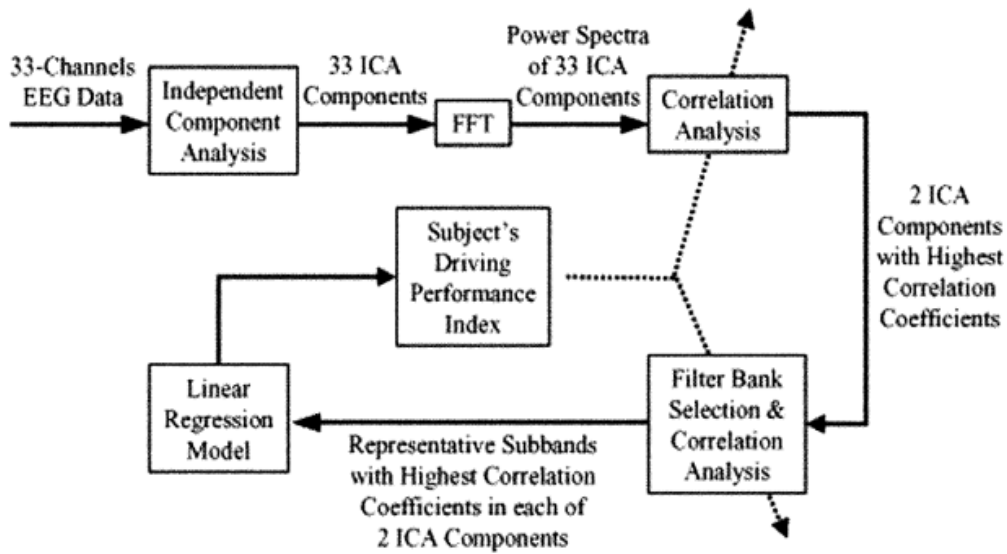


Fig. 1-2: Flowchart of EEG processing in drowsy estimation system [19]



Fig. 1-3: Scan NuAmps Express system (Compumedics Ltd., VIC, Australia)

In the supervised mode, supervised learning methods such as artificial neural network (ANN) could be used to classify different states of vigilance. But stimulus may introduce some noise. So in [43], the author proposed a semi-supervised learning algorithm which can quickly label huge amount of data. Here another author proposed another kind of semi-supervised learning method based on probabilistic principle component analysis (PPCA) to distinguish wake, drowsy and sleep in driving simulation experiment. After training with data of around 20 min (6–8 min for each state), they could directly use our method as a real time classifier to estimate driver's

vigilance state [44]. Although this method could greatly reduce the training time, but it still must be used in off-line analysis. In our target, we wanted to find a non-training and unsupervised method, and easily implement to an on-line detecting system.

1.3 Motivation

To avoid tragedies, a real-time physiological signal monitoring system of drowsiness detection is required to prevent traffic accidents. However, users' mobility is limited by the inconvenience of traditional BCI (heavy and large EEG machine). Besides, recent studies used one kind of bio-signal as EEG or EOG only to detect drowsiness. Nevertheless, the accuracy of detection is not high enough with one physiological signal used only. Thus, an inexpensive, convenient, portable, wireless and multi-parameter of bio-signal used platform with long battery life that can be carried indoors or outdoors are desired.

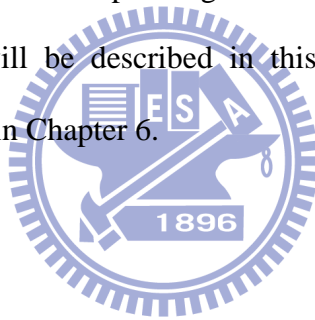
In this study, not only a real-time wireless brain computer interface for drowsiness detection was proposed, but also parameters of EOG were used. The spontaneous eye blink can be determined by EOG measurement and is considered to be a suitable ocular indicator of fatigue and alertness level [22, 24]. It offers several advantages, since it represents a normal, simply observable and easily accessible phenomenon that reflects the influence of central nervous activation without voluntary manipulation[24]. Recent studies show that the analysis of eye blinks can provide some information for physiologists to quantify drowsiness. There are many parameters of eye blinks, such as duration, frequency, closing time, opening time, amplitude and so on. The blink duration and opening time are especially subject to characteristic modifications with increasing drowsiness. Besides, frequency

(percentage of eyelid closure) was also used as the indicator by previous research to determine user was drowsy or not [22-26]. To increase accuracy of drowsiness detection, parameters of EOG signal were used in our study and we would stress the importance of correlation between drowsiness with EOG signal.

A wearable, wireless and real-time bio-signal acquisition system was designed for long-time EEG/EOG monitoring, and a DSP module with bio-feedback as buzzer or bio-stimulator was also introduced. An algorithm of drowsiness detection based on [45] was proposed to reduce the complexity of computation. Different from previous ICA-based algorithm of drowsiness detection, it used the statistics properties of alpha/theta rhythm and blink duration in alert state to build up the alert model. Consequently, a derivation from the alert model can be used to detect drowsiness. The most useful advantage of this algorithm was that the differences between individual and environment in different people or measurements could be removed, and every analysis was independent. Moreover, with the advantage of low computational complexity, it is easy to be implemented in our portable DSP module.

1.4 Organization of Thesis

In Chapter 2, it will describe that what are EEG and EOG signals, virtual reality driving simulation environment, and algorithms implemented in this thesis, which including EEG/EOG preprocessing and unsupervised approach. In Chapter 3, it will introduce how to implement a wireless portable bio-signal acquisition system and DSP module in hardware design. In Chapter 4, it will explain the detail of driving performance, unsupervised algorithm, and how to accomplish them. In chapter 5, it will introduce the driving performance sorting analysis then the method of driving performance and unsupervised approach will be verified with 10 real experimental subjects' driving trajectories and corresponding EEG and EOG signals, the procedures and results of verification will be described in this chapter. Finally it will have conclusions and future works in Chapter 6.



Chapter 2 Material and Method

We developed the BCI system according to the steps of Fig. 2-1. The portable bio-signal acquisition system which we designed was used in input device of BCI. The EEG and EOG raw data continually transmitted to DSP module, hence, the following three steps: signal preprocessing, features extraction, and classifier were processed in DSP module. The algorithm we chose was according to unsupervised approach (N. R. Pal, 2008 [45]) and automatic EOG analysis (B. Jammes, 2008[23]). The user interface can output real-time EEG and EOG signals and the results of drowsy detection. If the results were determined as drowsiness by algorithm, DSP module would call the buzzer to output a warning voice or generate stimulation by the muscular bio-stimulator to wake user up as a bio-feedback application.

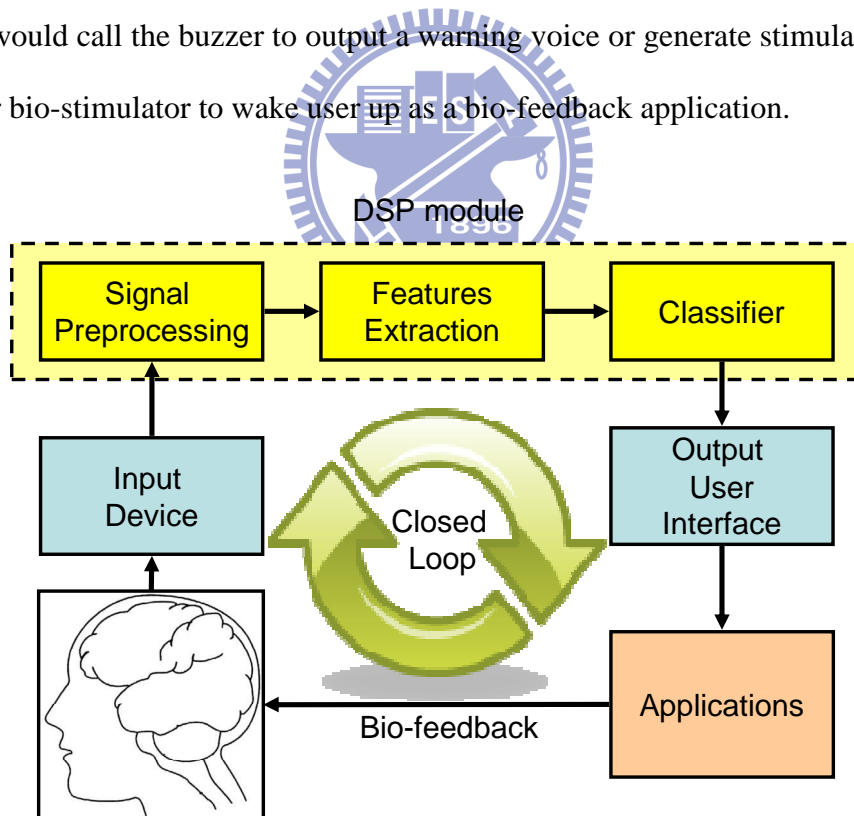


Fig. 2-1: A typical BCI system architecture

In off-line analysis, we wanted to verify the relationship between users's driving trajectories and corresponding EEG and EOG signals. Before analyzing, we assumed

that driving trajectories were directly proportional with variance of theta, alpha spectrum and blink duration. So we designed a driving simulation experiment and used our portable bio-signal acquisition system to observe and record driving information and actual EEG and EOG raw data at one time. There were 10 subjects' EEG and EOG raw data recorded and every trail was at least 25 minutes. Our analysis included two parts: one was to analyze the driving trajectories, and another was to analyze the corresponding EEG and EOG signals. The first step of driving trajectories processing was to analyze the driving performance. On the other hand, we also analyzed EEG and EOG signals. First, we used FFT to get the theta and alpha band information, and then used both two information built up an alert model, computing covariance matrix and mean vector of theta and alpha spectra. Furthermore, compute MDT and MDA continually by using unsupervised method. Second, we calculated the derivative of EOG signals. The EOG velocity was acquired, and then a threshold was applied to select blinks. Next, the duration of these blinks was computed as the reference of drowsiness. After finishing whole data analysis, we used binary classification test, sensitivity and specificity, to verify the drowsiness hit rate. Every experimental trial was separated and sorted, hence, the corresponding MD* (MDT and MDA) and duration of blinks were also sorted. Defining the threshold of both information which been processed to decide the drowsiness or alertness, and to analyze the drowsy accuracy.

2.1 EEG Signal Acquisition

Electroencephalography (EEG) is the recording of electrical activity along the scalp produced by the firing of neurons within the brain. In clinical contexts, EEG

refers to the recording of the brain's spontaneous electrical activity over a short period of time, usually 20–40 minutes, as recorded from multiple electrodes placed on the scalp [55]. When measuring from the scalps, recorded EEG signal is about 10-100uV for a typical adult human. And a common system reference electrode is connected to the other input of each different amplifier. These amplifiers amplify the voltage between the active electrode and the reference (typically 1,000–100,000 times, or 60–100 dB of voltage gain). The EEG is typically described in terms of rhythmic activity and transients. The rhythmic activity is divided into bands by frequency. The common band of EEG is shown as Table 2-1. Following the classification of EEG, Theta and Alpha band are related to drowsiness. Thus, when the subjects become drowsy, both bands will increase their power.

Table 2-1: Common band of EEG

Type	Frequency (Hz)	Normally
Delta	<4	Slow wave sleep for adults
Theta	4~7	Drowsiness, idling, or arousal in children and adults
Alpha	8~12	Relaxed, reflecting, or closing the eyes
Beta	12~30	Alert or working

There are high correlation between drowsiness and EEG obtained from the location of OZ in the international 10–20 EEG system [56]. Therefore, in this study, we only monitored EEG in the location of OZ. Here, three EEG electrodes were used. One was input, one was reference, and the other was ground. According to a modified International 10–20 EEG system and refer to right ear lobe as depicted in Fig. 2-2. We used the following notations: F: Frontal lobe. T: Temporal lobe. C: Central lobe. P: Parietal lobe. O: Occipital lobe. "Z" refers to an electrode placed on the mid-line. The input data was placed on OZ, ground was fixed on the center of forehead, and reference was pasted behind the right ear.

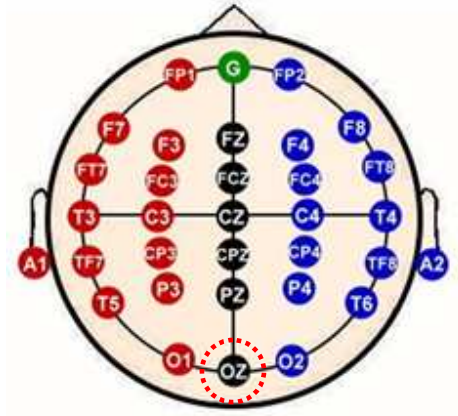


Fig. 2-2: International 10-20 system

Raw EEG data were recorded with 12-bit quantization level at the sampling rate of 256 Hz. And a simple moving average filter was used to remove 60 Hz power line noise and other high-frequency noise.

2.2 EOG Signal Acquisition

Electrooculography (EOG) is a technique for measuring the resting potential of the eyeball. Mostly, there are two electrodes placed above and below the eye, and the resulting signal is called vertical EOG. If the eye is moved from center position toward left or right, then one of the electrodes would see the positive side of the eyeball and the other would see the negative side. There would be a potential difference between the electrodes. If we assumed the resting potential as a constant, then the potential difference become a measure for the eye position called eye movement measurements [46]. Eye movement measurements usually used as a reference of stages of sleep which included three main stages called: awake, REM and NREM. Eye movement is significantly difference during these three stages, so lots of research of sleep used this measurement to observe variation. In this study, the

vertical EOG was derived using three electrodes: input, reference and ground. One electrode was placed above the right eye as the input and the other below the right eye as the reference signal. There was also an electrode as ground fixed on the center of forehead (the same as the ground signal of EEG). A sampling rate of 256Hz was used; because of the principal measurement range of EOG is about 50uV-3500uV, the gain was set 2,000 times. Besides, the parameters of EOG which used in our study were blink behaviors, so feature of these blink behaviors was listed in Table 2-2. The recommended derivation of EOG was shown as Fig 2-3.

Table 2-2: Feature of blink behaviors

Behavior	Description
Blink amplitude	A typical blink has an amplitude of 400uV
Blink duration	Nearly 200ms – 400ms for one blink
Blink frequency	About 15-20 times per minutes for a relaxed person

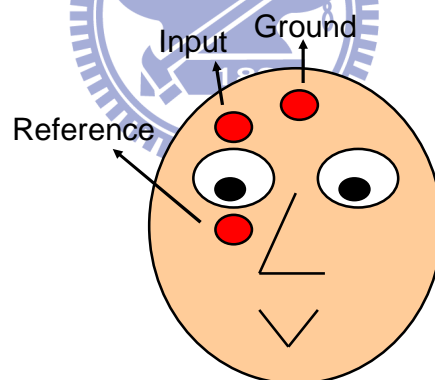


Fig. 2-3: The recommended derivation of EOG

2.3 Virtual Reality Driving Simulation Environment

In this study, a lane-keeping driving experiment was utilized to investigate driving performance under different levels of drowsiness. Here, a virtual reality (VR)-based cruising environment was developed to simulate a car driving at 100 km/hr on a straight four-lane highway at night [19], [57]. During the driving

experiments, all scenes move according to the displacement of the car and the subject's maneuvering of the wheels which make the subject feel like driving the car on a real road. The VR environment was shown in Fig. 2-4.



Fig. 2-4: The overview of surrounded VR scene. The VR-based highway scenes are projected into surround screen with seven projectors.

In our experiments, the driving speed was fixed at 100 km/hr and the car was drifted away from the center of the cruising lane automatically and randomly by the system to mimic the effects of a non ideal road surface. The driver was asked to maintain the car along the center of the cruising lane. All subjects involved in this study had good driving skill and hence when the subject was alert, his/her response time to the random drift was short and the deviation of the car from the center of the lane was small. However, when the subject became not alert / drowsy, both the response time and the car's deviation were high. Note that, in all our experiments, the subject's car was the only car cruising on the VR-based freeway. Although, both response time and the deviation from the central line are related to the subject's driving performance, in this study, we use the response time as a measure of

performance of the subjects. The driving task was shown in Fig. 2-5.

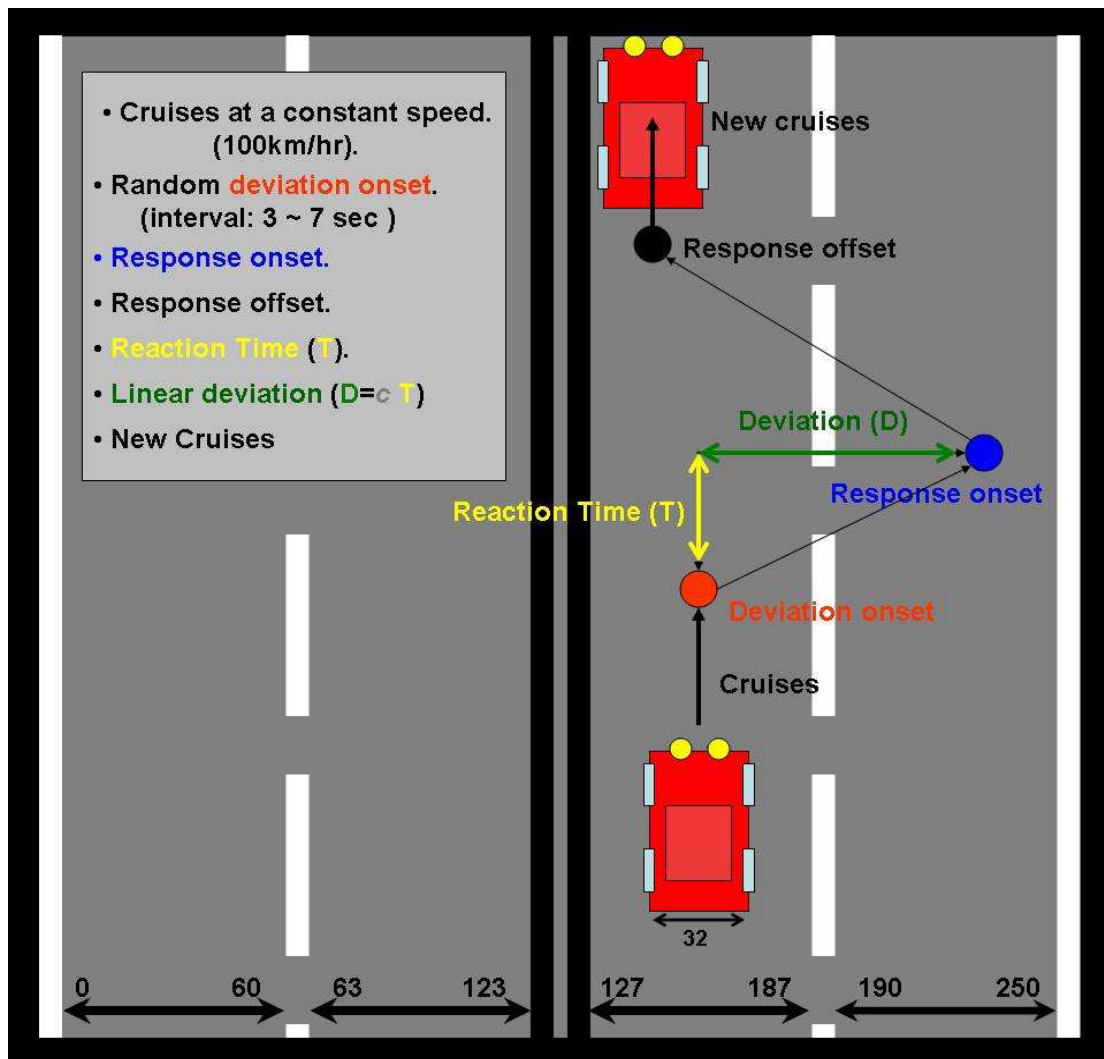


Fig. 2-5: The digitized highway scene. The width of highway is equally divided into 256 units and the width of the car is 32 units. An example of the deviation event, the car cruised with a fixed velocity of 100 km/hr on the VR-based highway scene and it was randomly drifted either to the left or to the right away from the cruising position with a constant velocity. The subjects were instructed to steer the vehicle back to the center of the cruising lane as quickly as possible [56].

In order to synchronize the records of driving trajectory and raw bio-signal data, a C# program was designed to record both of them at the same sampling rate. The driving trajectory produced from the VR-based cruising environment program, and raw bio-signal data obtained by portable bio-signal acquisition system were transmitted to C# program via RS232 and Bluetooth respectively. After finishing

the experiment, both driving trajectory and raw bio-signal data were saved in a text file. Thus, we could investigate the correlation between driving performance and results of unsupervised approach. The illustration of synchronization between the driving trajectory and bio-signal data was shown in Fig. 2-6.

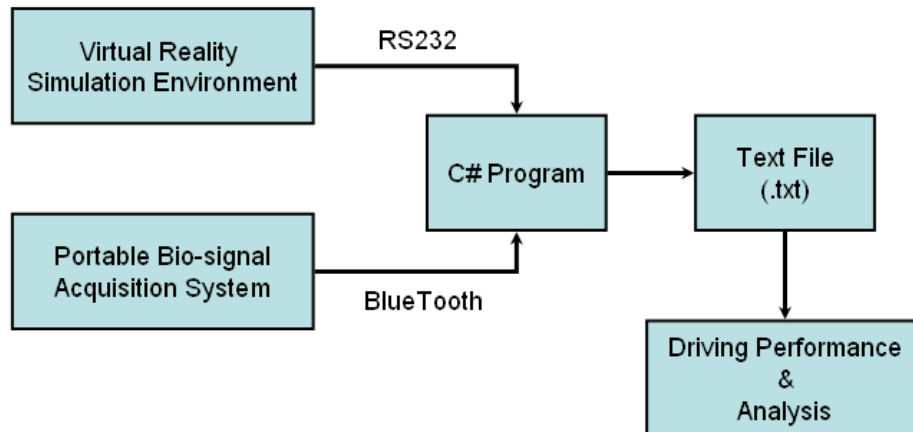


Fig. 2-6: Illustration of synchronization between the driving trajectory and bio-signal data



2.4 EEG Preprocessing

The EEG preprocessing steps were shown in Fig. 2-7. First, a simple moving average filter (low-pass filter with a cutoff frequency of 32 Hz) was used to remove 60 Hz power line noise and other high-frequency noise. In order to simplify the computation, raw EEG data were down-sampled to sampling rate of 128 Hz. Then a 640-point Hanning window was designed to save 5 seconds EEG information and the frequency resolution was set as 256-point, as Fig. 2-8 shown. In our study, Hanning window was chosen because the frequency resolution and spectral leakage are both good for each application. Finally, the power in the frequency band of alpha rhythm (8 ~ 12Hz) and theta rhythm (4 ~ 7Hz) was extracted.

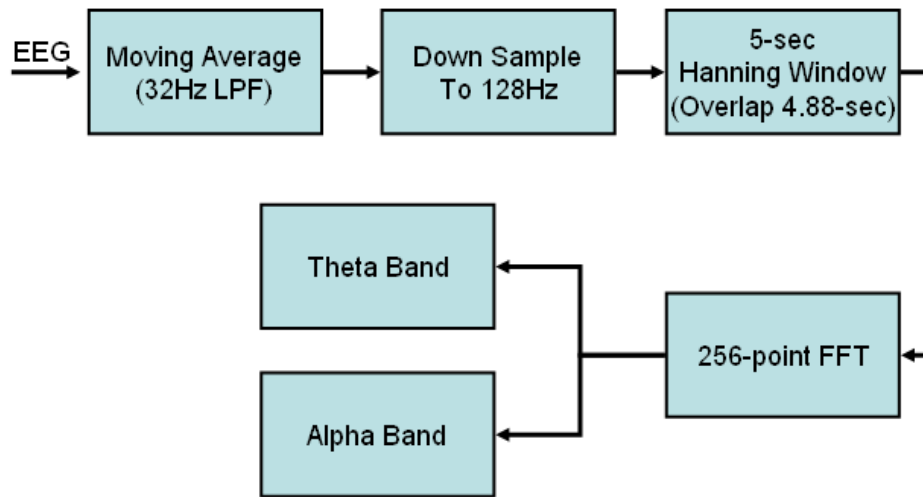


Fig. 2-7: Steps of EEG preprocessing

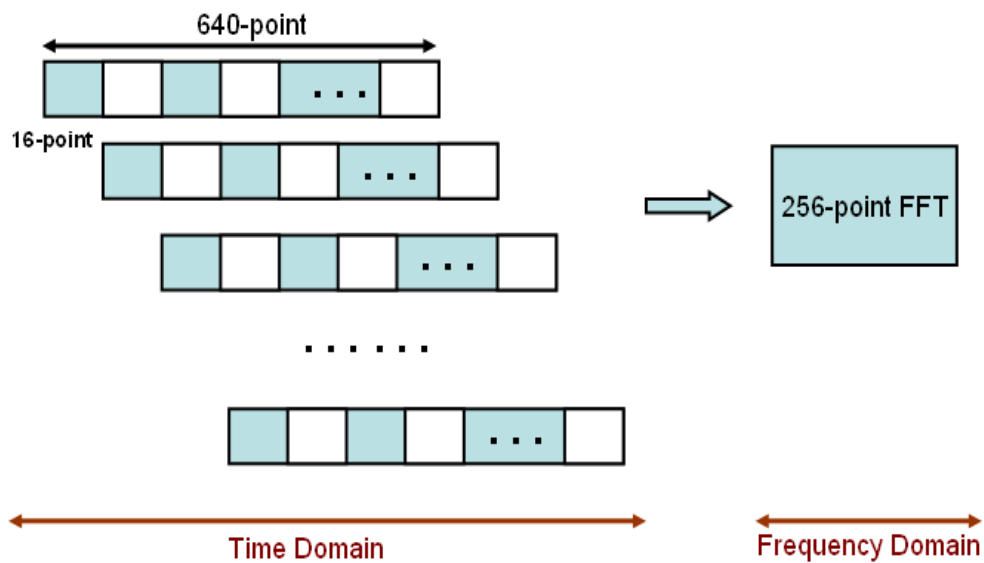


Fig. 2-8: Illustration of 5-second moving window with 4.88-second overlap

2.5 EOG Preprocessing

EOG preprocessing was introduced in this section. Comparing to EEG preprocessing, EOG preprocessing was simpler to implement. Behavior of EOG emphasized in our study was blink, so the steps of EOG preprocessing were aimed at

preprocessing for blink detection. First, we had to define the initial threshold parameters. The values of threshold were empirically selected after analyzing a set of EOG signals recorded as user was in alert state before experiments. According to these threshold parameters then we could acquire the closing time, the opening time of the blinks and other parameters of blink. Second, a 10-Hz low pass filter was used in order to remove frequencies above 10-Hz. Finally, the derivative of the filtered signal called EOG velocity need to be computed. To combine EOG velocity and initial threshold parameters then we could define if the event of EOG raw data was a blink or not, and acquired the parameters we needed. The steps of EOG preprocessing were shown in Fig. 2-9.

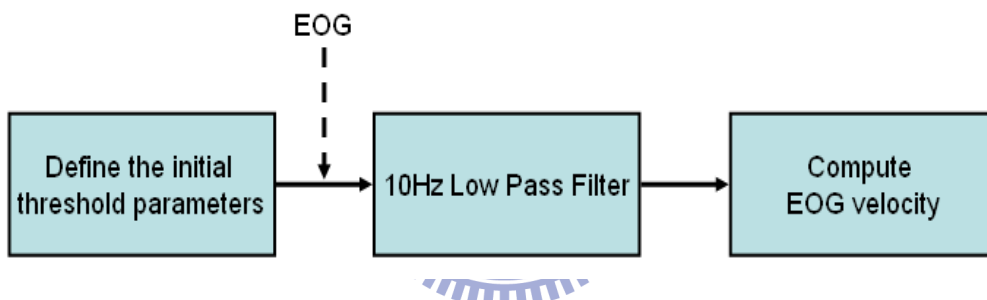


Fig. 2-9: Steps of EOG preprocessing

2.6 Unsupervised Analysis of EEG and EOG

It is recognized that the changes in EEG spectra in the theta band (4~7Hz) and alpha band (8~12Hz) reflect changes in the cognitive and memory performance [58]. Other studies have reported that EEG power spectra at the theta band [59], [60] and/or alpha band [61], [62] are associated with drowsiness, and EEG log power and subject's driving performance are largely linearly related. Besides, blink of EOG is also recognized as an important parameter for detecting drowsiness[23]. There are lots of parameters could be extracted from blinks, for instance: amplitude, duration and so on. Blink duration is an significant information as a result of it becomes longer when

subjects become drowsy, and the changes of blink amplitude reflect the drowsiness level too; the amplitude is small when subjects feel drowsy[24],[25].

As above researches said, these findings have motivated us to derive the alert model of the driver using not only the alpha-band and theta-band EEG power spectrum computed using OZ channel output recorded in the first few minutes of driving, but also the duration of blinks from subjects to increase the accuracy of drowsiness detection. The unsupervised analysis of EEG is introduced first. The choice of the OZ channel is explained in the Experimental Results section. We emphasize that the few minutes of data used to find the alert model are not necessarily collected from the very beginning of driving session because different factors, such as walking of driver by a few meters to reach the garage, may influence the EEG signal generated at the very beginning. The specific window to be used for generation of the alert model is selected by Mardia test [63]. We assume that if the subject/driver is in an alert state, then the EEG power spectra relating to theta band (as well as that relating to alpha band) would follow a multivariate normal distribution. The parameters of the multivariate normal distributions characterize the models. Using the alpha-band and theta-band EEG power, we identify two normal-distribution based models. Then, we assess the deviation of the current state of the subject from the alert model using Mahalanobis distance (MD). We assume that when the subject continues to remain alert, his/her EEG power should resemble the sample data used to generate the model and hence would match the alert model or template. If the subject becomes drowsy, then its power spectra in the alpha band (and also in theta band) will deviate from the respective model and hence MD will increase. With a view to reducing the effect of spurious noise, MDs are smoothed over a 20-sec moving windows, the window is moved by 0.125-sec steps.

Next, we focus on the analysis of EOG signal. In our study, lots of blink behaviors are extracted by our algorithm in the beginning. To base on section 2.5, after EOG velocity and initial threshold parameters are all prepared, we could use the closing and opening threshold to define closing time and opening time as parameters. Besides, computing the difference between the starting point of closing time with end point of opening time then we could acquire the value of blink duration. On the other hand, blink amplitude is computed by using maximum value of one blink to subtract the value of EOG baseline. After above procedure, amplitude of blinks, duration of blinks, closing time of closures and opening time of closures are all acquired. However, some of these parameters could not reflect the variation when subjects become drowsy, for example: the difference of closing time of closures is little between alert and drowsiness[22]. At last, duration is the only parameter we used in our study to determine the subjects are drowsy or not. We assumed when subjects are remaining alert, duration of blinks would be short. In contrast, when subjects feel drowsy, duration of blinks would become longer. 6-second averaged signal of duration before every event of driving performance occurred is extracted by our algorithm to reduce the effect of spurious noise and to be the index for detecting drowsiness.

We then study the relationship between smoothed Mahalanobis distance, duration of blinks and subject's driving performance by computing the correlation between them. Fig. 2-10 shows the overall flow of the EEG and EOG data analysis. In this figure, after the models are identified, the preprocessed alpha band and theta band power data directly go to the blocks for computation of MDA and MDT respectively. Besides, blink duration is computed at the same time. The block for computation of "Combination" makes a linear combination of MDT, MDA and duration of blinks.

Finally, all of these parameters are used in correlation analysis with the driver's performance.

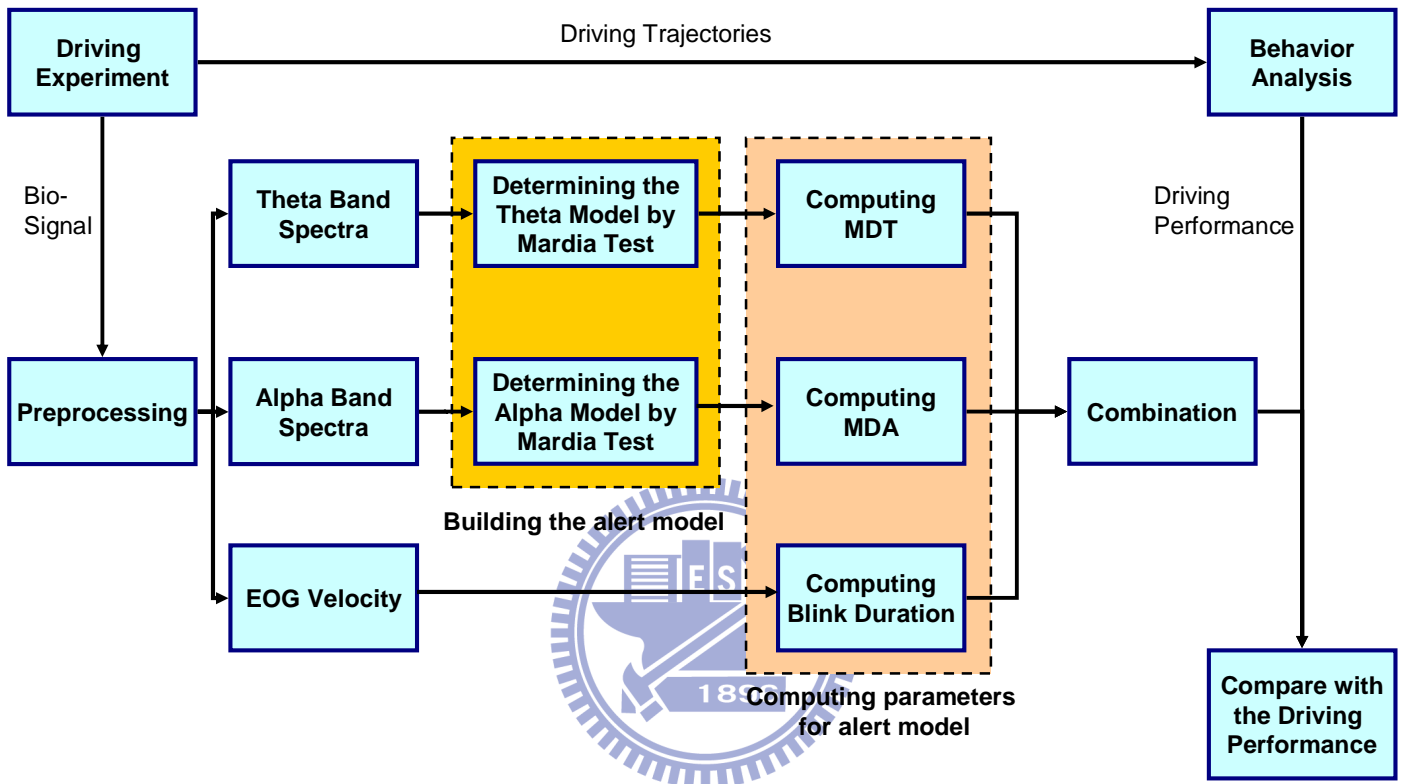


Fig. 2-10: The flowchart of the EEG and EOG analysis method.

Chapter 3 Hardware Frameworks

In this chapter, we focus on this portable system hardware. Following the design flowchart, we will introduce the design methods of hardware circuits and firmware structures steps by steps.

3.1 System Overview

In order to online-measure and analyze EEG and EOG signals, the whole hardware framework of our system mainly contains two sub-systems: One is portable bio-signal acquisition system and the other is DSP module. First, EEG and EOG signals were measured by our portable acquisition module continually. After EEG and EOG signals were acquired, these tiny signals would be amplified. Noise except the frequency band of these bio-signals would be removed by filters in our portable acquisition module. Then filtered EEG and EOG signals would be digitized by analog-to-digital converter and transmitted to the DSP module via Bluetooth. In this study, Linux kernel μ Clinux was used as the operation system in DSP module to handle user's applications. The major tasks of DSP module were to receive EEG and EOG signals via Bluetooth, and to execute the program of online drowsiness level detection, which monitored the variation of power of users' alpha rhythm and theta rhythm. Besides, the difference of blink duration was also monitored. The program of online drowsiness level detection would collect EEG data under alertness for first 3 minutes to build EEG alert model, and then calculated drowsiness level by assessing the power variation of alpha and theta rhythm every 2 seconds. In addition, the duration of every blink was also calculated by our module. If the power or duration variation exceeded the threshold of alert model, the DSP module would send warning

tone of buzzer or generate an electrical stimulation to wake up user. The whole hardware framework is shown as Fig. 3-1.

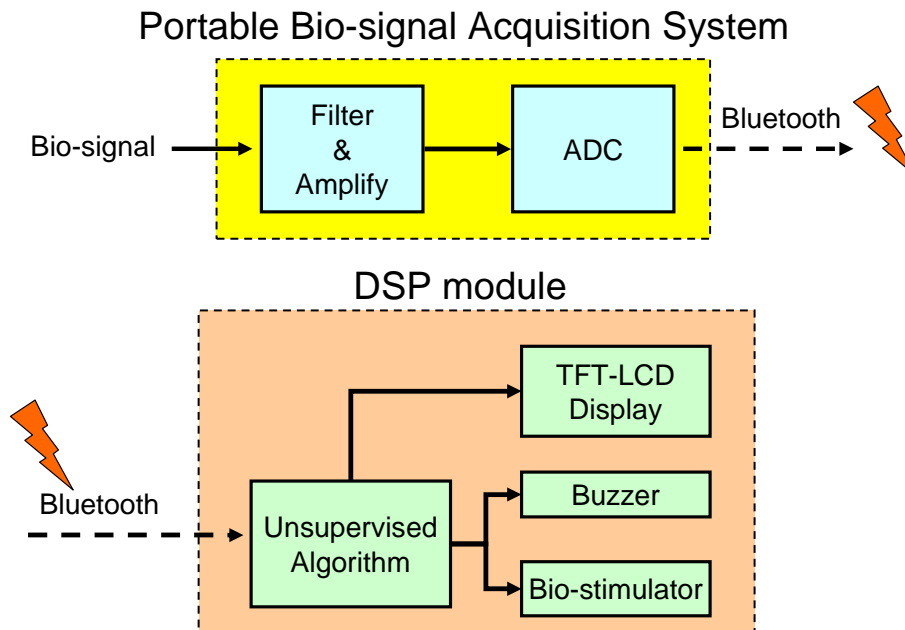


Fig. 3-1: Illustration of hardware framework of our system

3.2 Portable Bio-signal Acquisition System

The portable bio-signal acquisition unit combines the power, amplifier, band pass filter, ADC, wireless controller, and data encoding into one. It is a light weight, wireless monitor for recording physiological signals. It owns 4-channel bio-signal measurement, includes EEG x2 and EOG x2. The portable bio-signal acquisition unit mainly contains four parts: (1) front-end filter circuit, (2) analog to digital converter, and digital controller, (3) power management circuit and (4) wireless transmission. The diagram of the portable bio-signal acquisition unit is shown as Fig. 3-2.

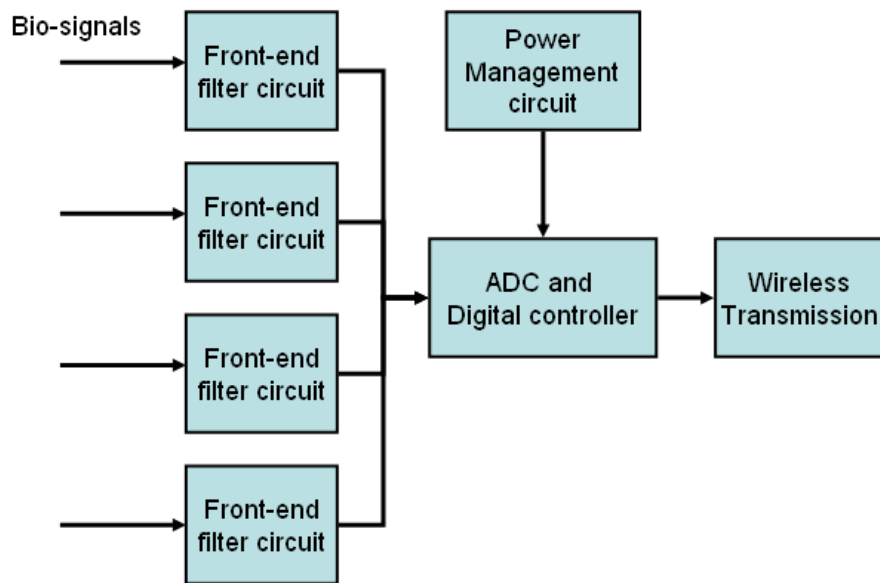


Fig. 3-2: Diagram of portable bio-signal acquisition unit

In our study, only one EEG and one EOG channel of this portable system were used. They were both amplified by bio-amplifier consisted of high-pass, low-pass filters and amplifier. The amplified signals then organized by Micro-processor MSP430. When the signal passed through the high-pass filter, all unnecessary low-frequency noise would be reduced or eliminated, as they passed through the low-pass filter, all unnecessary high-frequency noise would be reduced or eliminated. According to AASM recommendations and difference physiological potentials characteristics, the specification for EEG and EOG channels was shown in Table 3-1.

Table 3-1: Specification for various kinds of bio-sensors

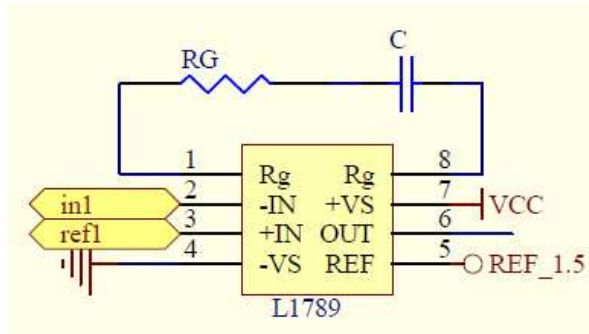
Sensor	Input Signal Range	Gain (Operation voltage:3V)	H.P. Corner F. (Hz)	L.P. Corner F. (Hz)	Sampling rate (Hz)
EEG	20uV-200uV	4500	0.1	45	256
EOG	50uV-3500uV	2000	0.3	45	256

3.2.1 Front-End Filter Circuit

The front-end circuit consisted of preamplifier, and band-pass filter. In some references, other circuit designs preferred to use unit gain filters and one variable gain amplifier. Moreover, they didn't use a high-pass filter to cut-off the noise in low frequency band. To improve them, we designed a 3 stages high pass filter and 2 stages low pass filter to get the clear EEG and EOG information without noise. Hence, adding the gain into filter tried to minimize the total size.

A. Preamplifier

Instrumental amplifier LT1789-1 was used as the first stage of analog amplifier. LT1789-1 owns an ultra low input current and a high common-mode rejection ratio (CMRR) about 90dB. A high CMRR is important in applications that the signal of interest is represented by a small voltage fluctuation superimposed on a (possibly large) voltage offset, or when relevant information is contained in the voltage difference between two signals. Instrumental amplifier LT1789-1 provided not only the function of gain, but also that of one stage high pass filter by adding a capacitor. The output voltage of the LT1789-1 is referenced to the voltage on the reference terminal. The preamplifier circuit design is shown in Fig. 3-3 and the simulation of preamplifier's gain response (EEG) is in Fig. 3-4.



$$\text{Gain} = 1 + (200\text{k}/R_G)$$

$$f_0 = 1 / (2 * R_G * C)$$

Fig. 3-3: The R_G decides the gain of preamplifier, and the high pass filter of preamplifier decided by R_G and C .

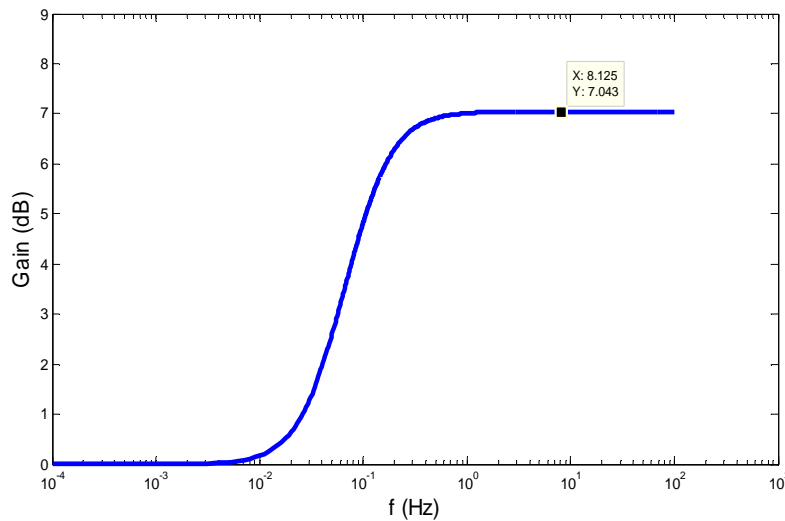
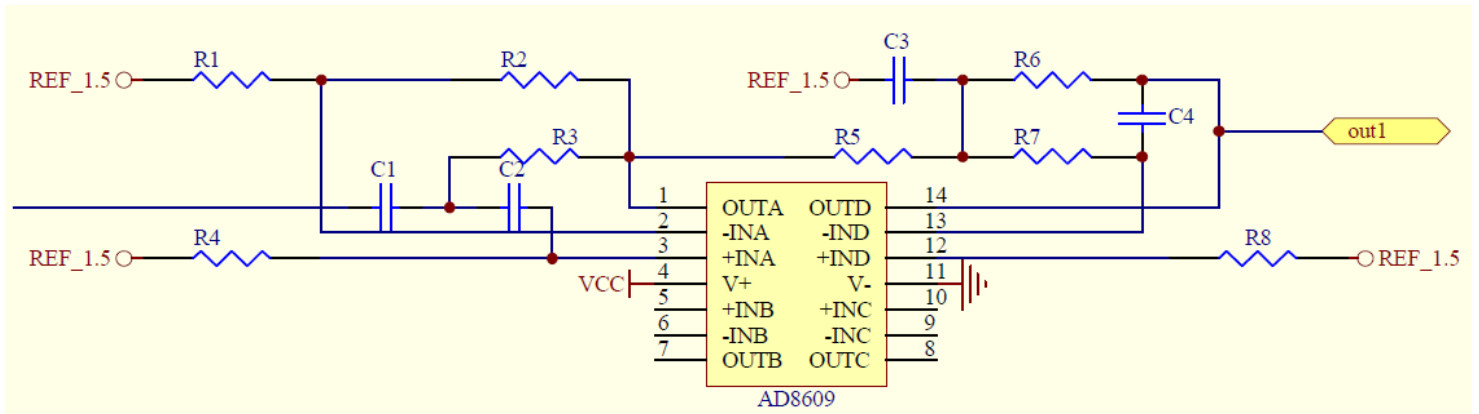


Fig. 3-4: Simulation of preamplifier's gain response (EEG)

B. Band pass filter

In this thesis, operational amplifiers were used to achieve the function of band-pass filter; the feature of op AMP is suitable for amplifying low-frequency signal. The AD8609 is quad micro-power rail-to-rail input and output amplifiers and low dc offset was chosen to be band pass filter. Fig.3-5 shows High-pass filter and Low-pass filter circuits. The 3dB cutoff frequency of high pass was decided

by passive components R3, R4, C1 and C2.



$$f_H = \frac{1}{2\pi\sqrt{R_3 R_4 C_1 C_2}}$$

Fig. 3-5: High-pass filter and Low-pass filter circuits

The passive components R7, R8, C3, and C4 decide the 3dB cutoff frequency

$$f_L = \frac{1}{2\pi\sqrt{R_6 R_7 C_3 C_4}}$$

A circuit of band-pass filters and amplifier is designed as shown in Fig. 3-5 and gain will be determined by passive components R1, R2, R5 and R7. The simulation results of each channel are shown as Fig.3-6 and Fig.3-7.

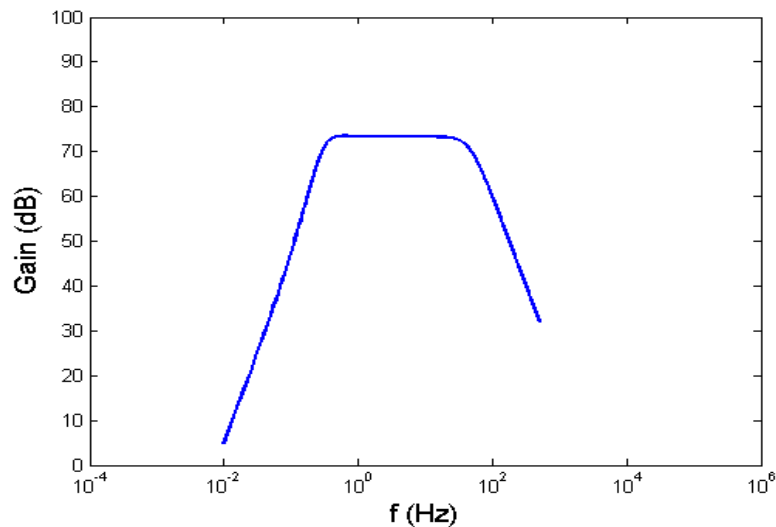


Fig. 3-6: Simulation results in EEG channel of amplifier and band-pass filter

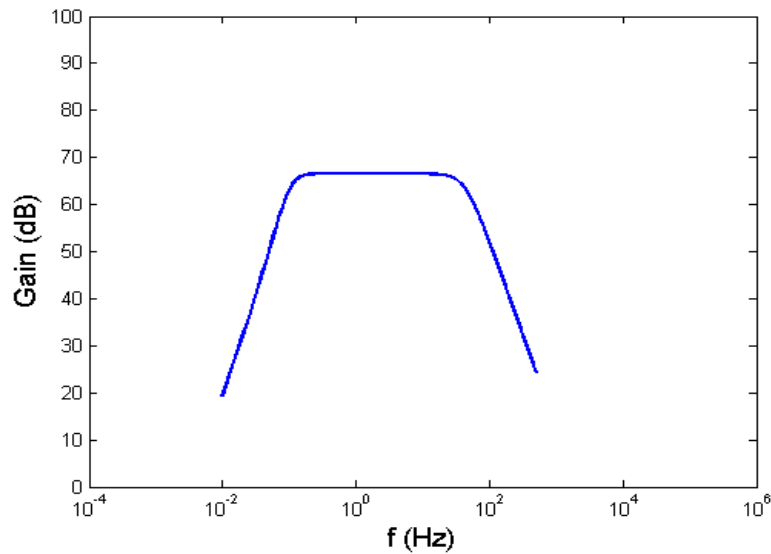


Fig. 3-7: Simulation results in EOG channel of amplifier and band-pass filter

3.2.2 Analog to Digital Converter and Digital Controller

For the data acquisition system, it needs a controller to organize the working of ADC and encode the digital data to Bluetooth module by UART port. The MSP430 is particularly well suited for wireless RF or battery powered applications. The MSP430 incorporates a 16-bit RISC CPU, peripherals, and a flexible clock system that interconnect using a von-Neumann common memory address bus (MAB) and memory data bus (MDB) shown as Fig. 3-8. The clock system is designed specifically for battery-powered applications. Dedicated embedded emulation logic resides on the device itself and is accessed via JTAG using no additional system resources. We configure with built-in 16-bit Timer_A, a fast 12-bit A/D converter, one universal serial synchronous/asynchronous communication interfaces (USART) and 4M Hz external oscillator to development our design[51].

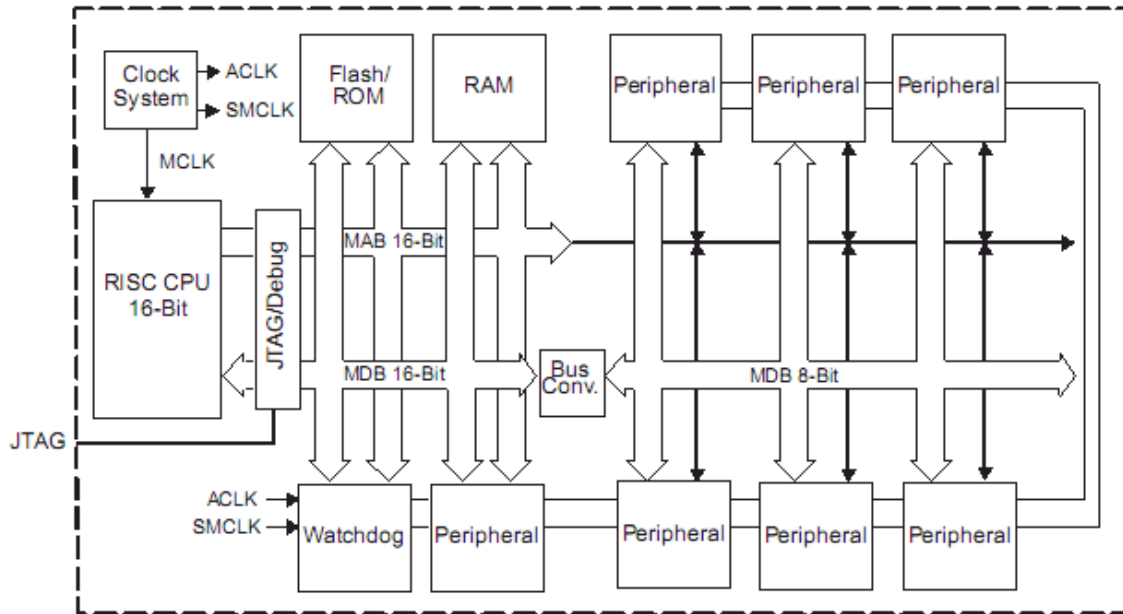


Fig. 3-8: MSP430 Architecture [51]

Timer_A triggers Analog to Digital Converter, and buffers the output data of ADC until buffer full. And then all buffer data will be transmitted via USART. The operating flow chart in MSP430F1611 was shown in Fig. 3-9.

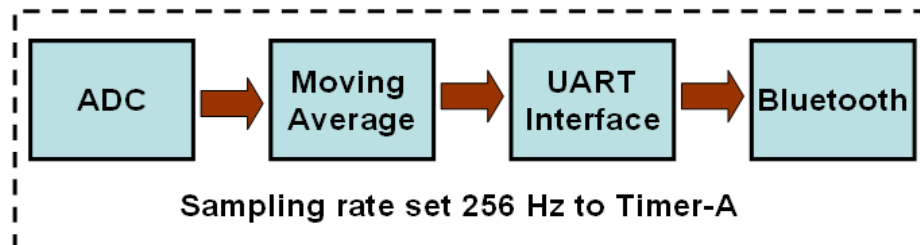


Fig. 3-9: Operating flow chart in MSP430F1611

A. Timer Interrupt

The interrupt function of MSP430F1611 is based on inner timer/counter register, called Timer_A, to count a specific time value. The counter value TACCR0 had to be set first, as shown in Fig. 3-10. When the timer counted to the TACCR0 value, the TACCR0 CCIFG interrupt flag would be set. When the timer counted from TACCR0 to zero, the TAIFG interrupt flag would be set. In our portable bio-signal acquisition

module, 4MHz crystal oscillator was used as system clock of MSP430F1611. Thus, if the sampling rate of our acquisition module is set to 256 Hz, TACCR0 has to be set to 15625.

$$TACCR0 = 4M / 256 = 15625$$

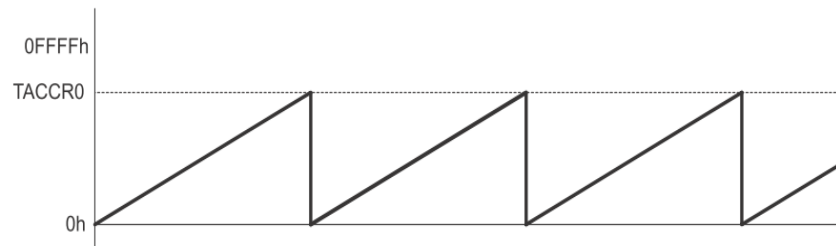


Fig. 3-10: Timer_A up mode for interrupt function of MSP430F1611

B. Analog to Digital Converter

In this system, by passing the signal through wireless, it needs an analog to digital converter to convert the continuous signal to discrete number. To suit with the filtered and amplified signal from front-end circuit, built in ADC of MSP430 was chosen to be an analog to digital converter.

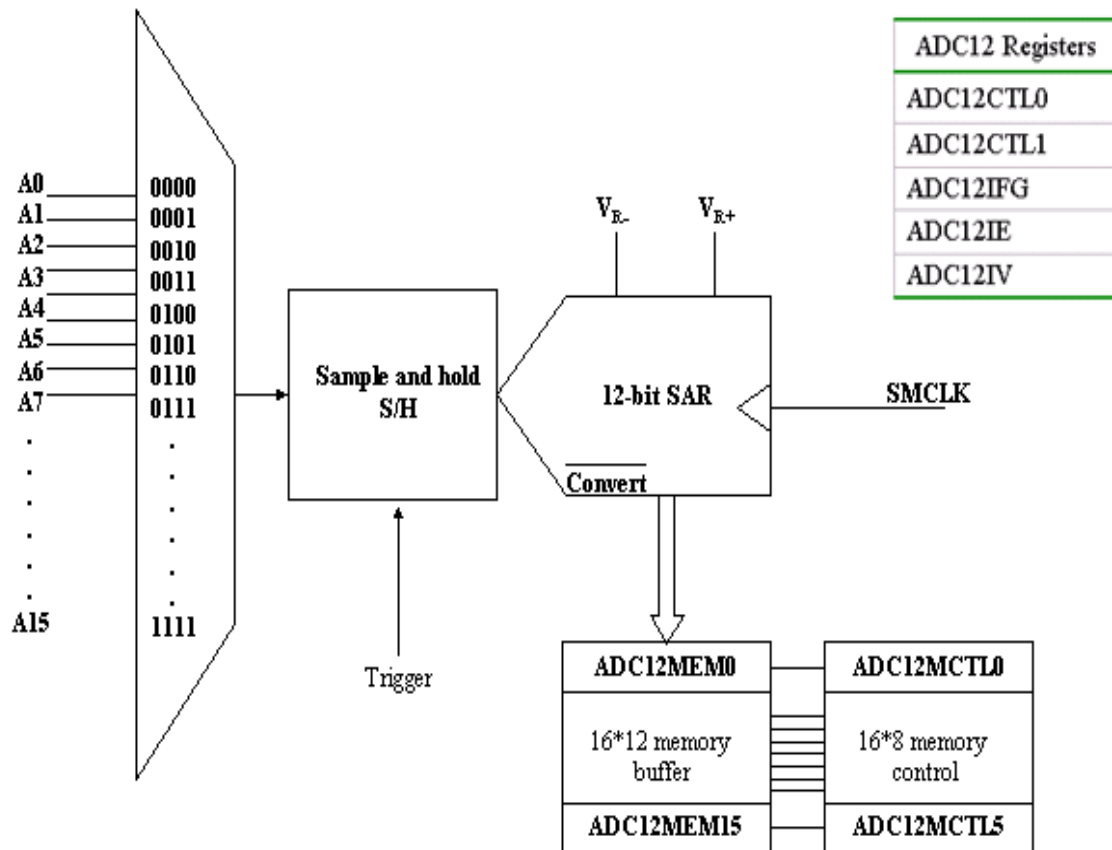


Fig. 3-11: ADC12 Block Diagram [51]

Fig. 3-11 shows ADC12 Block Diagram. The ADC12 module supports fast, 12-bit analog-to-digital conversions. The module implements a 12-bit SAR core, sample select control, reference generator and a 16 word conversion-and-control buffer. The conversion-and-control buffer allows up to 16 independent ADC samples to be converted and stored without any CPU intervention [51]. The ADC12 inputs are multiplexed with the port P6 (A0-A7) pins, which are digital CMOS gates. An analog-to-digital conversion is initiated with a rising edge of the sample input signal SHI. The signal SHI will be set by interrupt routine of timer A at 256Hz. The ADC12 module is configured by three control registers, ADC12CTL0, ADC12CTL1 and ADC12MCTLx. Those registers are set to enable core, select conversion clock, set conversion mode, sample and input channels define. In our system, we used the “multiple channels, single conversion each” mode. In this mode, a sequence of

channels is sampled and converted once. Each conversion requires 6 ADC12CLK cycles; include conversion and result restored into ADC12MEMx conversion memory registers. Fig. 3-12 shows a diagram for sampling time and conversion time of ADC with trigger by timer A. Here, the total sampling and conversion time less then 7812 clocks. Therefore, the conversion time of ADC is fast enough to fit the requirement of the sampling rate of the whole system. The ADC result of each channel will be 12 bits long in the form of an unsigned integer whose value is: $4095 * \frac{A_x - V_{r-}}{V_{r+} - V_{r-}}$

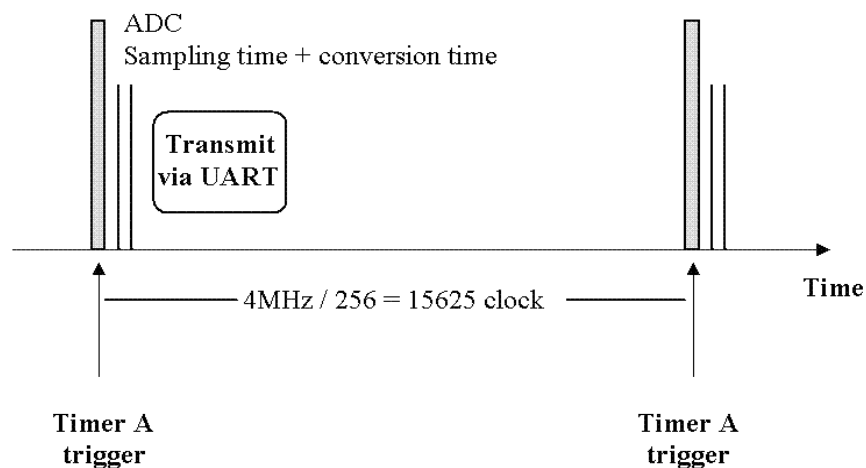


Fig. 3-12: Diagram of the sampling and conversion with timer A trigger

When conversion results are written to a selected ADC12MEMx, the corresponding flag in the ADC12IFGx register is set. An interrupt request is generated if the corresponding ADC12IEx bit and the GIE bit are set. After ADC12IFGx register set, the interrupt service routine of ADC started. In the interrupt service routine, we buffered ADC12MEMx. Next, a moving average filter was used to remove 60-Hz power line interference, and then filtered signal data was encoded before wireless transmission [Fig. 3-13].

FF	62	Channel 1_low byte	Channel 1_high byte	Channel 2_low byte	Channel 2_high byte
----	----	--------------------	---------------------	--------------------	---------------------

Fig. 3-13: Data format

C. Moving Average

Moving average, also called rolling average or running average, is usually used to analyze a set of data points by creating a series of averages of different subsets of the full data set. Moving average can be applied to any data set, however, it is most commonly used with time series data to smooth out short-term fluctuations and highlight longer-term trends or cycles. The choice between short- and long- term, and the setting of moving average parameters depends on the requirement of application. Mathematically, moving average is a type of convolution and is similar to a low-pass filter used in signal processing. The moving average filter is optimal for a common task: reducing random noise while retaining a sharp step response. This makes it as the premier filter for time domain encoded signals.

Given a sequence $\{a_i\}_{i=1}^N$, the output of an n -moving average is a new sequence $\{s_i\}_{i=1}^{N-n+1}$ defined as the average of subsequences of n terms. The formula of moving averaging was shown as followings.

$$s_i = \frac{1}{n} \sum_{j=1}^{i+n-1} a_j \quad (3-1)$$

Therefore, the sequences s_n of n -moving averages when $n = 2,3$ can be expressed as

$$s_2 = \frac{1}{2} (a_1 + a_2, a_2 + a_3, \dots, a_{n-1} + a_n)$$
$$s_3 = \frac{1}{3} (a_1 + a_2 + a_3, a_2 + a_3 + a_4, \dots, a_{n-2} + a_{n-1} + a_n) \quad (3-2)$$

Fig. 3-14 shows the results of noise cancellation by using moving average. A function generator was used to generate sin wave, and our portable bio-signal acquisition system was used to record this signal. If our portable acquisition module

was close to some electric instruments, the signal recorded from the acquisition module would be easily influenced by noise of 60 Hz power line. In the above figure of Fig. 3-14, it showed that the original sin wave had been contaminated by 60Hz power-line noise. After filtering by using moving average with 5-point moving window, we found moving average could effectively remove power-line noise, as shown in the below figure of Fig. 3-14.

$$Num_of_window = \frac{SampleRate}{60} = \frac{256}{60} = 4.27 \quad (3-3)$$

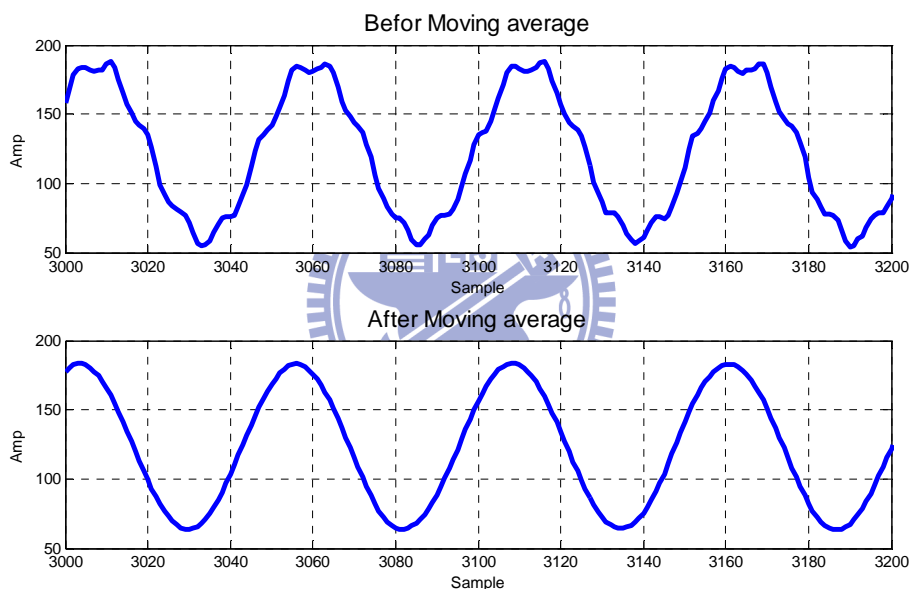


Fig. 3-14: Result of noise cancellation by using moving average

D. UART Interface

In asynchronous mode, USART connected MSP430 to external systems via two external pins, URXD and UTXD. In UART mode, USART transmitted and received characters at a bit rate asynchronously to another device. Timing for each character was based on the selected baud rate of USART. In our study, the transmitter and receiver used the same baud rate. For initializing UART, RX and TX had to be enable first, and then decided the baud rate of UART and disable SWRST. The required

division factor N for determining baud rate was listed as followings:

$$N = \frac{BRCLK}{\text{baud rate}} \quad (3-4)$$

Here, BRCLK was 4 MHz, and baud rate was 115200 bit/s. After initializing UART, the micro-controller could transmit data filtered by moving average to BLUE TOOTH module via UART.

3.2.3 Power Management

Power Management circuit in our portable bio-signal acquisition system includes two parts: one is power supply circuit, and the other is charging circuit.

A. Power Supply Circuit

In our portable bio-signal acquisition system, the operating voltage VCC was at 3V, and the virtual ground of analog circuit was at 1.5V. In order to provide stable 1.5V and 3V voltage, a regulator LP3985 was used to regulate battery voltage to 3V. LP3985 is a micro-power, 150mA low noise, and ultra low dropout CMOS voltage regulator. The maximum output current can support 550mA. Furthermore, the turn-on time can reach 200 μ s. A voltage divider circuit was used to divide 3V voltage into 1.5V, and a unity amplifier constructed from AD8628 was used to provide a voltage buffer. The total power supply circuit was shown in Fig. 3-15.

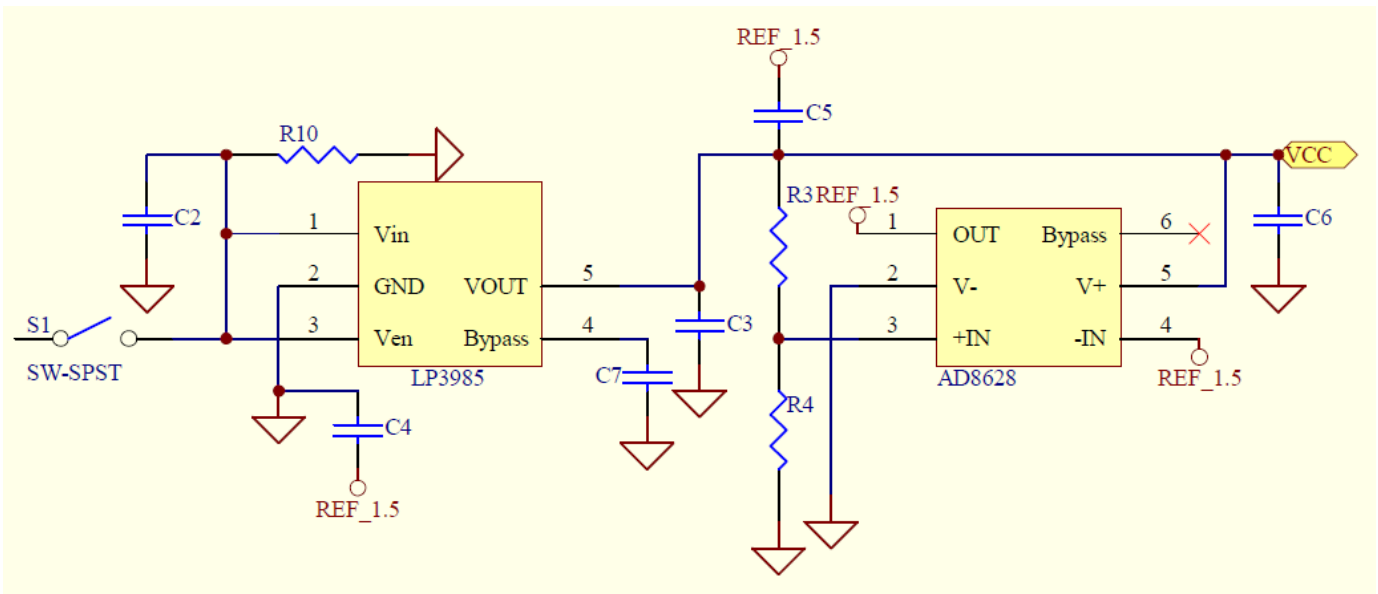


Fig. 3-15: Power supply circuit in portable bio-signal acquisition system

B. Charging Circuit

The charging circuit BQ24010DRC had integrated power FET and current sensor for 1-A charging applications. The maximum charging current can arrive at 1A. The battery's power would be detected automatically by charging circuit and switched to charging mode when battery's power was not enough. BQ24010DRC also protected battery to avoid over charging or over driving [64]. The charging circuit was shown in Fig. 3-16.

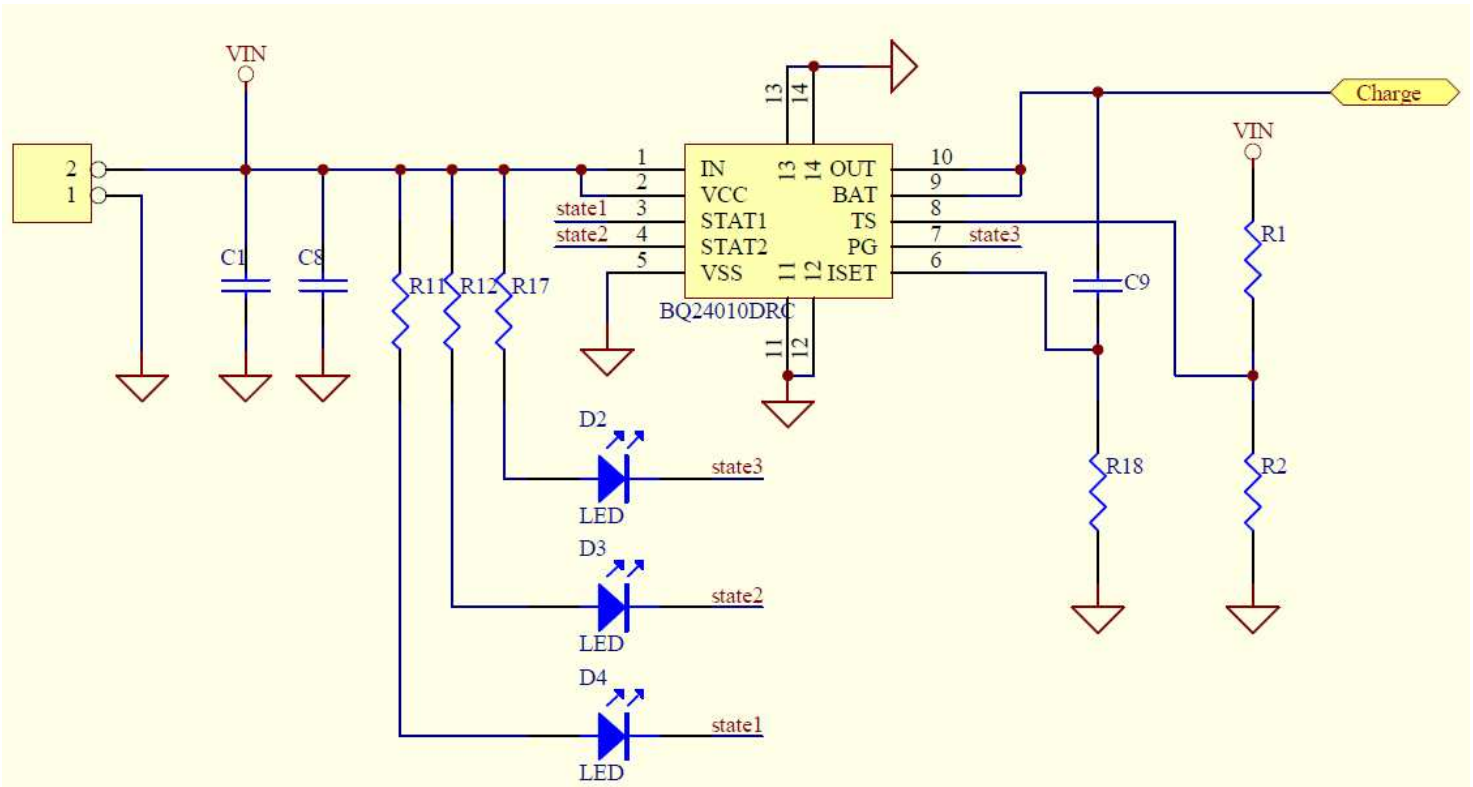


Fig. 3-16: Charging circuit in our portable bio-signal acquisition system

3.2.4 Wireless Transmission

Bluetooth is a wireless protocol utilizing short-range communication technology to facilitate data transmission over short distances from fixed and/or mobile devices. The intent behind the development of Bluetooth was the creation of a single digital wireless protocol, capable of connecting multiple devices and overcoming issues arising from synchronization of these devices. In this study, Bluetooth module BM0203 was used. BM0203 is an integrated Bluetooth module to ease the design gap and uses CSR BlueCore4-External as the major Bluetooth chip. CSR BlueCore4-External is a single chip radio and baseband IC for Bluetooth 2.4GHz systems including enhanced data rates (EDR) to 3Mbps. It interfaces to 8Mbit of external Flash memory. When used with the CSR Bluetooth software stack, it provides a fully compliant Bluetooth system to v2.0 of the specification for data and voice communications. All hardware and device firmware of BM0203 is fully

compliant with the Bluetooth v2.0 + EDR specification. Bluetooth operates at high frequency band to transmit wireless data, so it can be perfect worked by using a PCB antenna, as shown in Fig. 3-17.

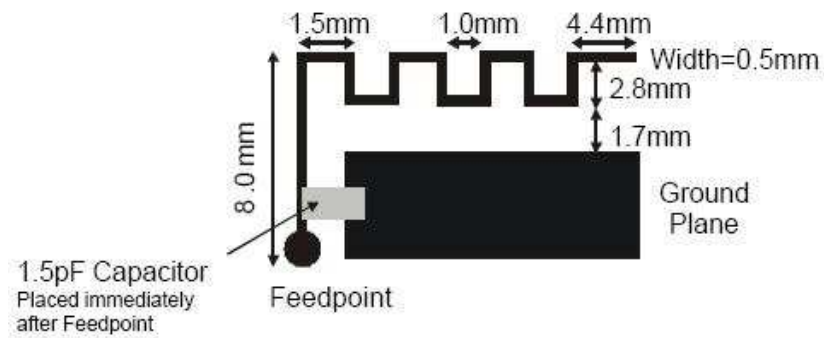


Fig. 3-17: PCB Blue Tooth antenna [64]

3.3 DSP Module

The goal of our DSP module is not only to build a back-end analysis platform but also to provide a bio-feedback mechanism by buzzer or stimulator. This module has greatly powerful calculating ability and supports various peripheral interfaces. After measuring and pre-processing EEG and EOG signals by our portable bio-signal acquisition system, these signals would be transmitted to this DSP module via Bluetooth module. Then, DSP module would process and analyze them. As soon as a drowsy state is detected, this module would warn the user by buzzer or stimulator. Furthermore, it can also use other peripheral interfaces to implement lots of applications [64].

3.3.1 DSP Framework

A powerful digital signal processor Analog Device BF533-STAMP was used in this DSP module, and its CPU speed can be up to 600MHz. There are two 16-bit

MAC Multiply-And-Accumulate used to execute 1200 lines addition and multiplication functions. Besides, DSP contains many independent DMA, Direct Memory Access, to effectively reduce the processing time of core. The system block diagram was shown in Fig. 3-18. In our study, Bluetooth module and UART both worked in the same UART interface.

TFT-LCD, an optional element depends on user's requirement, which is worked by using Memory Mapping, shared the same Memory Bus with SDRAM. In order to reduce the size of platform, traditional parallel NOR Flash was replaced with SPI Flash, and it shared with micro SD Socket, too. Furthermore, the DSP module also owned power management and charging circuits. Micro SD Socket provided the interface scalability, such as micro SD Card, Sensor, ADC, Wireless Card, etc. There is also a buzzer placed on the platform worked via GPIO interface for application. As a matter of fact, our DSP module is divided into two parts: the Master board and the Slave board. The elements introduced above are all placed in the Master board, for instance: SDRAM, micro SD socket, buzzer and so on. There are three circuits of stimulator placed on the Slave board; it also worked via GPIO interface from the Master board. In our application for drowsiness detection and warning, a buzzer and a stimulator are used as a bio-feedback to warn users when they become drowsy. The stimulation which generated by the circuit of stimulator will be introduced in the next session.

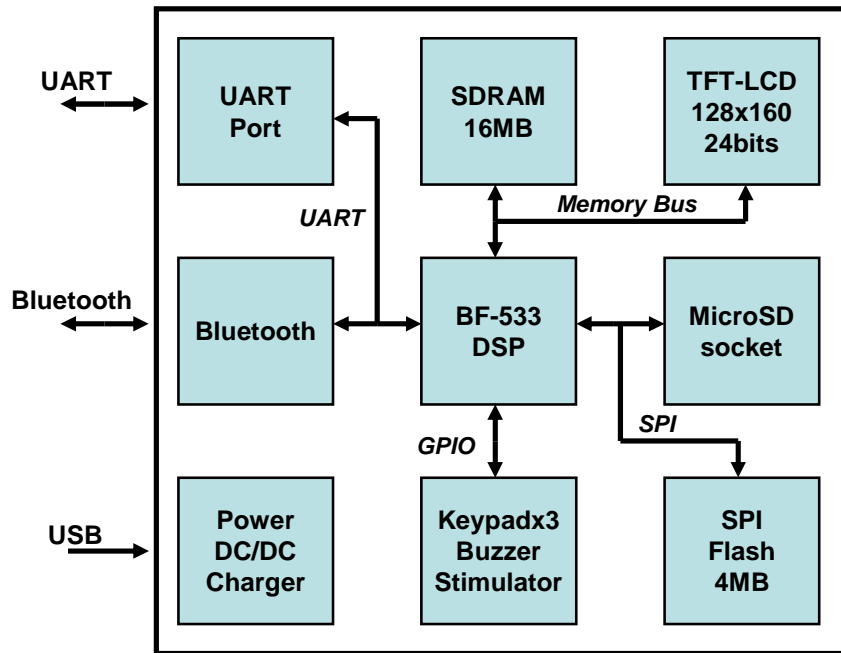


Fig. 3-18: The block diagram of DSP system [64]

3.3.2 The Circuit of Stimulator

The circuit of stimulator was placed on the Slave board to generate the stimulation for warning the user. The Master board and the Slave board communicated with each other via GPIO interface. It is a muscular bio-stimulator, which is small, portable set, designed for those aiming at look improvement in the beginning. Stimulator also provides muscles' stimulation and invigoration so it was used as the bio-feedback mechanism to warn user. The schematic circuit of Slave board was shown in Fig. 3-19.

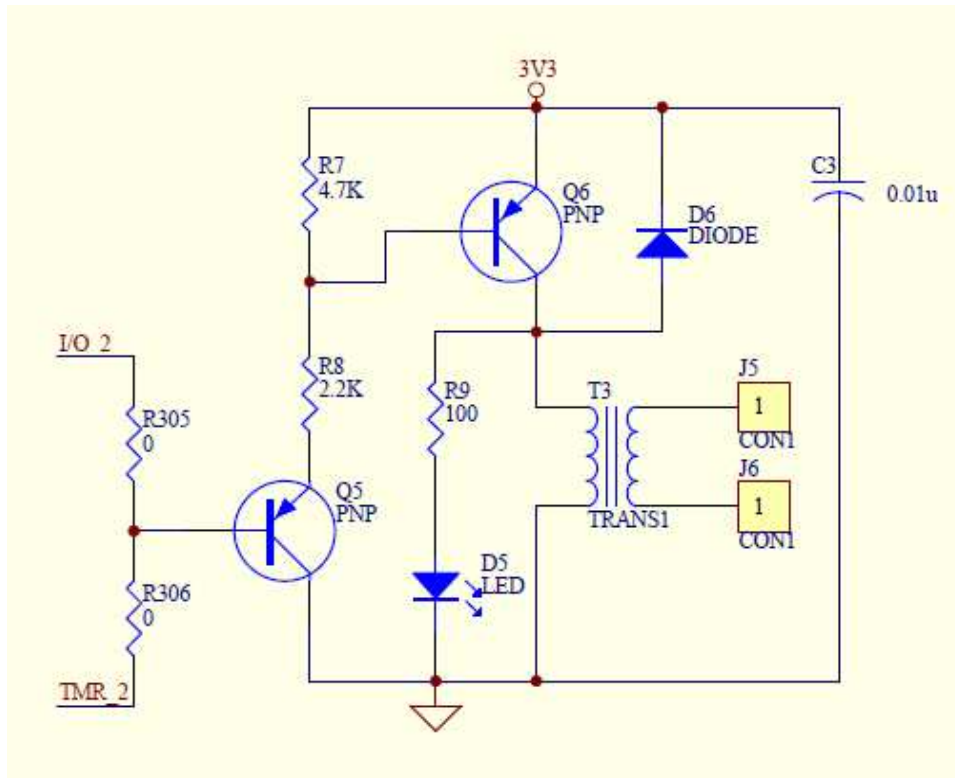


Fig. 3-19: The schematic circuit of Slave board

In every circuit of stimulator, there were two sources of pulse for user to select: Timer interface or GPIO interface. It was all depend on user's application. In our study, the GPIO interface was chosen. As soon as a drowsy state was detected by the DSP module, 150 μ Sec. pulses at about 80 Hz frequency would be generated and send to the Slave board via GPIO interface. Q1 acted as a buffer and Q2 inverted the polarity of the pulses and drove the Transformer. The amplitude of the output pulses was set by R1 and roughly displayed by the brightness of LED D1. D2 protected Q2 against high voltage peaks generated by T1 inductance during switching. The output signals would be generated by J1 and J2, which were directly connected to the electrodes. User only need taped the electrodes to the skin at both ends of the chosen muscle then the stimulator could be worked. The output voltage is about 60V positive and 150V negative but user is no need for fear of electric-shock danger, because the output current is so small and would be safe[72].

3.4 Hardware System Specification

A. Portable bio-signal acquisition system

Fig. 3-20 is the front-end analog circuit and digital control circuit of our portable bio-signal acquisition system. There are three leads in our portable bio-signal acquisition module for each channel, includes EEG or EOG input, reference, and virtual ground of the front-end analog circuit. The electrodes connected with the leads of virtual ground and EEG reference were placed on user's forehead and behind right ear respectively. On the other hand, the reference of EOG was placed below right eye. The specification of portable bio-signal acquisition system was listed in Table 3-2.

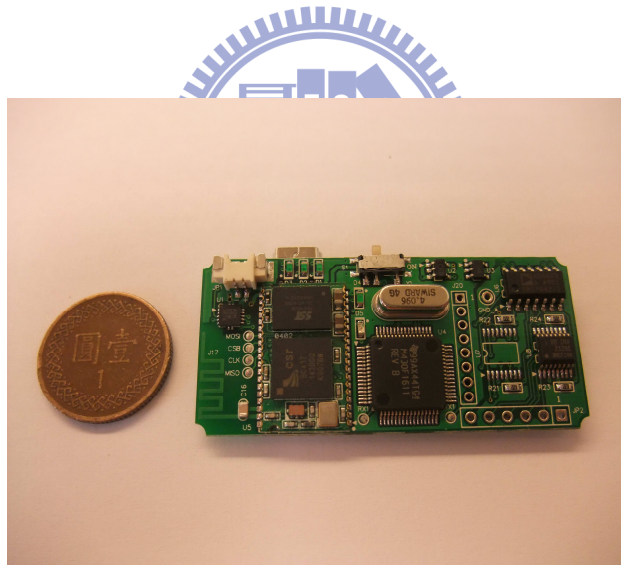


Fig. 3-20: The front-end analog and digital control circuit

Table 3-2: The spec of portable bio-signal acquisition system

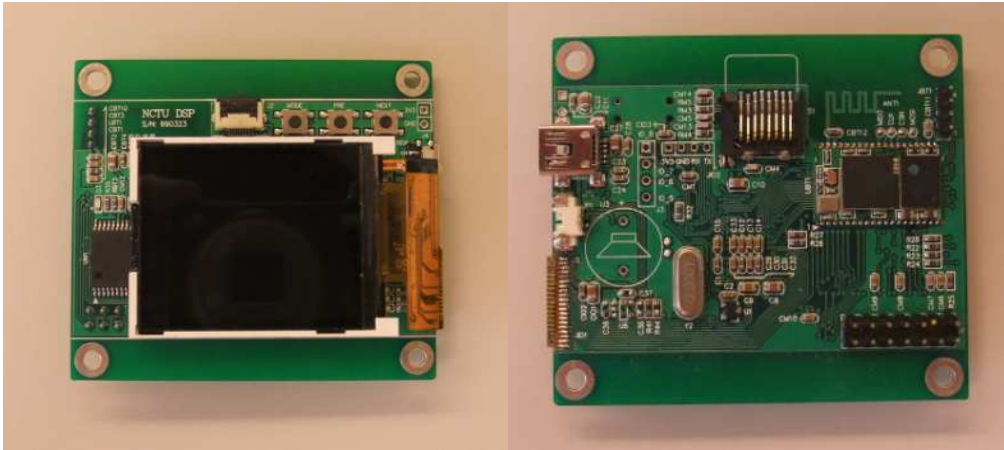
Type	Portable Bio-signal Acquisition System
Channel Number	1~4
System Output Voltage Range	0~3V
Gain	2000~5000
Bandwidth	0.1~100Hz
ADC Resolution	12bits
Output Current	29.5mA
Battery	Lithium 3.7V 450mAh 15~33hr
Full Scale Input Range	577 μ V
Sampling	256Hz
Input Impedance	greater than 10M Ω
Common Mode Rejection Ratio	77dB
Power Supply Rejection Ratio	88dB
Size	25mm x 54mm

B. DSP Module

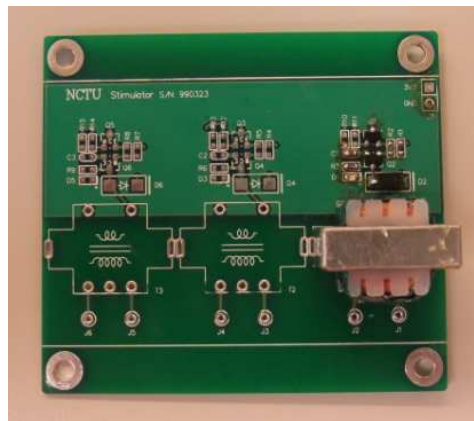
DSP module was divided into two parts: the master board and the slave board. The master board was shown in Fig. 3-21(a). CPU, SDRAM, buzzer and etc. were placed on the master board. Fig. 3-21(b) is the illustration of the slave board which included three circuits of stimulator. The specification of DSP module was listed in Table 3-3.

Table 3-3: The spec of DSP Module

Type	DSP Module
Chipset	ADI BF533
Speed (CLK)	600MHz (1200MAC)
SDRAM	16MB (Max 64MB)
Size	65mm x 45 mm
Storage	Micro SD
Transmission	BLUETOOTH
Display	TFT-LCD
Keypad	3
Battery	Lithium 3.7V 450mAh 15~33hr
Application(GPIO)	Buzzer, Bio-stimulator



(a)




(b)

Fig. 3-21: (a) Master board of DSP module (b) Slave board of DSP module

Chapter 4 Unsupervised Approach

Based on the unsupervised analysis flowchart in Fig. 2-10, we will further discuss the details of every analysis diagrams in the following sessions. In order to find out the real driving behavior information, first we calculate the driver's driving performance by using the record in simulation experiment. Moreover, we use the unsupervised analysis method to analyze the corresponding EEG and EOG information, including the preprocessing, alert model construction, blink duration, and computation of the deviation using Mahalanobis distance method.

4.1 Driving Performance



The VR-based four-lane straight highway scene was applied in the experiment. In this scene, the four lanes from left to right are separated by a median stripe and the distance from the left side to the right side of the road was equally divided into 256 points indicating the position of the vehicle as the digital output signal of the VR scene at each time instant. The width of each lane and the car is 60 units and 32 units, respectively. Fig. 2-5 shows an example of the driving performance represented by the vehicle deviation trajectories. VR driving simulation environment will randomly start a deviation event to move the car to right or left side in the car driving experiments. Subjects needs to sense those sudden movements and trying to make a reversely turn to back to the third lane. At one time, the VR environment also outputs the driving events inside the data of car trajectories, as deviation event start trigger, response onset trigger; and response offset trigger. Fig. 4-1 shows the example of deviation event.

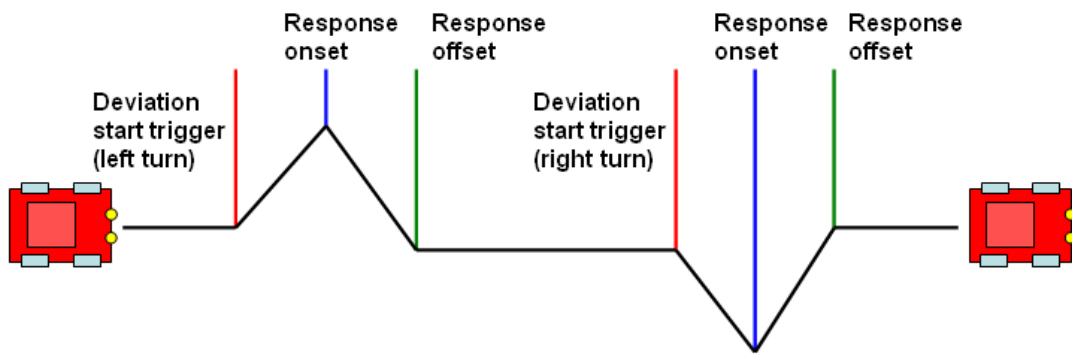


Fig. 4-1: The example of deviation event and car trajectories

Two parameters would be acquired from every deviation event called “reaction time” and “deviation”. In our study, deviation was not used because it could lead to an error. The road of our VR scene was divided into only 256 points and users need to keep the car on the third lane. For example, a user kept the car at the point 140 first, then a deviation event of right side triggered. If this user fall asleep at that time who might not able to make a reversely turn immediately and the car would just deviate to the boundary of the fourth lane: point 250. Suppose this user still not makes a reaction for the event, the numeric of deviation should become larger. However, owing to the limit of our VR scene, the results of deviation would be still at point 250 and can not be used. Simultaneously, reaction time was also computed by our system and not affected by the limitation of our VR scene: the longer user made no reaction, the longer “reaction time” would be, so it was used to validate our approach. The method of index is introduced as follow: reaction time of every event was acquired by computing the difference of “Response onset” and “Deviation start trigger” first, and then two successive reaction time of deviation event was compared at a time for observing the variation. Once the latter reaction time was larger than the former, we would use this result to compare with MDA, MDT, blink duration and implement in correlation analysis with the driver’s performance. We emphasize that this index is

used only to validate our approach, and it is not as an input to develop the model for the alert state of the subject.

4.2 Construction of the Alertness Model

In order to investigate the relationship between the measured EEG/EOG signals and subject's cognitive state, and to quantify the level of the subject's alertness in previous studies [65]-[67], we need to quantify the volunteer's drowsiness level in this experiment at first. When subjects fall drowsy, they often exhibit relative inattention to environments, eye closure, less mobility, failure to motor control and making decision. Hence, the vehicle deviation was defined as the subject's drowsiness index.

In our approach for every subject in every driving session a new model will be constructed. Consequently the inter-session variability between subjects is no more important; these are taken into account automatically. To develop the alert model we make a few mild but realistic assumptions as follows:

- (1) The subject is usually very alert immediately after he/she starts the driving session.
- (2) Subject's cognitive state can be characterized by the power spectrum of his/her EEG.
- (3) When the person is in alert state, it can be modeled reasonably well using a multivariate distribution of the power spectrum.
- (4) The alert model expresses well the EEG spectra when the subject remains alert or return to alert state from drowsiness.

One might argue that the subject may already be in a drowsy state when he/she begins driving. If that is really true, then that can be detected by checking the consistency between two alert models derived using data in two successive time intervals. In other words, we can check whether the two alert-models identified in two successive time intervals are statistically same or not. If the subject was already in a drowsy state, then he/she will either move to a deep drowsy/sleepy state or will transit to an alert state. In both cases, the two models will not be statistically consistent.

In our study, a multivariate distribution was used to model the distribution of power spectrum in the alert state. In particular, at every 0.125 second, we calculate the power spectrum vector in p dimension. In our experiment theta band is located in 16~31(4~7Hz), and alpha band is located in 32~48 (8~12Hz). In this way, a set of $n=480$ data vectors $\{\mathbf{x}_1, \dots, \mathbf{x}_{480}\}$ is generated in every minute. We use 3 minutes of spectral data to derive the alert model. The alert model is represented and characterized by a multivariate normal distribution $N(\boldsymbol{\mu}, \boldsymbol{\Sigma}^2)$, where $\boldsymbol{\mu}$ is the mean vector and $\boldsymbol{\Sigma}$ is the variance-covariance matrix.

We use the maximum likelihood estimates for $\boldsymbol{\mu}$ and $\boldsymbol{\Sigma}^2$. After finding the alert model we check whether the EEG spectrum in alpha band (also in theta band) indeed follows a multivariate normal using Mardia's test [68], [69]. If the model passes the Mardia's test, we accept that model as the alert model. Otherwise, we move the data window by one minute and again use the next 3 minutes of data to derive and validate the model using Mardia's test. Once a model is built, a significant deviation from the model can be taken as a departure from alertness. Note that, we are saying "departure from alertness" which is not necessarily drowsiness. For example, the subject could be excited over a continued conversation over a mobile phone. In this case, although the person is not drowsy, he/she is not alert as far as the driving task is concerned and

hence needs to be cautioned. Thus our approach is more useful than typical drowsiness detection systems. A consistent and significant deviation for some time can be taken as an indicator of drowsiness.

For the sake of completeness, we briefly explain the Mardia's test of multi-variate normality. Given a random sample, $X=\{\mathbf{x}_1, \dots, \mathbf{x}_n\}$ in \mathbb{R}^p , Mardia [68], [69] defined the p-variate skewness and kurtosis as:

$$b_{1,p} = \frac{1}{n^2} \sum_{i=1}^n \sum_{j=1}^n \{(\mathbf{x}_i - \bar{\mathbf{x}})' S^{-1} (\mathbf{x}_j - \bar{\mathbf{x}})\}^3 \quad (4-1)$$

$$b_{2,p} = \frac{1}{n} \sum_{i=1}^n \{(\mathbf{x}_i - \bar{\mathbf{x}})' S^{-1} (\mathbf{x}_i - \bar{\mathbf{x}})\}^2 \quad (4-2)$$

In (1) and (2) $\bar{\mathbf{x}}$ and S represent the sample mean vector and covariance matrix, respectively. In this case of university data, $b_{1,p}$ and $b_{2,p}$ reduces to the usual university measures skewness and kurtosis, respectively. If the sample is obtained from a multivariate normal distribution, then the limiting distribution of $b_{1,p}$ is a Chi-square with $p(p+1)(p+2)/6$ degrees of freedom, while that of $\sqrt{n} (b_{2,p} - p(p+2))/8\sqrt{p(p+2)}$ is $N(0,1)$. Hence we can use these statistics to test multi-variate normality. In all our experiments, we have used the routines available for Mardia's test in the R-package [70]. On the other hand, EOG was also processed. In contrast to the alert model of EEG, the EOG preprocessing was simpler. The blink duration was recorded at the first 3 minutes, and then all of this blink duration was averaged to be the baseline of the alert state. During the experiment, the blink duration might become longer or shorter than the baseline. We could increase the accuracy of blink detection by comparing the blink duration of alert state.

4.3 Computation of the Deviation from the Subject

After the alert model is found, we use it to assess the subject's cognitive state. This was done by finding how the subject's present state, as represented by the EEG power spectra, and was different from the state represented by the alert model. The deviation of the present state from the model is computed using Mahalanobis distance [71] that can account for the covariance between variables while computing the distance. Let the alert model computed using the alpha band be represented by $(\bar{\mathbf{x}}, S)_A$ and that by the theta band be represented by $(\bar{\mathbf{x}}, S)_T$. Let \mathbf{x} be a vector representing the power spectra in the alpha band (or in the theta band) of the EEG of the subject at some time instant, then the deviation of the present state from the model is:

$$MD^*(\mathbf{x}) = \sqrt{(\mathbf{x}-\bar{\mathbf{x}})^T S^{-1} (\mathbf{x}-\bar{\mathbf{x}})} \quad (4-3)$$

In (3) if we use the alpha band model, then * is A, and for the theta band model and data, * will be T. Thus the deviation from the alpha band model will be denoted by MDA and that for the theta band model will be denoted by MDT. Similar to the pre-processing of the indirect alertness level index (driving performance), the MDA/MDT is also smoothed by the moving average method using a window with a window of 20 seconds. The moving average window is shifted by just one value (i.e., 2 sec). For a better visual display, we have scaled the MD* values by subtracting the average MD* computed over the training data used for finding the alert model.

We shall see later that the deviation from the alpha band model (i.e., MDA) or the theta band model (i.e., MDT) can be used to detect departure from the alert cognitive state.

4.4 Computation of the Blink Duration from the Subject

In this section, computation of the duration of blinks is introduced. Vertical EOG was used in our study to acquire the parameters of EOG. In Fig.4-2, there is an idea blink and the differentiation of this blink called EOG velocity. We analyzed this EOG velocity and characterized the behaviour of vertical EOG[23]. To base on the blink model, closing time starts at the time “cs” and finishes at “ce”, and the opening time starts at the time “os” and stop at “oe”.

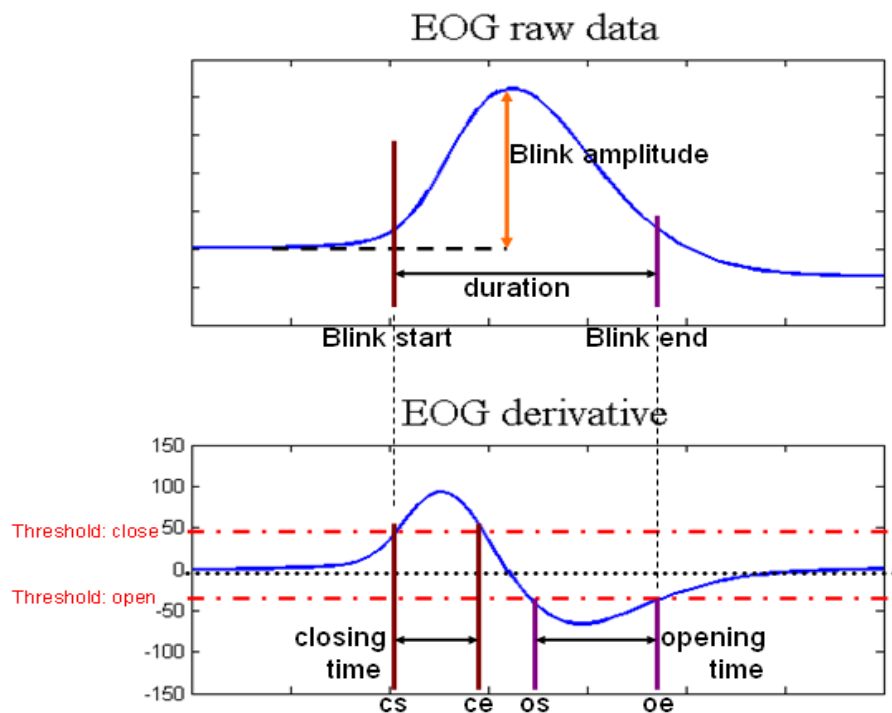


Fig. 4-2: Blink features

The values of closing and opening threshold were selected empirically because each driver's characteristics of EOG were different. Thus, EOG signals during many conditions(closed eyes, open eyes,etc) should be recorded before our experiment to ensure the accuracy. The computation consists of following basic steps[23],[26]:

- Step 1) Define the initial threshold parameters.
- Step 2) Filter out the frequencies above 10 Hz.
- Step 3) Compute the derivative(difference) of the filtered signal called EOG velocity.
- Step 4) Use closing and opening threshold to identify blinks. If the value of EOG velocity above closing threshold and which is followed by a value below opening threshold are identified as blinks.
- Step 5) Verify the satisfaction of some constraints, for example: duration must below the value of maximum duration, amplitude need to above the minimum amplitude and so on.

After these five steps, parameters of EOG could be acquired. In our study, closing time, opening time, duration and amplitude of blinks were all computed. However, correlation between driving performance and closing time was low. No matter user was drowsy or not, the value of closing time always kept at a constant. Amplitude of blinks would become small when user felt drowsy. In contrast with amplitude, opening time and duration would become larger as user turn from alert state into drowsy state. To simplify our study, blink duration which had highest correlation with driving performance was the only parameter selected to detect drowsiness.

This raises a natural question, can a combined use of MDA, MDC and duration do a better job than individual ones. To explore such a possibility we use a linear combination MDA, MDT and duration to compute a combined measure of deviation as:

$$\textit{Combination} = i \times \textit{MDT} + j \times \textit{MDA} + k \times \textit{Duration}$$

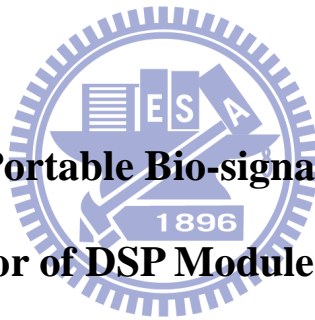
where $0 \leq i, j, k \leq 1$ and $i+j+k=1$. (4-4)



Chapter 5 Results and Discussion

In this chapter, it is separated into two parts including the performance of portable bio-signal acquisition system and the relationship between driving performance and unsupervised analysis. In the first segment, sine wave and alpha wave are used to test the performance correlation. In the next segment, we will discuss the unsupervised result by using correlation with driving performance, sorting analysis, and linear combination to find out the proportional relationship. Finally, we use the binary classification method to summarize the threshold from alertness to drowsiness, furthermore set the optimal threshold into the program of DSP module.

5.1 Performance of Portable Bio-signal Acquisition System and Bio-stimulator of DSP Module



In this section, the reliability of the proposed portable bio-signal acquisition system was examined. First, several sine waves with different frequencies generated by function generator were used as input signals to test whether the acquisition system can stably and validly acquire testing signals. Next, an arbitrary wave as EEG signal was generated by function generator, and the original arbitrary wave and the arbitrary wave recorded by our system were compared to test whether the characteristic of EEG signal was kept to ensure the reliability of our acquisition system. In addition, the effect of bio-stimulator was also examined in this section. When user became drowsy, bio-stimulation was generated without warning to make user alert and the corresponding EEG raw data was recorded simultaneously, and then these EEG data were analyzed to make sure if our bio-stimulator took effect on user.

A. Test for Sine Wave Signal

In this performance test, we tried to test the correlation between the sine-waves which were recorded actually by portable bio-signal acquisition system and the sin-waves which were generated by MATLAB function. The EEG signals which were recorded about 23 sec. The result between two conditions was shown in Fig. 5-1. And the correlation of total information could up to 0.9765.

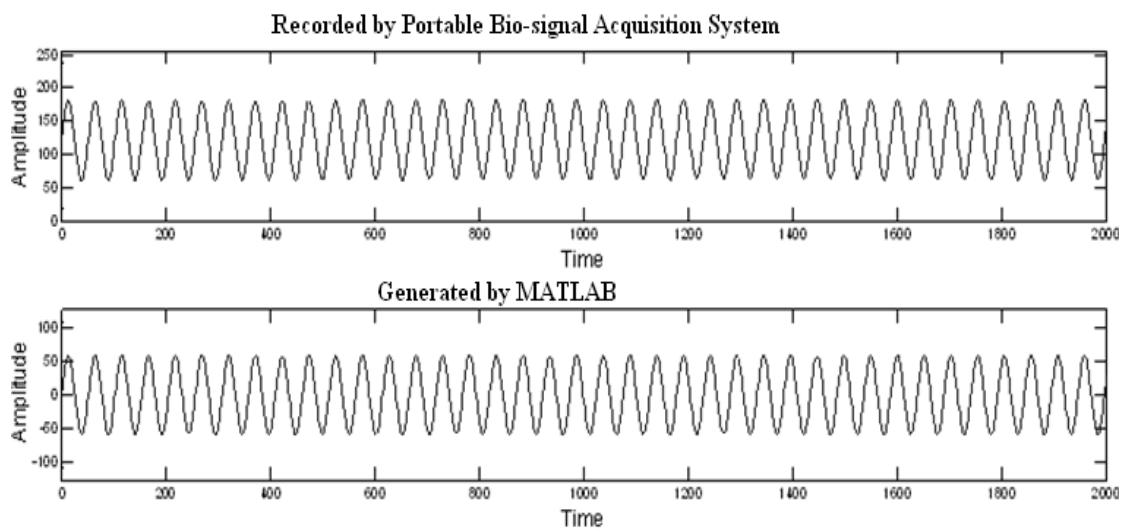


Fig. 5-1: The result between two conditions

B. Test for Arbitrary Wave Signal

An arbitrary wave as EEG signal was generated by using function generator. This arbitrary wave was scaled down 1000 times at first, then filtered and amplified by our system. After ADC processing, the processed digital signal would be transmitted to PC by Bluetooth and recorded by our program. To compare the original arbitrary wave and the signal recorded by our system, we could find out that recorded signal was smoother than the original and the amplitude was slightly smaller, but the characteristics of EEG were all kept by our system. Come to a conclusion, using moving average to remove noise of 60Hz might cause the recorded signal smoother. Besides, sampling rate of 256 points per second would reduce data volume and lead to

the decreased amplitude. The result of arbitrary wave test was shown in Fig. 5-2.

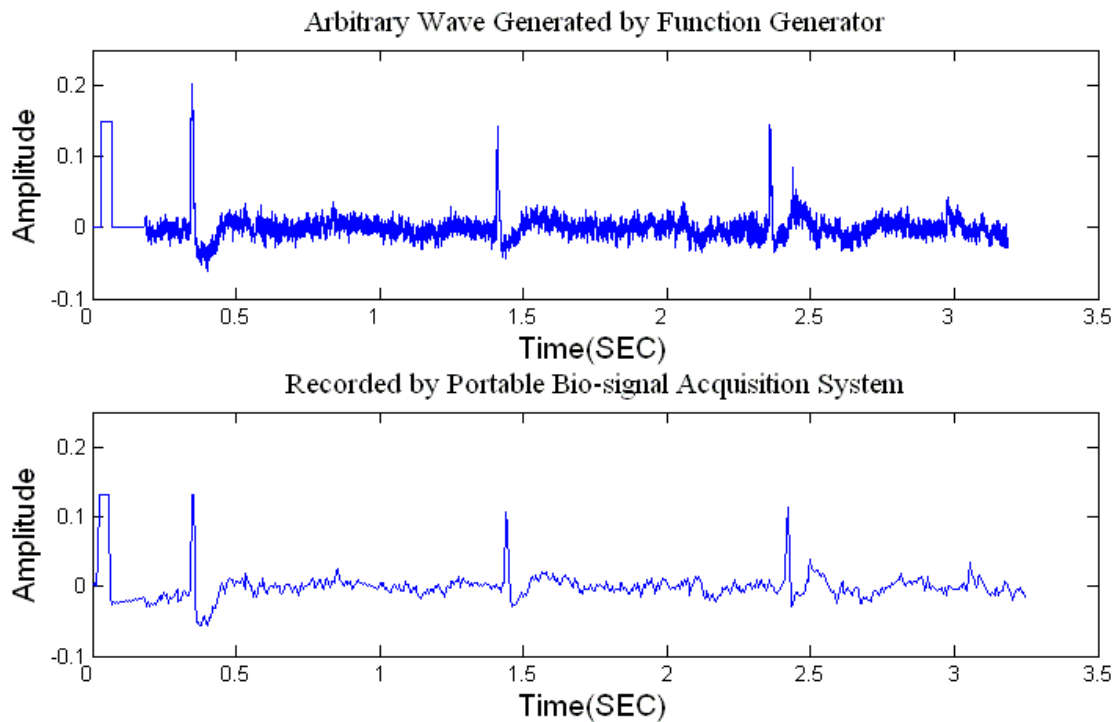


Fig. 5-2: The result of arbitrary wave test

C. Test for Bio-stimulator of DSP module

Bio-stimulation is one of bio-feedback mechanism of our DSP module. The utility of our bio-stimulator is to make mental state of user return alert and to avoid traffic accidents. To make sure the stimulus position of bio-stimulator can indeed take effect on user, traditional Chinese medical science was referenced in our study. Fengchi is in the posterior aspect of the neck, below the occipital bone and the depression of this point is like a well, when stimulating on this point can alleviate the tight muscle and refresh user. So, Fengchi was used as the stimulus position and it was shown in Fig. 5-3 [73].

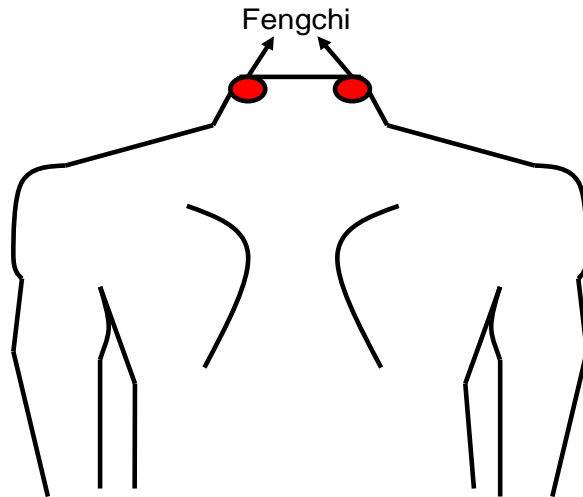


Fig. 5-3: The position of Fengchi

An experiment was designed that when user was driving the car of our virtual driving simulation environment, a pair of bio-stimulation electrodes were attached on Fengchi of neck. As soon as user became drowsy which defined in our study was reaction time of driving performance over 1 second, and then our bio-stimulator would switch on and generate bio-stimulation to alert user. The corresponding EEG raw data was recorded and analyzed to observe the difference between before, during and after bio-stimulation, and the result was shown in Fig. 5-4 and Fig. 5-5.

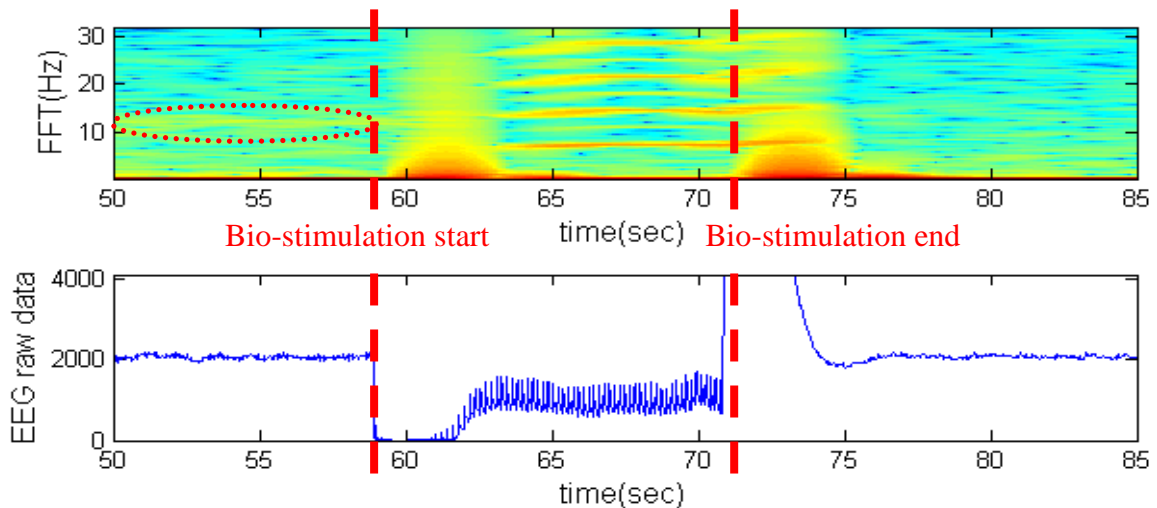


Fig. 5-4: Result of EEG raw data and corresponding frequency spectrum

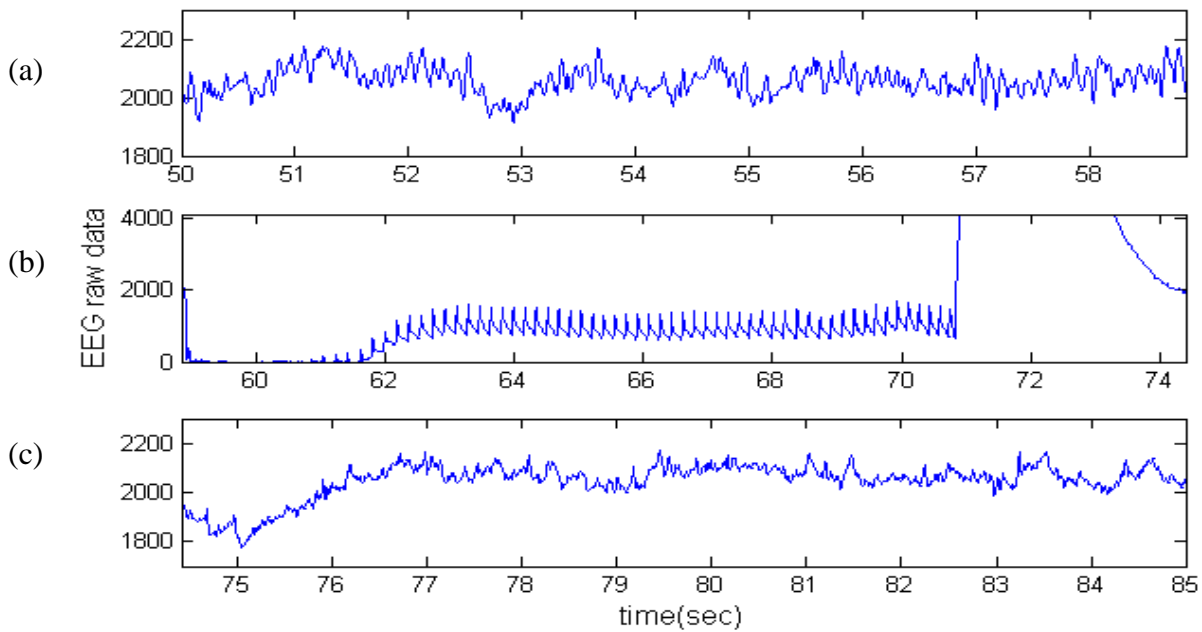


Fig. 5-5: Results of EEG raw data: (a) before bio-stimulation, (b) during bio-stimulation and (c) after bio-stimulation.

According to Fig. 5-4 and Fig. 5-5, EEG data in frequency domain showed that the main frequency of EEG was distributed among 8-12Hz (alpha-band) when user was in drowsy state (before second 59). As bio-stimulation was generated (second 59 through second 74) that the proportion of alpha-band was decreased and the main components of frequency domain were composed by the frequency of bio-stimulation. After stimulation was finished, frequency of alpha-band was significant reduced, and it means that user was become alert from drowsy state. On the other hand, observing EEG data in time domain that EEG data was mixed with stimulation signals during bio-stimulation generated and it proved that our bio-stimulator took effect on the user. Besides, as user was taking experiment, oral questioning was also implemented to ensure the mental state of user. Moreover, the result of oral questioning showed that when user was stimulated from drowsy state, the effect of bio-stimulator was significant and user became alert indeed. In conclusion, bio-stimulator can wake user up and keep user in alert state effectively.

5.2 Driving Performance and Unsupervised Analysis

In this section, we will show the results of algorithm in five parts. 1) Discussing the relationship between driving behavior information and unsupervised analysis in each event of deviation. 2) Separating the behavior trials hence find out the corresponding EEG and EOG data, then sorting both information check the connection between MDA, MDT, blink duration and the reaction time of driving performance. 3) Using linear combination of PPV and sensitivity to find out the optimized threshold of “Combination”(i × MDT + j × MDA + k × Duration) and check the maximum value of f-measure between these three information. 4) Applying this optimized threshold to 10 trials of experiment to ensure the usability of our algorithm. 5) In our study, the importance of blink duration is emphasized. So we use only two parameters of EEG (MDT, MDA) doing the same process to find out the optimized threshold and check the maximum value of f-measure between only MDT and MDA. Then we will accord the results of these two conditions (within and without parameter of blink duration) to compare and discuss. Finally, the result of comparison will be shown in the last part of this section.

5.2.1 Results of Unsupervised Analysis

Following the steps of preprocessing and the unsupervised analysis in above chapters, we used OZ channel which has the highest average correlation in 10-20 system [56] to record EEG signal. On the other hand, we used vertical EOG which has the largest amplitude of different kinds EOG measurements to make the parameters acquired more precisely. Then, we constructed $(\bar{\mathbf{x}}, S)_T$ and $(\bar{\mathbf{x}}, S)_A$ in the alert model that $\bar{\mathbf{x}}$ and S are mean vector and covariance matrix. Moreover, according to the results of FFT counted the MDT and MDA out. Besides, blink

duration was also extracted from the results of EOG velocity to be one of the parameter of drowsy detection.

There were four examples to show the results of reaction time, MDT, MDA and blink duration, as Fig. 5-6 through Fig. 5-9.

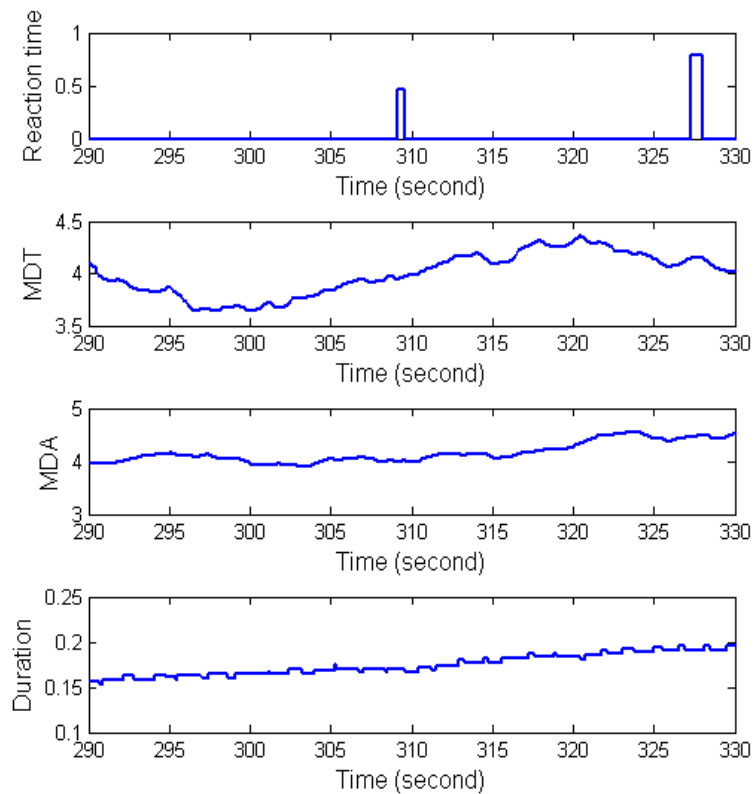


Fig. 5-6: Example 1 of driving performance and unsupervised analysis

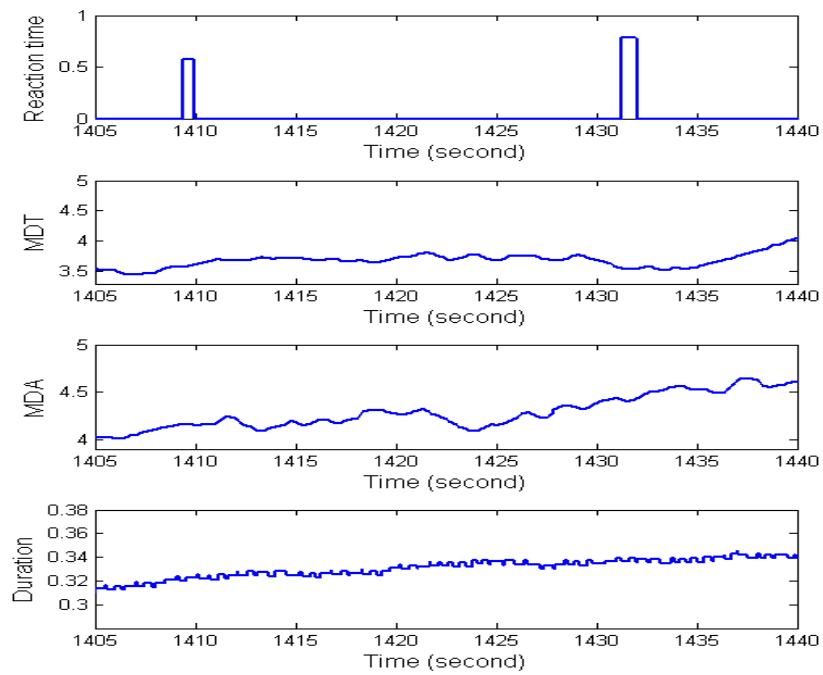


Fig. 5-7: Example 2 of driving performance and unsupervised analysis

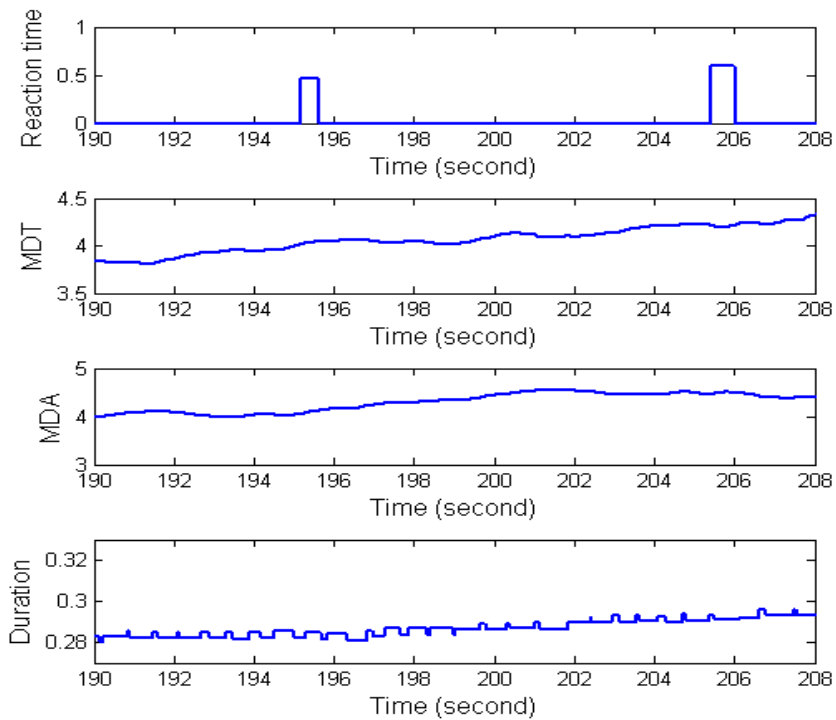


Fig. 5-8: Example 3 of driving performance and unsupervised analysis

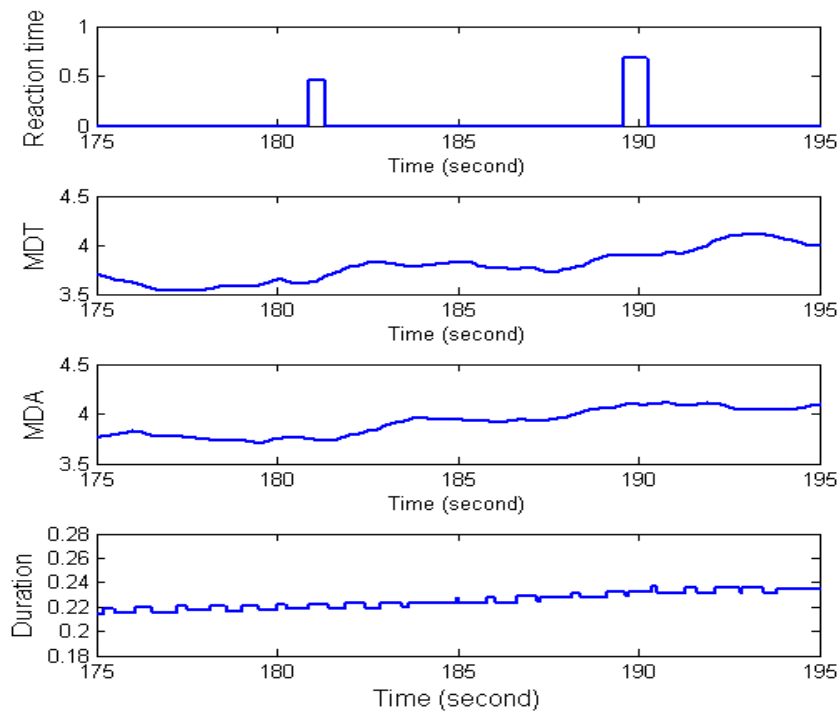


Fig. 5-9: Example 4 of driving performance and unsupervised analysis

From above four cases of unsupervised analysis, we could directly find out the relationship between unsupervised analyses and driving performance. When the latter value of reaction time was larger than the former it meant that user was become drowsy. Comparing to the variation of MDT, MDA and blink duration, these three parameters were all become larger as the value of reaction time was rising. According to those experimental results, we could asseverate that EEG and EOG signals would be influenced by behavior information when subjects become drowsiness.

5.2.2 Relationship between Driving Performance and Unsupervised Analysis

In reference (N. R. Pal, 2008 [45]) said, they investigated the relationship between the driver's performance and the concurrent changes in the EEG spectrum, and go on, they had sorted the EEG power spectra in alpha band by smoothed driving performance. The similar sorting was also done for power in the theta band. The result which they discovered was that theta and alpha spectrum were directly proportional to the deviation length of driving performance. Besides, in reference (P. P. Caffier, 2003 [23]) said, level of drowsiness had divided to four stages (Q1 - Q4) where Q1 meant most drowsy comparing to Q4 meant most alert. They computed across all measurements of the 60 participants and sorted the blink duration according to level of drowsiness. The results showed that blink duration was proportional to the level of drowsiness. The more drowsiness of the participant (Q1) the more large value of blink duration was.

Since the driving performance is an indirect index of the alertness level, we propose the sorted analysis method that sorts the smoothed log power spectra MD* and blink duration according to the driving performance index to assess the brain dynamics and blink variation corresponding to the transition from alertness to drowsiness in driving. This process is used to observe the features change as the increase of driving performance index.

This analysis flow is to separate total trials from the driving events. In our analysis, we assumed that the driving deviation and drowsiness state were direct proportional, so we decided to use the reaction time of driving deviation to be the information of driving performance analysis. Every trial would find out the corresponding EEG and EOG raw data. Hence, according to the alertness model in

first 3 minutes, the frequency domain spectrum under the deviation can be changed out by FFT, and continually, the MD* power can be transformed. The blink duration was also computed at the same time. Further, the trials are sorted following the length of reaction time, and the synchronized MD* power spectra and blink duration also be sorted together. In our study, 6-second EOG data before “Response onset” was extracted and averaged to increase the accuracy of synchronized duration. The width of road was divided into 256 points, and speed of car drifting after deviation onset was 64 points/sec; in other words, the car would drift 1/4 width of road and crash into the second lane or fourth lane in one second. After trials sorting, according to above theory, we can separate the sorting data into 4 segments: state 1(0.2~0.56s), state 2 (0.56~0.75s), state 3(0.75~0.94s), and state 4(over 0.94s). Then, the mean and standard deviation in every segment which we counted shows the relationship between driving performance and drowsiness state. The process of sorting analysis is shown as Fig. 5-10.

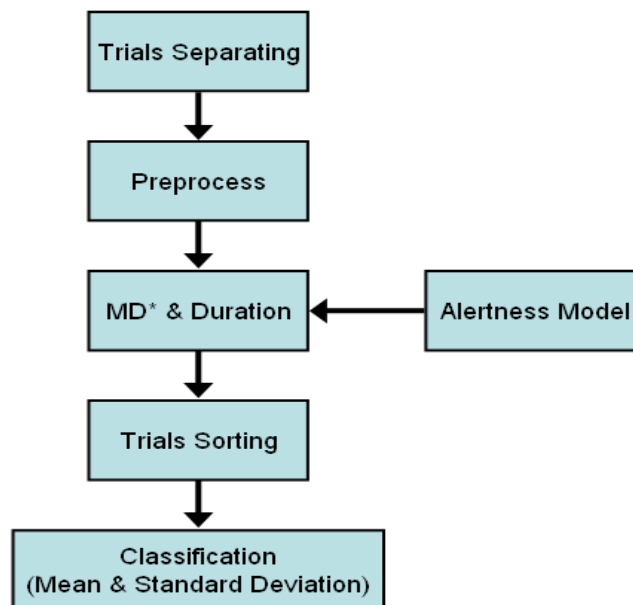


Fig. 5-10: Process of sorting analysis

Next, we checked how strongly MDA, MDT and duration were correlated with the driving performance. Fig. 5-11(a) showed the correlation between driving performance and MDA (across the 10 test subjects/sessions) while Fig. 5-11(b) and Fig. 5-11 (c) exhibited the same for MDT and blink duration. It was interesting to find out that Fig. 5-11 and the above theory exhibit almost the same behavior. In fact, the average MDA, MDT and blink duration increased more steadily with driving performance and proved that there was high correlation between these three parameters with driving performance.

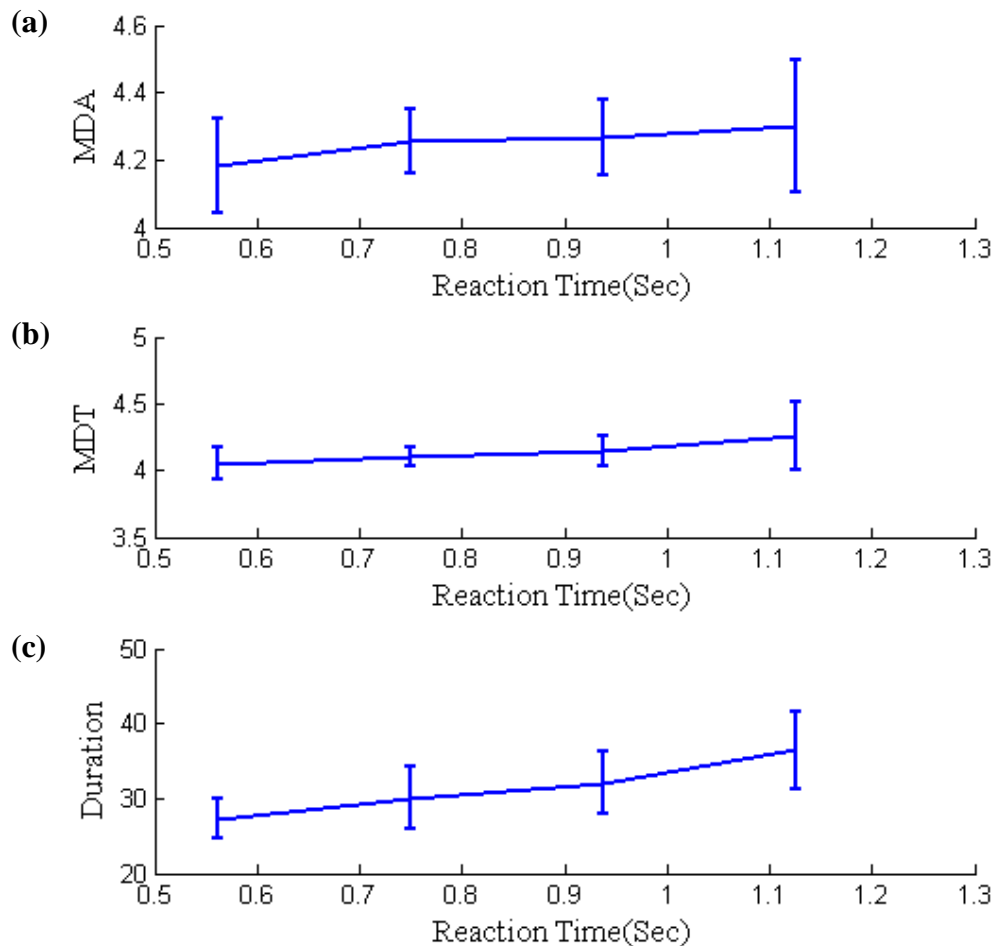


Fig. 5-11: The relationship between MDA/ MDT/ Duration and reaction time

5.2.3 Threshold Definition and Drowsiness Classification

In drowsiness classification, the true-false table is used to define sensitivity and specificity. Sensitivity and specificity are statistical measures of the performance of a binary classification test. The sensitivity measures the proportion of actual positives which are correctly identified as such (e.g. the percentage of drowsy people who are identified as having the condition); and the specificity measures the proportion of negatives which are correctly identified (e.g. the percentage of alert people who are identified as not having the condition). The relationship between sensitivity and specificity was shown in Fig. 5-12 and the description of binary classification test was in Table 5-1.

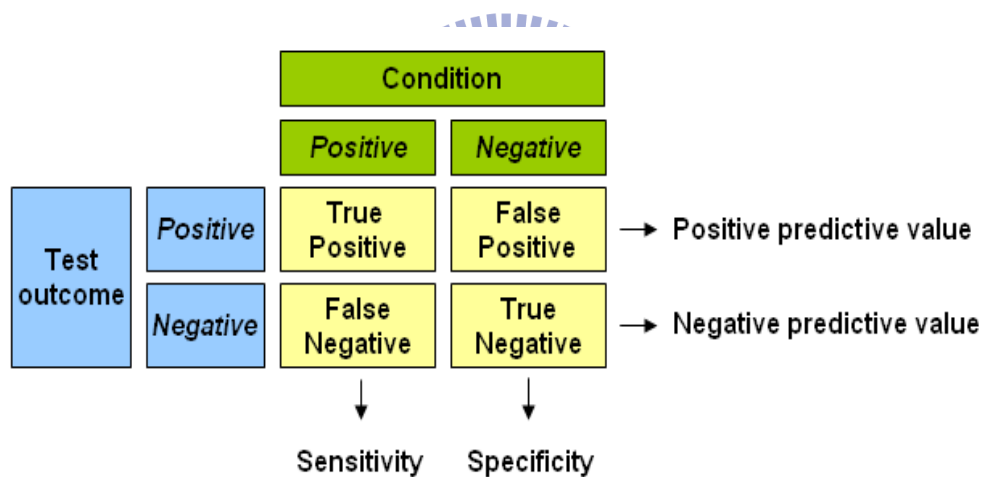


Fig. 5-12: The relationship between sensitivity and specificity

Table 5-1: The description of binary classification test

Type	Description
True positive	Drowsy people correctly diagnosed as drowsy
False positive	Alert people wrongly identified as drowsy
True negative	Alert people correctly identified as alert
False negative	Drowsy Sick people wrongly identified as alert

To define the drowsy state between driving performance with MD*/duration, we need to collect the parameters of true positive, false positive, and false negative, hence to analyze the sensitivity and positive predictive value.

A. Positive Predictive Value:

$$PPV = \frac{\text{number of True Positives}}{\text{number of True Positives} + \text{number of False Positives}} \quad (5-1)$$

The positive predictive value, or precision rate, or post-test probability of disease, is the proportion of patients with positive test results who are correctly diagnosed. It is the most important measure of a diagnostic method as it reflects the probability that a positive test reflects the underlying condition being tested for. Its value does however depend on the prevalence of the disease, which may vary.

B. Sensitivity:

$$\text{Sensitivity} = \frac{\text{number of True Positives}}{\text{number of True Positives} + \text{number of False Negatives}} \quad (5-2)$$

A sensitivity of 100% means that the test recognizes all drowsy people as drowsy. Thus in a high sensitivity test, a negative result is used to rule out the disease. Sensitivity alone does not tell us how well the test predicts other classes (that is, about the negative cases). In the binary classification, as illustrated above, this is the corresponding specificity test, or equivalently, the sensitivity for the other classes. However, sensitivity is not the same as the positive predictive value (ratio of true positives to combined true and false positives), which is as much a statement about the proportion of actual positives in the population being tested as it is about the test.

The calculation of sensitivity does not take into account indeterminate test results. If a test cannot be repeated, the options are to exclude indeterminate samples from analysis (but the number of exclusions should be stated when quoting sensitivity), or,

alternatively, indeterminate samples can be treated as false negatives (which gives the worst-case value for sensitivity and may therefore underestimate it).

After explaining the definitions of sensitivity and positive predictive value, then we can find out the optimized threshold of “Combination” step by step. First, because the results of MD* and blink duration had been normalized, it’s beneficial for us to collect all 10 subjects’ MD* and blink duration data to analyze. Second, we have to define the threshold of driving performance by taking the entire deviation events into account. The threshold of driving performance can be separated into 2 parts: alert and drowsiness. Further, we assume that deviation time is smaller than 1 second to be alert, and others are drowsiness. So the threshold of driving performance is defined as 1s. According to the value of threshold, all events can be separated to two conditions: drowsy and alert. Because we need to find out the optimized threshold of “Combination”, we use different kind conditions of linear combination and set the threshold of “Combination” from 20 through 40 respectively to calculate the corresponding PPV and sensitivity. In linear combination, according to these three conditions below:

$$1. \text{Combination} = i \times \text{MDT} + j \times \text{MDA} + k \times \text{Duration}$$

$$2. i + j + k = 1$$

$$3. 0 \leq i, j, k \leq 1$$

We calculated all kinds of combinations by i, j, k set as 0, 0.1, 0.2...0.8, 0.9, 1.

For example: $0.3 \times \text{MDT} + 0.3 \times \text{MDA} + 0.4 \times \text{Duration}$ and so on. Following these different combinations then PPV and sensitivity in different threshold of “Combination” could be acquired. There are too many kinds of combinations, so we

only showed 12 significant conditions in Fig. 5-13 and Fig. 5-14, we will explain these conditions later.

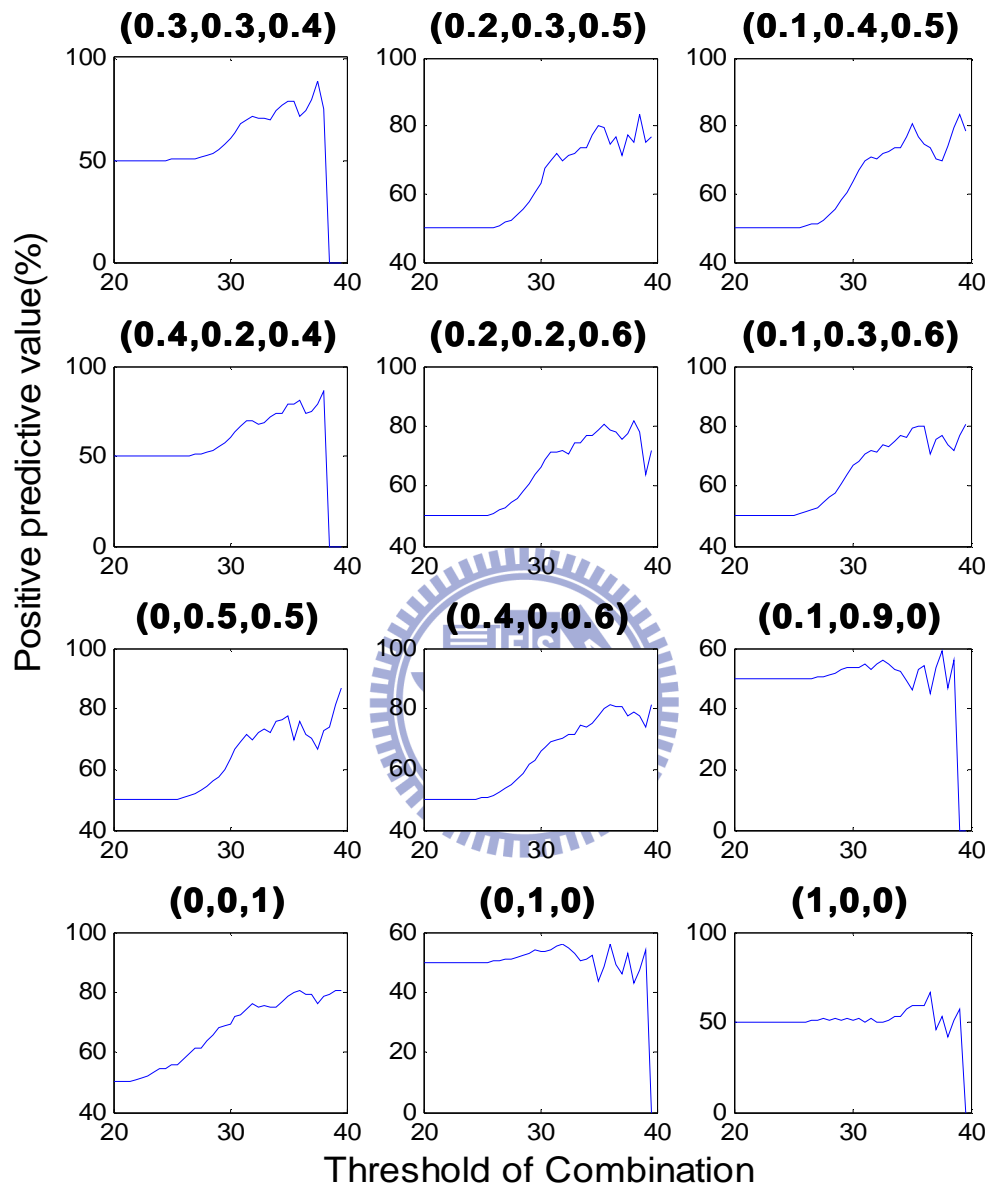


Fig. 5-13: Positive predictive value vs. threshold of “Combination” where the numeric in parentheses was sequentially expressed as (MDT, MDA, Duration)

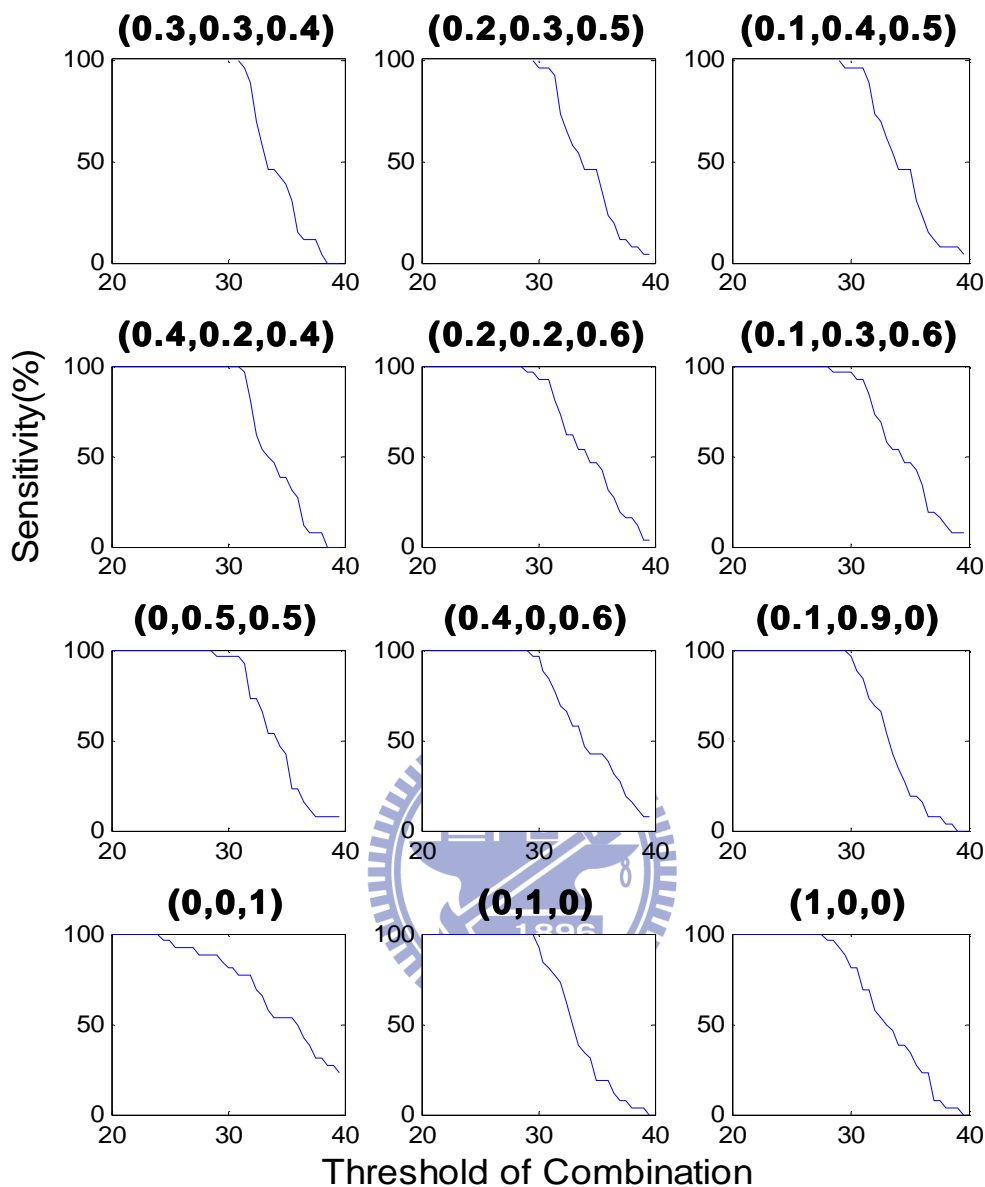


Fig. 5-14: Sensitivity vs. threshold of “Combination” where the numeric in parentheses was sequentially expressed as (MDT, MDA, Duration)

After calculating positive predictive value and sensitivity in different conditions of linear combination, we need to choose the optimized threshold of “Combination”. According to equation 5-3, the F-measure can be used as a single measure of performance of the test. In information retrieval positive predictive value is called precision, and sensitivity is called recall. The F-measure is the harmonic mean of precision and recall:

$$F - measure = 2 \times \frac{precision \times recall}{precision + recall} \quad (5-3)$$

The percent of F-measure means the ratio of drowsy accuracy actually. Both parameters are associated with drowsiness. In different linear combinational conditions, we could find out the maximum value of F-measure is in condition “i=0.3, j=0.3, k=0.4”. Come to a conclusion, the best linear combination of the “Combination” is composed of 0.3×MDT, 0.3×MDA and 0.4× Duration. The maximum value of F-measure, 80.91%, happened in the most suitable threshold of “Combination”, 31.5. Besides, the corresponding sensitivity is 96.15% and positive predictive value is 69.84%. There are too many conditions, so we only select 12 significant conditions listed in our study. The first 6 conditions are all composed of MDT, MDA and duration, and these conditions have higher value of f-measure between all of conditions. The next 3 conditions are only composed of two parameters and have the highest f-measure in each condition (MDA + duration, MDT + duration and MDT + MDA). The last 3 conditions are composed by only one parameter, and also have the highest f-measure in each condition. The results of different kind conditions of F-measure are shown as Fig. 5-15 and the results of binary classification test are listed in Table 5-2.

The reason of which F-measure was not high enough was described into 2 critical points:

1. We found out the relation between driving performance and MD*/duration, hence driving performance and MD*/duration were a sufficient condition but not a necessary condition. When MD*/duration value was high, the corresponding driving performance wasn't high too. There were other variables appending to user's EEG and EOG signals.

2. When subjects became drowsy, the MD* would increase, but would not happen immediately. This phenomenon which based on time domain appeared step by step. So we used trials of driving trajectories to analyze drowsiness was not sufficient to know the exact information of EEG.

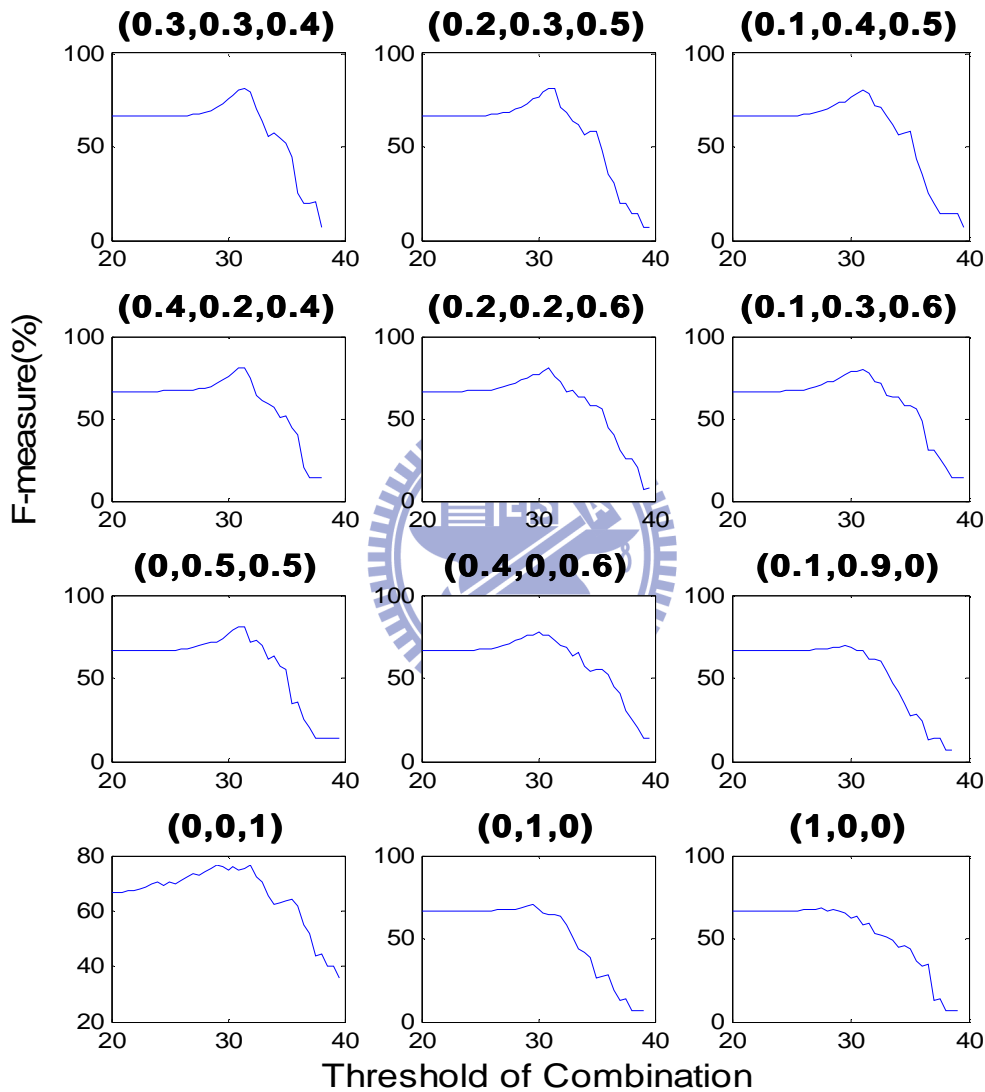


Fig. 5-15: F-measure vs. threshold of “Combination” where the numeric in parentheses was sequentially expressed as (MDT, MDA, Duration)

Table 5-2: The results of binary classification test

Combination (i, j, k)	Max F-measure (%)	Corresponding threshold	PPV (%)	Sensitivity (%)
(0.3, 0.3, 0.4)	80.91	31.5	69.84	96.15
(0.2, 0.3, 0.5)	80.87	31.5	71.96	92.31
(0.1, 0.4, 0.5)	80.67	31	69.48	96.15
(0.4, 0.2, 0.4)	80.59	31.5	69.36	96.15
(0.2, 0.2, 0.6)	80.22	31	70.93	92.31
(0.1, 0.3, 0.6)	80.18	31	70.87	92.31
(0.0, 0.5, 0.5)	80.55	31	69.31	96.15
(0.4, 0.0, 0.6)	78.34	30	66.10	96.15
(0.1, 0.9, 0.0)	69.54	29.5	53.31	100
(0.0, 0.0, 1.0)	76.88	29	67.99	88.46
(0.0, 1.0, 0.0)	70.11	29.5	70.11	100
(1.0, 0.0, 0.0)	68.22	27.5	68.22	100

$$\text{Combination} = i \times \text{MDT} + j \times \text{MDA} + k \times \text{Duration}$$

5.2.4 Test and Verify the Optimized Threshold

After the maximum result of f-measure is calculated, we have to validate if this linear combination and its corresponding threshold could actually work on all of the users. So we used the combination of highest value of f-measure (0.3, 0.3, 0.4) and its corresponding threshold: 31.5 to compute PPV, sensitivity and max f-measure of each subject. These 10 subjects' results of validation were listed on Table 5-3. To check the results of validation, we could find out the max f-measure of subject 5 was only 48.21. It may be caused by this subject's behavior of experiment. To review this subject's events of driving performance, it showed that one of the events determined as drowsy state, the corresponding MDT and MDA were higher than alert state. However, the corresponding blink duration was not increased when reaction time was become larger. We supposed that this subject might closed his eyes for a while as he felt drowsy, and result in the blink duration could not be computed correctly by our algorithm. Nevertheless, the average of max f-measure of other 9 subjects was 83.9%,

it meant that the optimized threshold and corresponding linear combination was useful for most users.

Table 5-3: 10 subjects' results of validation with MDT=0.3, MDA=0.3, Duration=0.4 and threshold set as 31.5

Subjects	Max F-measure (%)	PPV (%)	Sensitivity (%)
S1	87.96	78.50	100
S2	89.17	80.46	100
S3	95.73	91.82	100
S4	88.79	79.83	100
S5	48.21	46.54	50
S6	82.93	70.83	100
S7	79.23	65.60	100
S8	79.40	65.83	100
S9	71.26	55.36	100
S10	80.63	67.54	100

5.2.5 Comparison between MDT/MDA Only and with Blink Duration

In our study, one thing must be emphasized is that we not only used EEG signals as our parameters to detect drowsiness but also used EOG signals to increase the accuracy of our detection. To prove that linear combination with parameter of EOG signals was better than EEG signals only; we did the same process as unsupervised analysis mentioned before but calculated linear combination with only MDT and MTA.

$$MDC = a \times MDA + (1 - a) \times MDT, 0 \leq a \leq 1 \quad (5-4)$$

According to equation 5-4, the threshold of MDC was set from 20 ~ 40 respectively. In linear combination, we tried to separate into 9 conditions: a = 0.1, 0.2 ... 0.8, 0.9. Following these different conditions then sensitivity, positive predict value and corresponding max f-measure could be computed in different threshold

with only MDT and MDA. The results of binary classification test with only MDT and MDA were listed on Table 5-4.

Table 5-4: The results of binary classification test with only MDT and MDA

Types	Max F-measure (%)	Corresponding threshold	PPV (%)	Sensitivity (%)
MDC (a = 0.1)	68.30	28	51.87	100
MDC (a = 0.2)	68.33	28.5	51.89	100
MDC (a = 0.3)	68.63	29	52.24	100
MDC (a = 0.4)	68.88	29.5	52.53	100
MDC (a = 0.5)	68.84	29.5	52.49	100
MDC (a = 0.6)	68.85	29.5	52.50	100
MDC (a = 0.7)	69.01	29.5	52.69	100
MDC (a = 0.8)	69.29	29.5	53.01	100
MDC (a = 0.9)	69.54	29.5	53.31	100

The highest f-measure of MDC was 69.54% from all of combinations, and we can find out in Table 5-2 that the highest f-measure by using EEG and EOG signals was 80.91% higher than all of the max f-measure of MDC. We calculated the average max f-measure of all 9 conditions by using only MDT and MDA. Besides, the average max f-measure of 9 conditions by using three parameters was also calculated that these 9 conditions were the top nine combinations with higher value of f-measure. The result of comparison was shown in Fig. 5-16. It proved that drowsiness detection by using MDT, MDA and blink duration was better than only using MDT and MDA. According to the results, we can assert that blink duration has high correlation with driving performance and it is an important index to confirm user is drowsy or not.

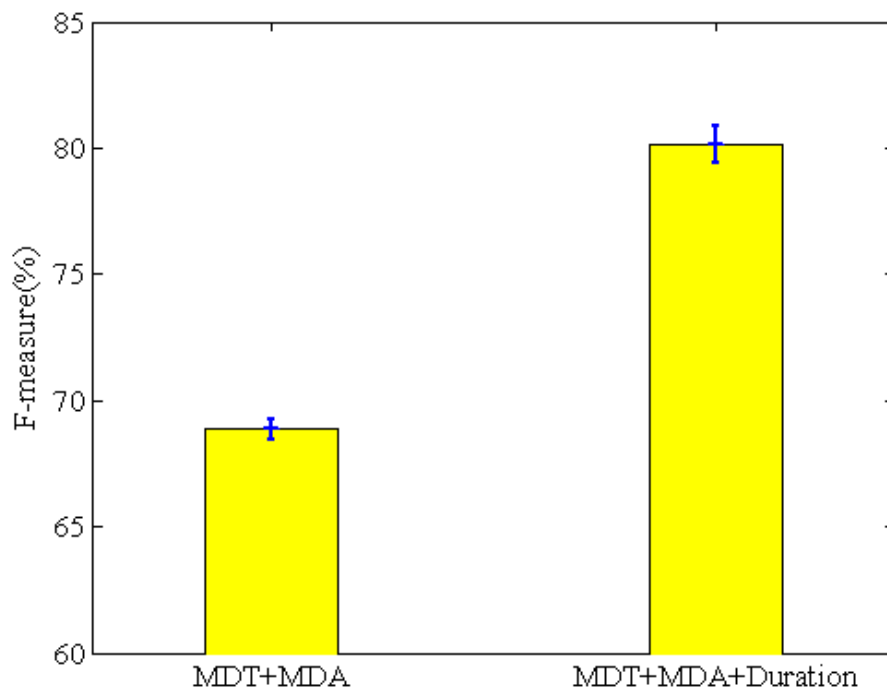


Fig. 5-16: The result of comparison between MDT/MDA only and with blink duration

5.2.6 DSP Module Programming

The flowchart of DSP module was shown in Fig. 5-17. In program development, we used multithread to build up a real-time analysis system, moreover to increase program's flexibility and the use of performance.

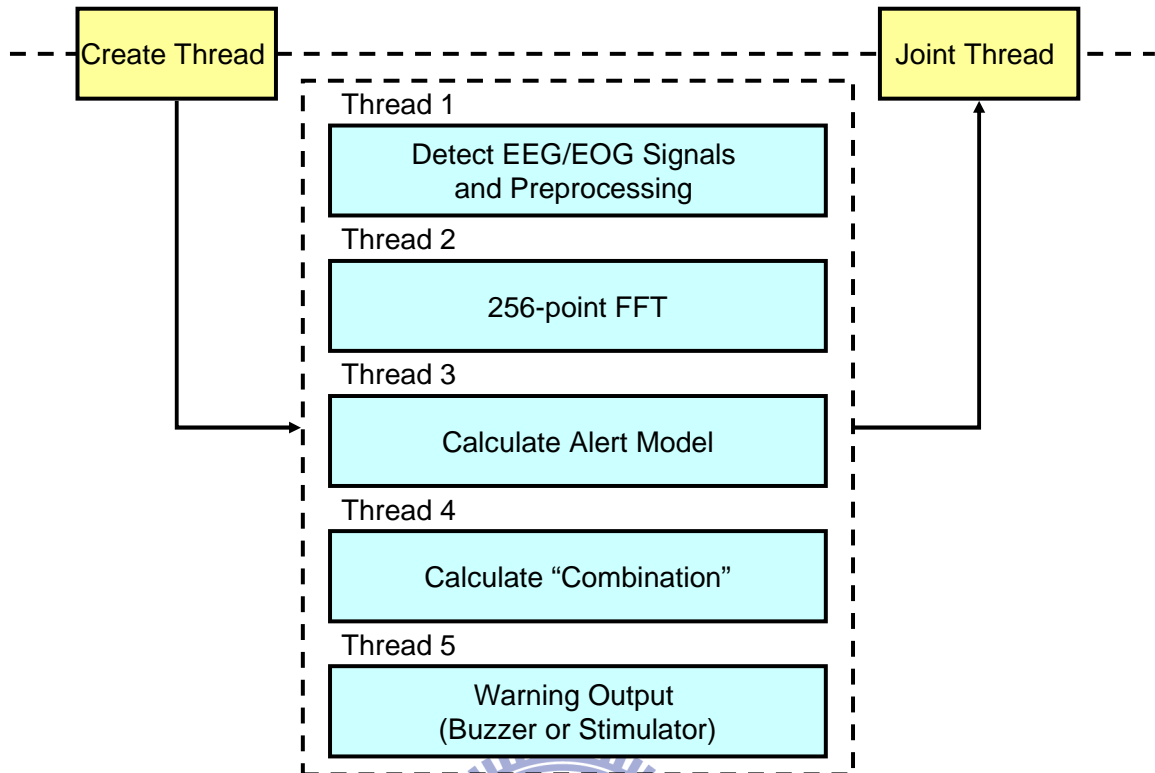


Fig. 5-17: The flowchart of DSP module program

Each thread is independent. In the DSP module's main loop, we just create the threads which we want and join them. The system kernel will automatically schedule those threads and decrease the system waiting cost. In thread 1, Real-time detect EEG/EOG raw data from Blue Tooth, and go on pass through two moving averages that one of them cut-off at 32Hz for EEG signal and another one cut-off at 10Hz for EOG signal, further down sample to 128 point in 1 second. Thread 2 handles FFT process. The FFT result will be transmit into 3 minute array in alert model. When array is full, the theta and alpha's mean vector and covariance matrix will computed in thread 3. Besides, average of user's blink duration at the first 3 minute is also computed to be the baseline in thread 3. Thread 4 mainly handles the MDT, MDA and blink duration converter, and then based on above optimal conclusion to calculate the "Combination" (0.3, 0.3, 0.4). If the values of "Combination" are higher than threshold in 31.5, the thread 5 will be switch on and make some warning voice or

generate stimulation in thread 5.

On the other hand, the program's user interface could directly tell user how was his / her physiological conditions. Further, let users easy handle this system. The user interface's flowchart was shown in Fig. 5-18. Following this flowchart, when the boot loader setup, the real-time drowsy detection program will be automatically started by DSP module. If user finished dress the portable bio-signal acquisition system over, he / she push the start button to start to detect real-time EEG and EOG raw data. Then the screen could print the real-time data. Furthermore, according to the mean vector, covariance matrix and baseline of EOG of our alert model, the linear combination of MDT, MDA and blink duration was counted continually, and the result value would also print on the screen's bottom side. Following Fig. 5-19 showed, the update time of screen we set was changed in every 1 second, so we could show total 1 second EEG/EOG raw data and result of "Combination" at the same time on the TFT-LCD. If a drowsiness state is detected by our system, a GPIO command from DSP module would be triggered to ring the buzzer or generate a bio-stimulation. In the other hand, user could push the quit button to end this program.

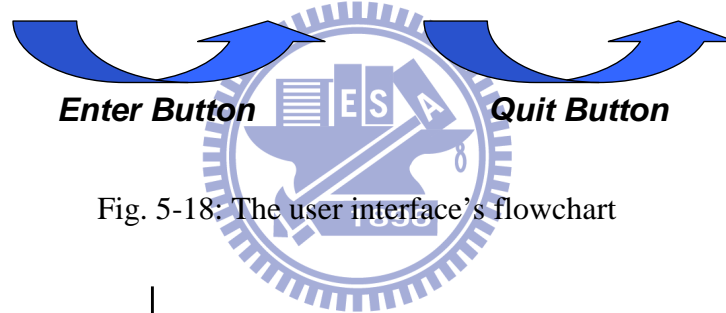
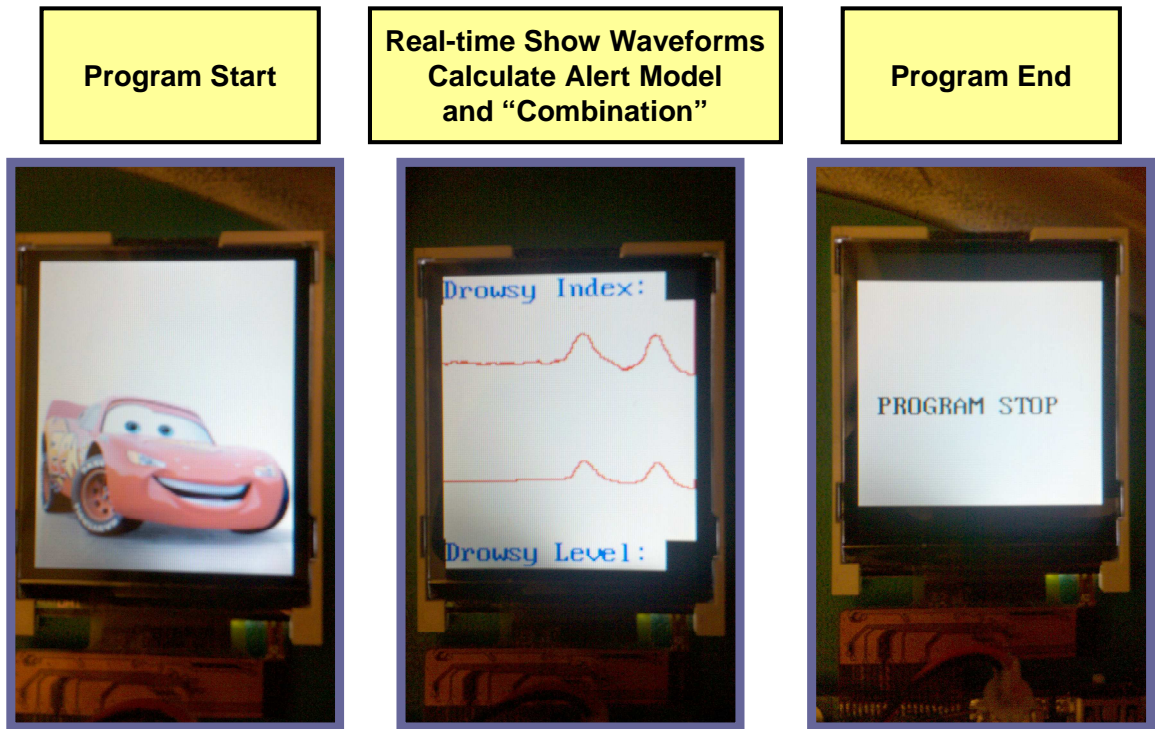


Fig. 5-18: The user interface's flowchart

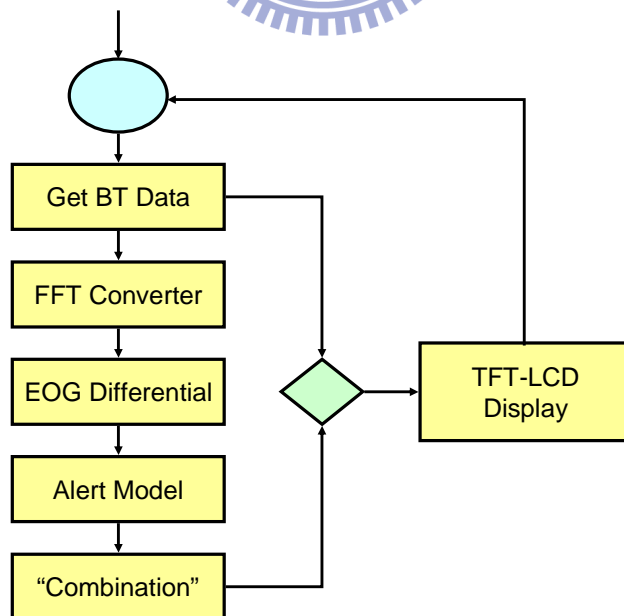


Fig. 5-19: The block diagram of dataflow

Chapter 6 Conclusions and Future Works

6.1 Conclusions

In our study, a real-time wireless system for drowsiness detection with bio-signal was proposed. A portable wireless bio-signal acquisition system and a DSP module with bio-feedback as buzzer or bio-stimulator were developed. Besides, we emphasized that not only EEG signal but also EOG signal used in our study to enhance the accuracy of drowsiness detection.

The portable wireless bio-signal acquisition system was designed to acquire EEG and EOG signals then transmit them into the DSP module wirelessly to detect drowsiness. In addition, our DSP module was equipped with bio-feedback device as buzzer or bio-stimulator for warning users that they were in drowsy state and waked them up. The modular approach applied in hardware and software design enables this system to be configurable for different application scenarios. Moreover, our bio-signal acquisition system is wearable, wireless and real-time, therefore, it is suitable for long-term bio-signal monitoring in users' daily life.

The algorithm based on [45] for drowsiness detection was also proposed in this study. It can effectively reduce computation complexity, and is suitable to be implemented in the DSP module. Besides, it is good at removing the differences between individual and environment in different people or measurements. Some previous studies indicated that the level of drowsiness is proportional with the increase of alpha and theta rhythms in EEG and blink duration in EOG. Under the assumption that reaction time of driving performance is proportional with the level of drowsiness, our experimental results showed that the power of alpha and theta

rhythms in EEG and blink duration in EOG increased indeed when the level of drowsiness increased no matter individually succeeding events or the results of average sorting including all of the experimental trials.

In this study, the levels of drowsiness were defined into two states: alert and drowsiness. These two states were used to determine all events of driving performance were drowsy or not first, and then the binary classification test was used to investigate the sensitivity and positive predictive value of our algorithm with different thresholds. Our experimental results with EEG and EOG signals showed that “Combination” with factor $0.3 \times \text{MDT}$, $0.3 \times \text{MDA}$ and $0.4 \times \text{duration}$ when threshold was set to 31.5 had the highest value of F-measure (F-measure = 80.91%, sensitivity = 96.15%, and positive predictive value = 69.84%) higher than the max f-measure value with only EEG signal used (F-measure = 69.54%). It proved that EOG is an important parameter to determine user is drowsy or not and using bio-signals (EEG and EOG) to detect drowsiness is better than EEG signal used only. However, the accuracy of our algorithm for drowsiness detection seems not good enough. This can be explained that each increase of alpha/theta rhythm and blink duration may not correspond to each drowsy event although the long-term increasing trend of power of alpha/theta rhythm and blink duration is proportional with the level of drowsiness.

6.2 Future Works

In future work, our system could combine with the utility of other physiological parameters, such as EKG and EMG, to improve both the sensitivity and positive predictive value. Besides, a non-linear algorithm as fuzzy neural network could be used to make the prediction more precise and increase the accuracy of drowsiness detection. On the other hand, the portable bio-signal acquisition system and DSP module could be integrated as one device to minimize the size of whole system and reduce the signal distortion result from using wireless transmission. Furthermore, there is a novel dry foam bio-signal electrode developed, fabricated and experimentally validated in our lab. The dry electrode was shown in Fig. 6-1:

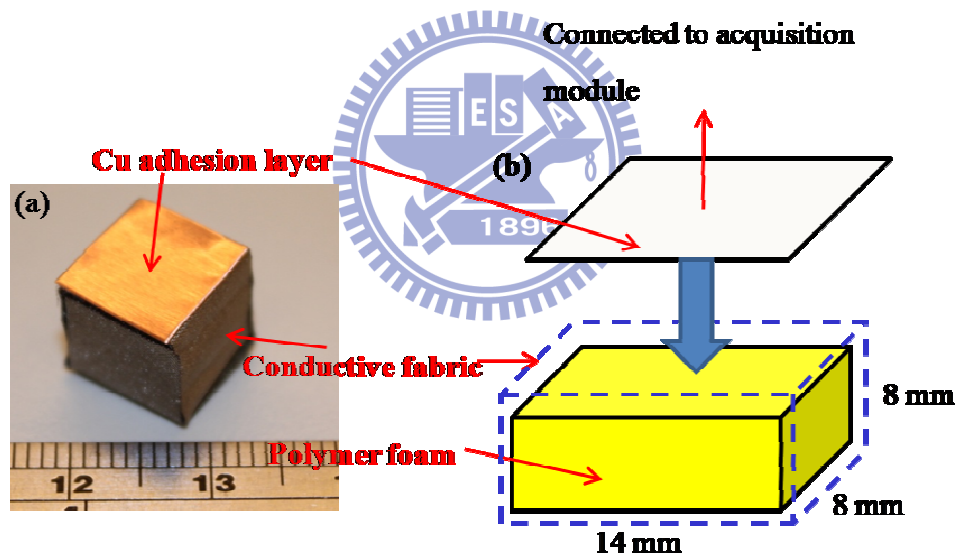


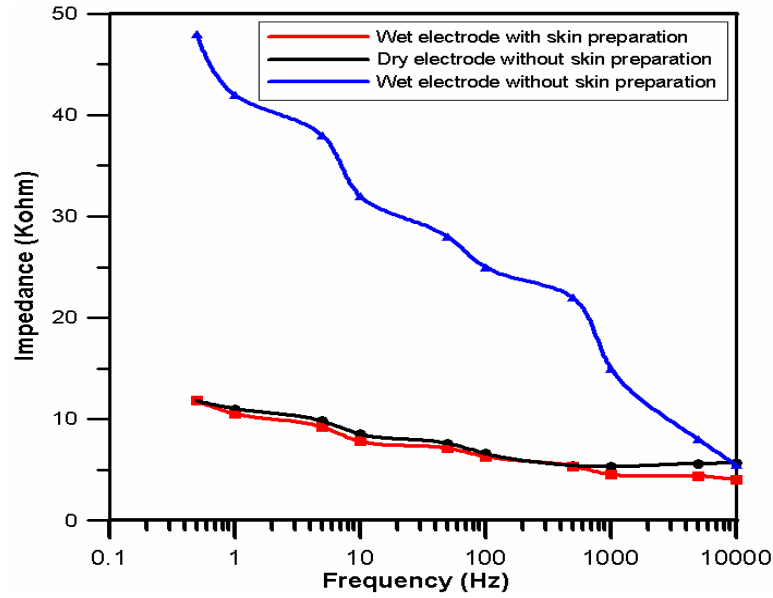
Fig. 6-1: (a) top view, (b) exploded view of the proposed dry foam EEG electrode. The foam electrode was covered by the conductive fabric on all surfaces and then paste on an Au layer.

The major merits of this dry foam electrode include follows: (1) It is applied with zero preparation of scalp, compared to the conventional wet electrodes, (2) the soft substrate of dry foam electrode is able to adapt to irregular scalp surface and the hairy site, and (3) Its fabrication process is low-cost. Therefore, compared to the standard wet electrodes, the proposed dry foam electrode provided a potential for routine and

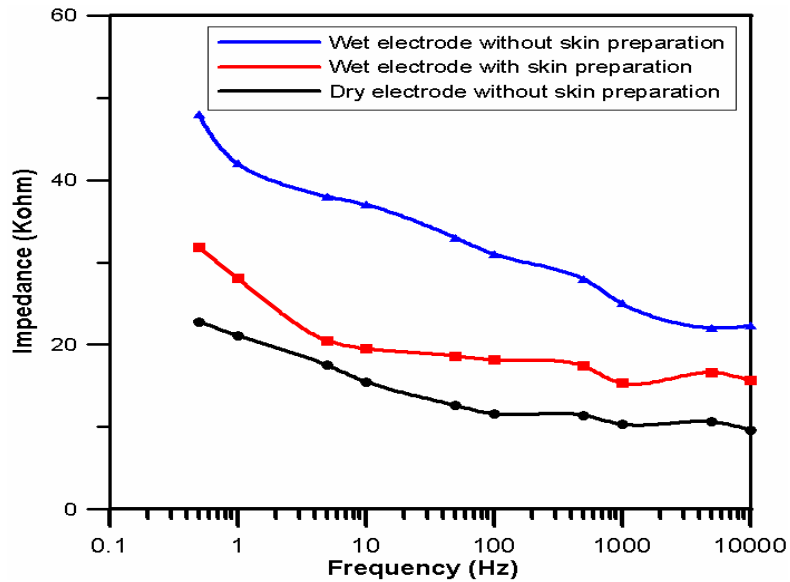
repetitive measurement, and also provided convenience, and comfort for clinical and research applications. The performance and signal quality of dry electrodes are introduced below:

A. Impedance Measurements

In order to test the impedance between the skin and electrode interface, two dry electrodes were placed on the forehead (4 cm apart), and then current was applied to the electrode pair to measure the impedance [49]. Nineteen tests were performed on five different participants. Two different electrodes were used: One is standard wet electrode and the other is dry foam electrode. Fig. 6-2(a) showed the impedance measurement under different conditions. Here, the black line denotes the impedance of dry foam electrode pair without skin preparation and conducting gel. Blue and red lines denote the impedances of conventional wet electrodes without and with skin preparation respectively. All of the conventional wet electrodes were applied with conduction gels. The results showed that the impedance between the skin and dry foam electrode without skin preparation and conducting gel is similar to that of the conventional wet electrode with skin preparation and conducting gel. Therefore, the conduction performance of dry foam electrode outperformed the conventional wet electrode [48, 49].



(a)



(b)

Fig. 6-2: Frequency characteristic of the proposed dry foam electrodes on (a) forehead and (b) hairy site.

Figure 6-2(b) showed the impedance measurement on the hairy site. It showed that, for dry foam electrode, the impedance on the hairy site nearly equals that on the hairless skin, but that on hairless skin is even lower. Evidently, the foam of dry foam electrode is soft enough to contact the skin properly, and the fabric layer is very stable. These properties make the standard skin preparation unnecessary. Certainly, dry

electrodes will hardly surpass the properties of the conventional electrodes with conduction gel. Fig.6-3 showed the impedance variation for different electrodes under long-term EEG measurement. For long-term EEG measurement, the impedance variation of the conventional wet electrode with conduction gel is more obvious than that of dry foam electrode. The impedance variation of dry foam electrode was observed in the range from 4 k to 26 k, and is in the acceptable range for normal EEG measurement [48, 54]. Furthermore, compared to the conventional wet electrode under long-term EEG measurement (5 hours), dry foam electrode can significantly provide better stability of the skin–electrode impedance. This result can be explained by that dry foam electrode does not need conduction gel, which is apt to drying.

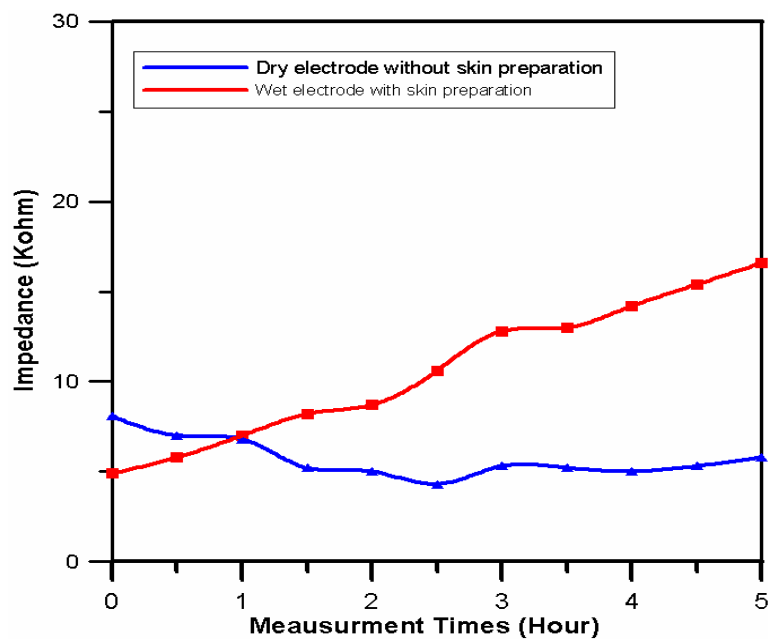


Fig. 6-3: Impedance variation of dry foam electrode and conventional wet electrode under long-term EEG measurement.

B. Comparison of the Signals between Dry/Wet Electrodes

Fig. 6-4(a) and Fig. 6-4(b) showed the placements and the results of EEG measurement by using dry/ wet electrode pairs in the locations of forehead (F10) and hairy site (POz) respectively. Fig. 6-4(c) showed the placements and the results of

EOG measurement by using different types of electrodes. The correlation between signals obtained by dry foam electrode and conventional wet electrode are typically in excess of 96.32 %, 92.18 % in the locations of forehead and hairy sites respectively. For EOG measurement, the correlation between EOG signals obtained by dry/wet electrodes is also very significant (in excess of 97.28 %). Therefore, the performance of bio-potential measurement by using dry foam electrode is almost identical to that of the conventional wet electrodes.



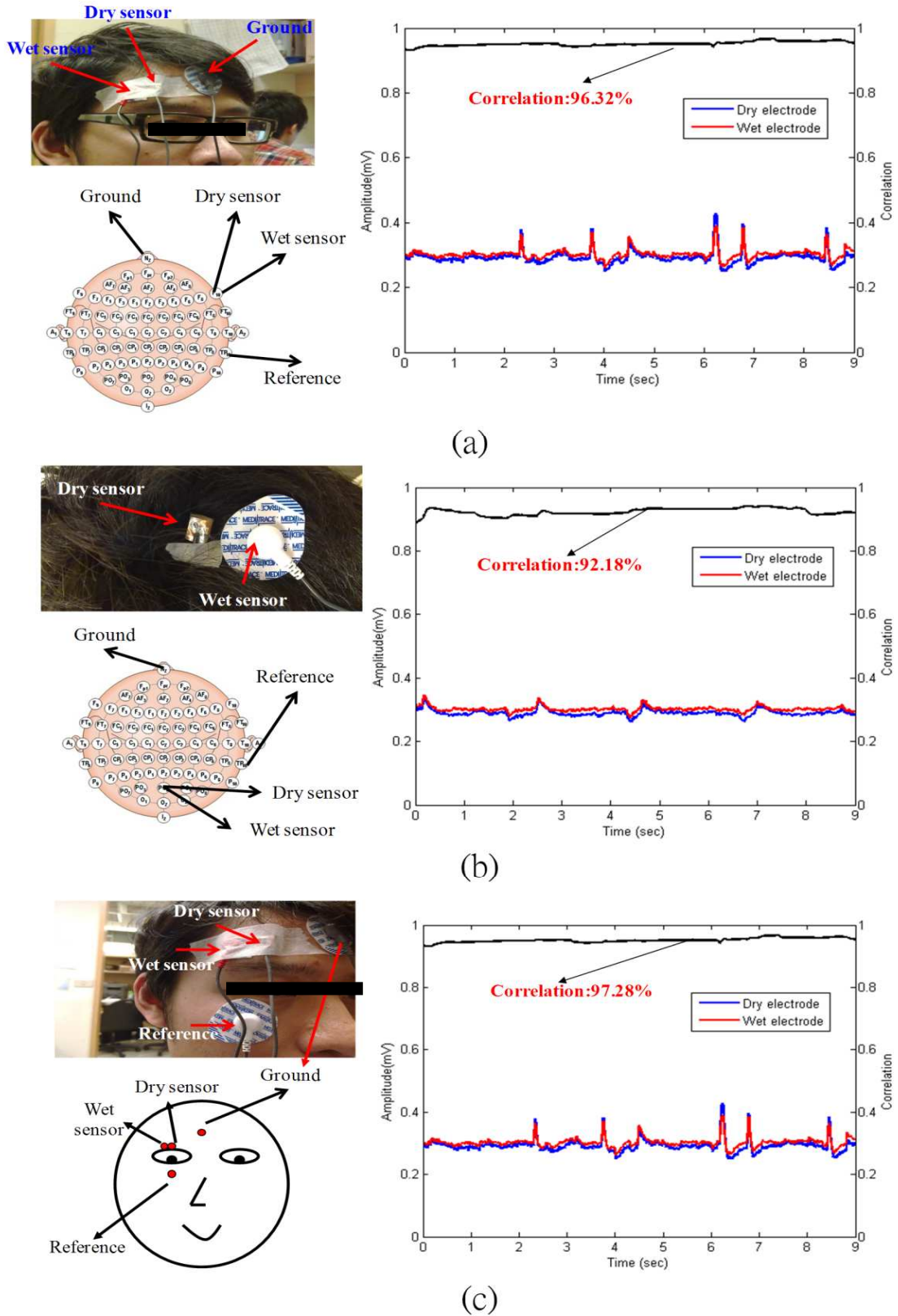


Fig. 6-4: Placements and results of (a) EEG measurement on forehead (F10), (b) EEG measurement on hairy site (POz), and (c) EOG measurement by using different types of electrodes.

In the future, we will integrate the dry foam electrode with our portable bio-signal acquisition system to become a more complete and convenient system. Using this system could simplify the procedure of bio-signal acquired preparation and also maintain the stability and make user feel comfortable. Come to a conclusion, our system is feasible for further extension, and within above future works could make our system more complete and better.



References

- [1] Agence France-Presse, Manila, 23rd. [Online]. Available : <http://www.ylps.tp.edu.tw/traffic/news.html>
- [2] K. A. Brookhuis, D. D. Waard, and S. H. Fairclough, "Criteria for driver impairment," *Ergonomics*, Vol 46, 433-445, 2003.
- [3] J. Connor, R. Norton, S. Ameratunga, E. Robinson, I. Civil, R. Dunn, J. Bailey, and R. Jackson, "Driver sleepiness and risk of serious injury to car occupants: population based case control study," *BMJ*, 324: 1125, 2002.
- [4] J. A. Horne, and L. A. Reyner, "Sleep related vehicle accidents," *BMJ*, 310: 565-567 , 1995.
- [5] G. Maycock, "Sleepiness and driving: the experience of UK car drivers," *Journal of Sleep Research*, 5: 229-237, 1996.
- [6] G. Maycock, "Sleepiness and driving: the experience of heavy goods vehicle drivers in the UK," *Journal of Sleep Research*, 6: 238-244, 1997.
- [7] NHTSA, Traffic safety facts 2001: A compilation of motor vehicle crash data from the fatality analysis reporting system and the general estimates system. In: NHTSA's National Center for Statistics and Analysis, Washington, DC, 2002.
- [8] NSF, Sleep facts and stats, National Sleep Foundation, Washington, DC. [Online]. Available: <http://www.sleepfoundation.org/>
- [9] S. G. Mason, A. Bashashati, M. Fatourechi, K. F. Navarro, and G. E. Birch, "A comprehensive survey of brain interface technology designs," *Ann. Biomed. Eng.*, vol. 35, no. 2, pp. 137-169, 2007.
- [10] A. Eskandarian, and A. Mortazavi, "Evaluation of a Smart Algorithm for Commercial Vehicle Driver Drowsiness Detection," *Intelligent Vehicles Symposium, 2007 IEEE* , vol., no., pp.553-559, 13-15 June 2007.
- [11] M. Suzuki, N. Yamamoto, O. Yamamoto, T. Nakano, and S. Yamamoto, "Measurement of Driver's Consciousness by Image Processing -A Method for Presuming Driver's Drowsiness by Eye-Blinks coping with Individual Differences -," *Systems, Man and Cybernetics, 2006. SMC '06. IEEE International Conference on* , vol.4, no., pp.2891-2896, 8-11 Oct. 2006.

- [12] F. Wang, and H. Qin, "A FPGA based driver drowsiness detecting system," *Vehicle Electronics and Safety, 2005. IEEE International Conference on*, vol., no., pp. 358-363, 14-16 Oct. 2005.
- [13] T. Hamada, T. Ito, K. Adachi, T. Nakano, and S. Yamamoto, "Detecting method for drivers' drowsiness applicable to individual features," *Intelligent Transportation Systems, 2003. Proceedings. 2003 IEEE*, vol.2, no., pp. 1405-1410 vol.2, 12-15 Oct. 2003.
- [14] T. Hong, and H. Qin, "Drivers drowsiness detection in embedded system," *Vehicle Electronics and Safety, 2007. ICVES. IEEE International Conference on*, vol., no., pp.1-5, 13-15 Dec. 2007.
- [15] I. Park, J. H. Ahn, and H. Byun, "Efficient Measurement of Eye Blinking under Various Illumination Conditions for Drowsiness Detection Systems," *Pattern Recognition, 2006. ICPR 2006. 18th International Conference on*, vol.1, no., pp.383-386, 2006.
- [16] M. J. Flores, J. M. Armingol, and A. Escalera, "Real-time drowsiness detection system for an intelligent vehicle," *Intelligent Vehicles Symposium, 2008 IEEE*, vol., no., pp.637-642, 4-6 June 2008.
- [17] H. Su, and G. Zheng, "A Partial Least Squares Regression-Based Fusion Model for Predicting the Trend in Drowsiness," *Systems, Man and Cybernetics, Part A: Systems and Humans, IEEE Transactions on*, vol.38, no.5, pp.1085-1092, Sept. 2008
- [18] T. C. Chieh, Mustafa, M. Marzuki, Hussain, Aini, Hendi, S. Farshad, Majlis, and B. Yeop, "Development of vehicle driver drowsiness detection system using electrooculogram (EOG)," *Computers, Communications, & Signal Processing with Special Track on Biomedical Engineering, 2005. CCSP 2005. 1st International Conference on*, vol., no., pp.165-168, 14-16 Nov. 2005.
- [19] C. T. Lin, R. C. Wu, S. F. Liang, W. H. Chao, Y. J. Chen, and T. P. Jung, "EEG-based drowsiness estimation for safety driving using independent component analysis," *Circuits and Systems I: Regular Papers, IEEE Transactions on*, vol.52, no.12, pp. 2726-2738, Dec. 2005.
- [20] C. T. Lin, S. F. Liang, Y. C. Chen, Y. C. Hsu, and L.W. Ko, "Driver's drowsiness estimation by combining EEG signal analysis and ICA-based fuzzy neural networks," *Circuits and Systems, 2006. ISCAS 2006. Proceedings. 2006 IEEE International Symposium on*, vol., no., pp.4 pp.-2128, 2006.

- [21] H. J. Eoh, M. K. Chung, and S. H. Kim, "Electroencephalographic Study of Drowsiness in Simulated Driving with Sleep Deprivation," *International Journal of Industrial Ergonomics*, Volume 35, Issue 4, pp. 307-320, April 2005.
- [22] Y. S. Kim, *et al.*, "Helmet-based physiological signal monitoring system," *European Journal of Applied Physiology*, vol. 105, pp. 365-372, Feb 2009.
- [23] B. Jammes, *et al.*, "Automatic EOG analysis: A first step toward automatic drowsiness scoring during wake-sleep transitions," *Somnologie-Schlafforschung und Schlafmedizin*, vol. 12, pp. 227-232, 2008.
- [24] P. P. Caffier, *et al.*, "Experimental evaluation of eye-blink parameters as a drowsiness measure," *European Journal of Applied Physiology*, vol. 89, pp. 319-325, May 2003.
- [25] S. Y. Hu and G. T. Zheng, "Driver drowsiness detection with eyelid related parameters by Support Vector Machine," *Expert Systems with Applications*, vol. 36, pp. 7651-7658, May 2009.
- [26] H. Su and G. T. Zheng, "A partial least squares regression-based fusion model for predicting the trend in drowsiness," *Ieee Transactions on Systems Man and Cybernetics Part a-Systems and Humans*, vol. 38, pp. 1085-1092, Sep 2008.
- [27] J. R. Millan, and J. Mourino, "Asynchronous BCI and Local Neural Classifiers: An Overview of the Adaptive Brain Interface Project," *IEEE Transactions on Neural Systems and Rehabilitation Engineering*, vol. 11, pp. 159-161, 2003.
- [28] E. L. Glassman, "A Wavelet-like Filter based on Neuron Action Potentials for Analysis of Human Scalp Electroencephalographs," *IEEE Transactions on Biomedical Engineering*, vol. 52, pp. 1851-1862, 2005.
- [29] D. J. McFarland and J. R. Wolpaw, "Sensorimotor Rhythm-based Braincomputer Interface (BCI): Feature Selection by Regression Improves Performance," *IEEE Transactions on Neural Systems and Rehabilitation Engineering*, vol. 13, pp. 372-379, 2005.
- [30] C. Neuper, A. Schlogl, and G. Pfurtscheller, "Enhancement of Left-right Sensorimotor EEG Differences during Feedback-regulated Motor Imagery," *Journal of Clinical Neurophysiology*, vol. 16, pp. 373-382, 1999.

- [31] R. Stein, D. Weber, Y. Aoyagi, A. Prochazka, J. Wagenaar, S. Shoham, and R. Normann, "Coding of Position by Simultaneously Recorded Sensory Neurons in the Cat Dorsal Root Ganglion," *The Journal of Physiology*, vol. 560, pp. 883-896, 2004.
- [32] S. Lemm, B. Blankertz, G. Curio, and K. R. Muller, "Spatio-spectral Filters for Improved Classification of Single Trial EEG," *IEEE Transactions on Biomedical Engineering*, vol. 52, pp. 1541-1548, 2005.
- [33] B. Kamousi, Z. Liu, and B. He, "Classification of Motor Imagery Tasks for Brain-computer Interface Applications by Means of Two Equivalent Dipoles Analysis," *Transactions on Neural Systems and Rehabilitation Engineering*, vol. 13, pp. 166-171, 2005.
- [34] L. Qin, L. Ding, and B. He, "Motor Imagery Classification by Means of Source Analysis for Brain Computer Interface Applications," *Journal of Neural Engineering*, vol. 1, pp. 135-141, 2004.
- [35] G. R. Muller-Putz, R. Scherer, C. Neuper, and G. Pfurtscheller, "Steady-State Somatosensory Evoked Potentials: Suitable Brain Signals for Brain-Computer Interfaces," *IEEE Transactions on Neural Systems and Rehabilitation Engineering*, vol. 14, pp. 30-37, 2006.
- [36] C. W. Anderson, E. A. Stolz, and S. Shamsunder, "Multivariate Autoregressive Models for Classification of Spontaneous Electroencephalogram during Mental Tasks," *IEEE Transactions on Biomedical Engineering*, vol. 45, pp. 277-286, 1998.
- [37] T. N. Lal, M. Schroder, T. Hinterberger, J. Weston, M. Bogdan, N. Birbaumer, and B. Scholkopf, "Support Vector Channel Selection in BCI," *IEEE Transactions on Biomedical Engineering*, vol. 51, pp. 1003-1010, 2004.
- [38] B. Graimann, J. E. Huggins, S. P. Levine, and G. Pfurtscheller, "Toward a Direct Brain Interface Based on Human Subdural Recordings and Wavelet-Packet Analysis," *IEEE Transactions on Biomedical Engineering*, vol. 51, pp. 954-962, 2004.
- [39] J. del R. Millan, M. Franze, J. Mourino, F. Cincotti, and F. Babiloni, "Relevant EEG Features for the Classification of Spontaneous Motor-related Tasks," *Biological Cybernetics*, vol. 86, pp. 89-95, 2002.

- [40] R. Palaniappan, R. Paramesran, S. Nishida, and N. Saiwaki, "A New Brain-Computer Interface Design Using Fuzzy ARTMAP," *IEEE Transactions on Neural Systems and Rehabilitation Engineering*, vol. 10, pp. 140-148, 2002.
- [41] F. Cincotti, L. Bianchi, G. Birch, C. Guger, J. Mellinger, R. Scherer, R. N. Schmidt, O.Y. Suarez, and G. Schalk, "BCI Meeting 2005- Workshop on Technology: Hardware and Software," *IEEE Transactions on Neural Systems and Rehabilitation Engineering*, vol. 14, pp. 128-131, 2006.
- [42] J. R. Wolpaw, G. E. Loeb, B. Z. Allison, E. Donchin, O. F. Nascimento, W. J. Heetderks, F. Nijboer, W. G. Shain, and J. N. Turner, "BCI Meeting 2005- Workshop on Signal and Recording Methods," *IEEE Transactions on Neural Systems and Rehabilitation Engineering*, vol. 14, pp. 138-141.
- [43] L. C. Shi, H. Yu, B. L. Lu, "Semi-supervised clustering for vigilance analysis based on EEG," *Proceedings of 20th International Joint Conference on Neural Networks*. 1518-1523, 2007.
- [44] J. W. Fu, M. Li, and B. L. Lu, "Detecting Drowsiness in Driving Simulation Based on EEG," *Autonomous Systems – Self-Organization, Management, and Control Proceedings of the 8th International Workshop*, Shanghai, China, October 6-7, 2008.
- [45] N. R. Pal, C. Y. Chuang, L. W. Ko, C. F. Chao, T.P. Jung, S. F. Liang, and C. T. Lin, "EEG-Based Subject- and Session-independent Drowsiness Detection: An Unsupervised Approach," *EURASIP Journal on Advances in Signal Processing*, Volume 2008, 11 pages, July, 2008.
- [46] Electrooculography, from wikipedia, the free encyclopedia, [Online]. Available: <http://en.wikipedia.org/wiki/Electrooculography>
- [47] C. T. Lin, I. F. Chung, L. W. Ko, Y. C. Chen, S. F. Liang, and J. R. Duann, "EEG-based assessment of driver cognitive responses in a dynamic virtual-reality driving environment," *IEEE Transactions on Biomedical Engineering*, vol. 54, pp. 1349-1352, 2007.
- [48] N. V. Thakor, "Biopotentials and electro-physiology measurement," in the measurement, Instrumentation, and Sensors Handbook, ed: CRC Press, 1999, pp. 74-1.
- [49] J. G. Webster, *Medical Instrumentation: Application and Design*, 3rd edition ed.: John Wiley & Sons Inc, 1998.

- [50] J.M.R. Delgado, W.L. Nastuk, "Electrodes for Extracellular Recording and Stimulation,; in *Physical Techniques in Biological Research*", New York: Academic Press,1964.
- [51] Texas Instrument. [Online]. Available:
<http://focus.ti.com/lit/ug/slau049f/slau049f.pdf>
- [52] C. T. Lin, L. W. Ko, J. C. Chiou, J. R. Duann, R. S. Huang, T. W. Chiu, S. F. Liang, and T. P. Jung, "Noninvasive neural prostheses using mobile and wireless EEG," *Proceedings of the IEEE*, vol. 96, pp. 1167-1183, 2008.
- [53] C.-T. Lin, Y.-C. Chen, T.-Y. Huang, T.-T. Chiu, L.-W. Ko, S.-F. Liang, H.-Y. Hsieh, S.-H. Hsu, and J.-R. Duann, "Development of wireless brain computer interface with embedded multitask scheduling and its application on real-time driver's drowsiness detection and warning," *IEEE Transactions on Biomedical Engineering*, vol. 55, pp. 1582-1591, 2008.
- [54] A. Searle and J. Kirkup, "A direct comparison of wet, dry and insulating bioelectric recording electrodes," *Physiological Measurement*, vol. 21, pp. 271-283, 2000.
- [55] Electroencephalography, from wikipedia, the free encyclopedia, [Online]. Available: <http://en.wikipedia.org/wiki/Electroencephalography>
- [56] 莊玠瑤，“利用虛擬實境模擬系統偵測駕駛員從清醒至打瞌睡過程之腦波變化”，國立交通大學，碩士論文，民國九十七年。
- [57] C. T. Lin, R. C. Wu, T. P. Jung, S. F. Liang, and T. Y. Huang, "Estimating alertness level based on EEG spectrum analysis," *EURASIP J. Appl. Signal Process*, vol. no. 19, pp. 3165–3174, Mar. 2005.
- [58] W. Klimesch, "EEG alpha and theta oscillations reflect cognitive and memory performance: a review and analysis," *Brain Research*, vol 29, pp. 169–195, 1999
- [59] S. Makeig and T. P. Jung, "Tonic, phasic, and transient EEG correlates of auditory awareness in drowsiness," *Cognitive Brain Research*, vol. 4, pp. 15-25, 1996.
- [60] S. Makeig, T. P. Jung, and T. J. Sejnowski, "Awareness during drowsiness: dynamics and electrophysiological correlates," *Canadian Journal of Experimental Psychology*, vol., 54, pp.266-273, 2000.

- [61] M. A. Schier, "Changes in EEG alpha power during simulated driving: a demonstration," *International Journal of Psychophysiology*, vol. 37, pp.155-162, 2000.
- [62] S. L. Joutsiniemi, S. Kaski, and T. A. Larsen, "Self-organizing map in recognition of topographic patterns of EEG spectra," *IEEE Transactions on Biomedical engineering*, Vol. 42, no. 11, 1995.
- [63] K. V. Mardia, "Mardia's Test of Multinormality," in *S. Kotz and N.L. Johnson, eds., Encyclopedia of Statistical Sciences*, vol. 5, pp. 217-221, 1985.
- [64] 賴家達, "無線嵌入式生醫平台", 國立交通大學, 碩士論文, 民國九十七年。
- [65] S. Makeig and T. P. Jung, "Changes in alertness are a principal component of variance in the EEG spectrum," *NeuroReport*, vol. 7, pp. 213-216, 1995.
- [66] T. P. Jung, S. Makeig, M. Stensmo, and T. J. Sejnowski, "Estimating alertness from the EEG power spectrum," *IEEE Trans. Biomed. Eng.*, vol. 44, no. 1, pp. 60-69, Jan. 1997.
- [67] S. Makeig and M. Inlow, "Lapses in alertness: Coherence of fluctuations in performance and EEG spectrum," *Electroencephalography. Clin. Neurophysiol.*, vol. 86, pp. 23-35, 1993.
- [68] K. V. Mardia. "Applications of some measures of multivariate skewness and kurtosis in testing normality and robustness studies," *Sankhyā, Ser B*, vol. 36, no. 2, pp. 115-128, 1974.
- [69] K. V. Mardia. "Tests of univariate and multivariate normality," In: *S. Kotz et al., editors, Handbook of Statistics*, vol. 1, pp. 279-320, 1980.
- [70] The R project for statistical computing, [Online]. Available: <http://www.r-project.org/>
- [71] P. C. Mahalanobis, "generalised distance in statistics," *Proceedings of the National Institute of Science of India* pp. 49 The R Project for Statistical Computing -55, 1936.
- [72] How to build Muscular Bio-Stimulator, [Online]. Available: <http://www.high-voltage-lab.com/231/muscular-bio-stimulator>
- [73] 風池穴小用, [Online]. Available: <http://tinyurl.com/2arkkbw>